THE UNIVERSITY OF OKLAHOMA

GRADUATE COLLEGE

A STUDY OF ELECTROFLUIDMECHANICAL INTERACTIONS IN BOILING HEAT TRANSFER

A DISSERTATION

SUBMITTED TO THE GRADUATE FACULTY

in partial fulfillment of the requirements for the

degree of

DOCTOR OF PHILOSOPHY

BY

JOHN L. EE OLINGER

Norman, Oklahoma

1968

A STUDY OF ELECTROFLUIDMECHANICAL INTERACTIONS

IN BOILING HEAT TRANSFER

APPROVED BY

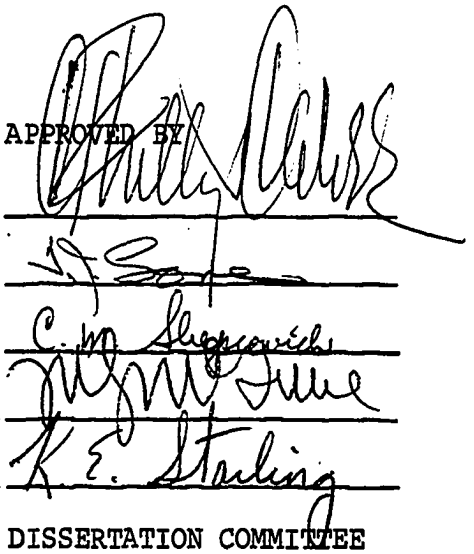

DISSERTATION COMMITTEE

ACKNOWLEDGEMENTS

The author is indebted to a multitude of persons and institutions for their assistance and encouragement during the course of this work. Most of those who were either in or associated with the Chemical Engineering Department during the years from 1963 to 1968 contributed in some way to this work. Of all these people the following are those whose contributions were particularly noteworthy.

Dr. C.Phillip Colver, who not only directed this research, but whose patience was severely tested on a number of occasions.

Drs. R.L. Mednick and F.E. Merliss, and the personnel at the OURI Machine Shop for assistance in the construction of the equipment and acquisition of the data.

Mr. J.B. Turner and Mr. H.H. West for their open-mindedness and constant availability which resulted in many stimulating discussions.

Mrs. Mary Ann Piety and Miss Mary Elaine Walter whose assistance in the preparation of this work following the author's departure from the University of Oklahoma was invaluable.

Drs. Michael Bobal, Walter Bornhorst and Mr. John Minardi of the University of Dayton for their ideas in data interpretation and complete cooperation in seeing that this work was completed.

Celanese Chemical Co., Phillips Petroleum Co., NASA, The University of Oklahoma Graduate School and Department of Chemical Engineering all of whom provided financial aid.

E. I. duPont de Nemours Co. for donation of the Freon-112 used in this work.

Finally, special appreciation is due my parents who without a doubt sacrificed the most during all my years as a student.

TABLE OF CONTENTS

TABLE OF CONTENTS--Continued

APPENDICES (Continued)

LIST OF TABLES

LIST OF TABLES--Continued

LIST OF TABLES--Continued

LIST OF ILLUSTRATIONS

LIST OF ILLUSTRATIONS--Continued

LIST OF ILLUSTRATIONS--Continued

A STUDY OF ELECTROFLUIDMECHANICAL INTERACTIONS IN BOILING HEAT TRANSFER

CHAPTER I

INTRODUCTION

Figure 1 shows the shape of a curve generated from pool boiling heat transfer data. This is a log-log plot of heat flux as a function of ΔT, where ΔT is the temperature difference between the heated surface and the saturated liquid. The general shape of this curve, commonly known as the boiling curve, has been reproduced experimentally by many investigators using many different liquids. As shown in Figure 1, the boiling curve is divided into four regions, namely the convective, nucleate, transitional, and film boiling regions. In each of these regions the mechanism of heat transport is different. This difference in mechanism of the boiling process in the various regions accounts for the peculiar shape of the curve.

From a practical standpoint, the boiling curve provides the necessary information to obtain the conductance term,

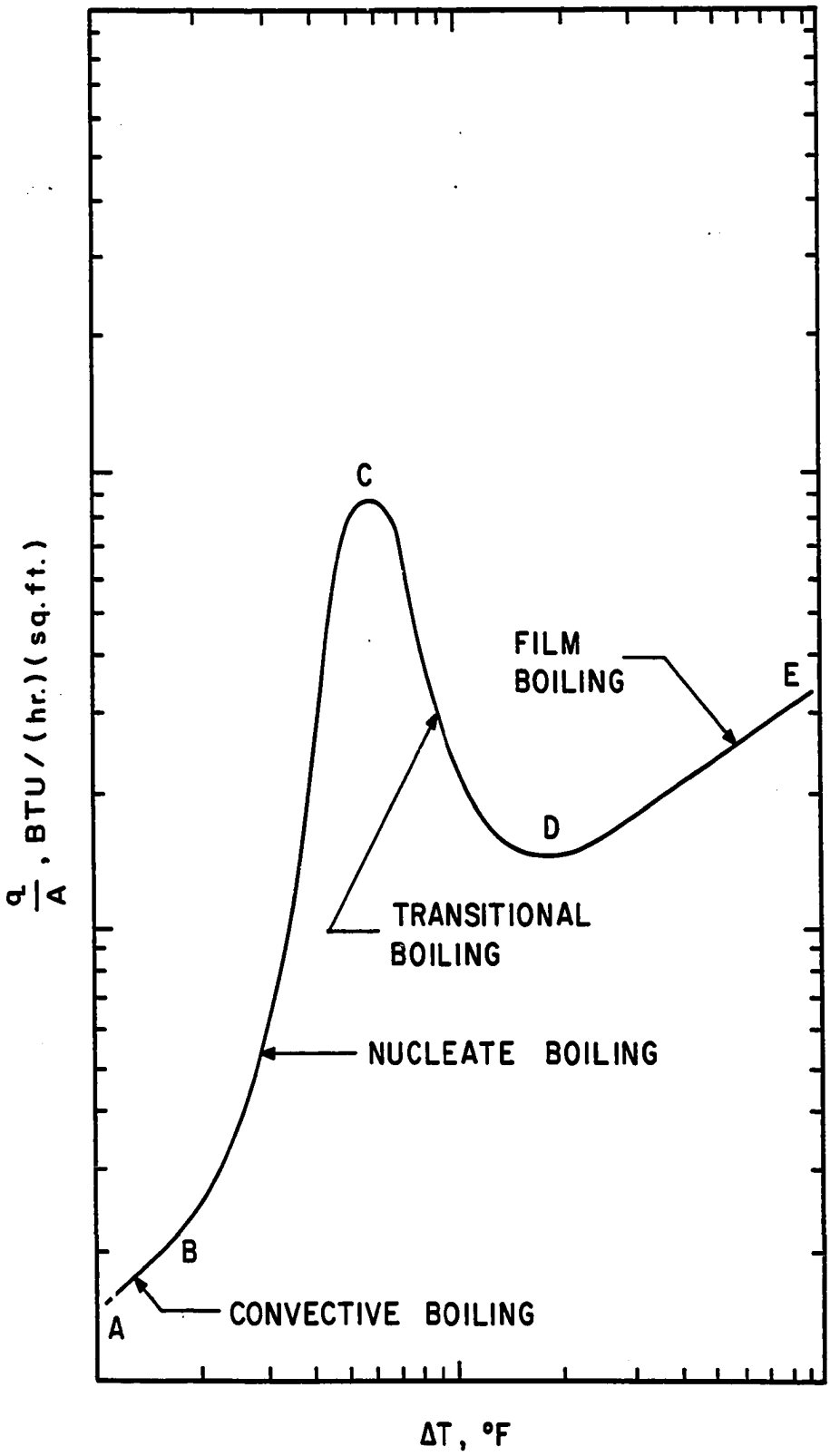

Figure 1. Typical Pool Boiling Curve

or heat transfer coefficient. The aforementioned parameters are related by the following rate expression for heat transfer,

$$\frac{q}{A} = h\ \Delta T \qquad (1)$$

where h is the heat transfer coefficient. To the design engineer, one of the most important features of the boiling curve is the maximum through which the heat flux goes with increasing ΔT. The heat flux at this maximum point is commonly referred to as the burnout heat flux, or the first critical heat flux, and represents the limit for practical and economical operation of boiling equipment. Thus, the determination of the factors which influence burnout has been the object of intense investigation. While these investigations have shown that the burnout heat flux can be favorably affected by operation at elevated pressure, through use of forced convection boiling rather than pool boiling, and by judicious choice of a liquid, a great deal more information is required to fully characterize the factors affecting the burnout heat flux. Since normal boiling operations approach burnout from the nucleate boiling regime, an understanding of nucleate boiling is basic to an understanding of burnout. Because of the complex fluid motion in nucleate boiling, however, an adequate analysis of the associated heat transfer process is exceedingly

complex. In addition to this, the heat transfer in nucleate boiling is greatly affected by the heat transfer surface properties. Investigations have shown that such difficult-to-characterize variables as heat transfer surface material, roughness and aging have a definite effect on nucleate boiling and burnout heat flux. Other pertinent variables are geometry, size, and orientation of the surface.

The heat flux restriction imposed by the burnout heat flux is circumvented by increasing the total heat transfer area in order to operate boiling equipment at a heat flux safely below the burnout value. In some boiling heat transfer applications, the area which can be obtained for heat transfer is severely limited. A good example of such a case is the heat transfer problem in a nuclear reactor, where the core size and geometry are an intimate part of the reactor design. With the size fixed by these considerations, the area which can be obtained for heat transfer is limited. In order to achieve the desired heat flux levels, the heat transfer rate must be increased. In boiling heat transfer, this means increasing the peak or burnout heat flux.

In view of the increasing importance of devices such as the nuclear reactor, in which high heat fluxes are extremely desirable, there has been an increasing interest in developing new techniques whereby the peak heat flux in nucleate boil-

ing can be increased. One of the promising techniques thus far developed involves the use of an intense electric field. Investigations in this area have shown that for certain fluids and electrode configurations, the peak heat flux can be significantly increased. While this effect has been experimentally demonstrated, the mechanism by which the electric field affects the boiling curve is not clearly understood.

Describing the effect of an electric field on the boiling process is by no means an easy problem. It involves an interpretation of the interaction of two separate phenomena, boiling heat transfer and electrofluidmechanics, neither of which is well understood. Since the boiling process is both a heat transfer problem and a two-phase flow problem, a better understanding of the electric field effects on boiling heat transfer would contribute to electrofluidmechanics and to boiling heat transfer. Considering that favorable electric field effects have been demonstrated in other areas of heat transfer, such as condensation, it is felt that more knowledge of electric field fluid interactions could lead to the profitable application of electrofluidmechanics to other physical processes.

This investigation was undertaken primarily to attempt to provide a better understanding of electric field effects on boiling heat transfer. It was hoped that by using the

previous work in this area, and by performing supplemental experimental work, some of the puzzling phenomena observed could be interpreted and possibly incorporated into a more general interpretation of electric field fluid interactions.

CHAPTER II

BACKGROUND AND LITERATURE SURVEY

Basic Principles of Electrofluidmechanics

Suppose a positively charged particle is placed between the two electrodes which are charged to a certain potential difference. Because of coulombic attraction the particle will experience a force which will cause it to drift toward the negatively charged electrode. The magnitude of this force is shown in Equation (2), where $\vec{E}$ is the electric field intensity in the region between the charged plates.

$$\vec{F} = \vec{E}\, q^{+} \tag{2}$$

If the terminals of the electrodes are reversed, the motion of the charged particle is also reversed. Such motion of a charged particle in an electric field, as exists between capacitor plates, is commonly referred to as electrophoresis. Electrophoresis is independent of the configuration of the charged plates or electrodes, that is, independent of whether the electric field is uniform or non-uniform. As long as the electrodes remain charged the particle is accelerated toward

the oppositely charged plate. A net motion occurs, however, if the direction of the electric field does not oscillate equally in time. If the potential is intermittently reversed on an equal time of application basis, as occurs with an AC voltage, the particle merely vibrates back and forth and the net motion is, in effect, zero.

Let us now suppose that a neutral particle carrying an equal amount of positive and negative charge is placed between the charged electrodes. It is easy to see that the particle will be oriented in the field so that the positive end of the particle is closest to the negatively charged electrodes and the negative end of the particle is closest to the positive electrode. In addition, the particle becomes strained or polarized. If the electrode arrangement is such that the generated electric field is uniform, the particle remains in this aligned and strained position but no net motion occurs. If the electrode configuration is such that the generated electric field is non-uniform, one end of the particle experiences a greater force than the other and the particle begins to move in the direction of increasing electric field intensity. Such motion of neutral particles is referred to as <u>dielectrophoresis</u>. The magnitude of the force from dielectrophoresis on a homogeneous unit volume of such dipoles is shown below.

$$\vec{F}_V = \frac{\epsilon_o}{6} (K-1) (K+2) \vec{\nabla}(\vec{E}\cdot\vec{E}) \qquad (3)$$

In this equation, K represents the dielectric constant of the medium and ϵ_o the permittivity of free space. As can be seen from Equation (3), the existence of this force is dependent on the presence of a non-uniform electric field. If an AC voltage is applied with an electrode arrangement giving a non-uniform electric field, a net force will still be present, as the field non-uniformity is determined solely by the electrode arrangement and not by the polarity.

The phenomena defined and described above as electrophoresis and dielectrophoresis are the prime electric field effects on fluids. The study and interpretation of these effects is the main concern in electrofluidmechanics. While the effects of electrophoresis have been observed and studied for some time, the effects of dielectrophoresis have only recently received much attention. The interest in dielectrophoretic phenomena was generated with the discovery that major external effects could be achieved with an intense non-uniform electric field, and that these effects could be attained with a very low power expenditure.

In any real situation, electrophoresis and dielectrophoresis occur simultaneously. The occurrence of the electro-

phoretic phenomena and its associated charge gives rise to many complexities which make an interpretation of electric field effects on fluids much more difficult than described above. Velkoff [28], in a paper on electrofluidmechanics, discusses some of these complexities and also some of the other secondary phenomena (not mentioned here) arising as a result of the electric field.

Boiling Studies With Applied Electric Fields

The phenomena which result on applying intense non-uniform electric fields to fluids are often quite peculiar and unexplainable. Pohl [22,23], in articles published in the 1950's, demonstrated experimentally some of these uncommon phenomena. In general, his results showed that the electric field could be used to produce a fairly efficient pumping action of nonconducting liquids, to cause continuous separations in coarse suspensions, to cause selective precipitation, and to produce mixing. Although works concerning electrofluid interactions appeared in the literature as early as the late 1930's, it appears that no great interest in electrofluidmechanical phenomena developed until Pohl's work during the 1950's. Choi [6] and Holmes [11] give surveys of much of the early work performed in this area.

Since the time of Pohl's work, electrofluidmechanical phenomena have been used with significant achievements in

boiling heat transfer and condensation heat transfer. In the area of boiling heat transfer, which represents the largest portion of applied electrofluidmechanics, the effect of an applied electric field has been to generate electrophoretic and dielectrophoretic forces, which tend to enhance boiling heat transfer by increasing convection and by extending the range of nucleate boiling to significantly higher heat fluxes. Some data showing these effects on the complete boiling curve are shown in Figures 2 and 3. These figures show data reported by Choi [6] and Markels and Durfee [14,15]. Others contributing significantly in this area are Kronig and Ashmann [1], and Bonjour, Verdier, and Weil [5]; both studies were similar and primarily in the region of convective boiling heat transfer. In general, all investigators studying non-uniform electric field effects on convective boiling, burnout heat flux, and film boiling have shown the same type of effects, namely that heat transfer can be significantly increased at very low expenditures of electrical energy. For the particular types of electrode geometries studied, they have shown that amplification factors of several hundred can be achieved. The amplification factor, AF, is given by Equation (4) and is defined as the amount of additional heat that can be transferred at a fixed ΔT, through use of an applied electric field per unit of input electrical energy.

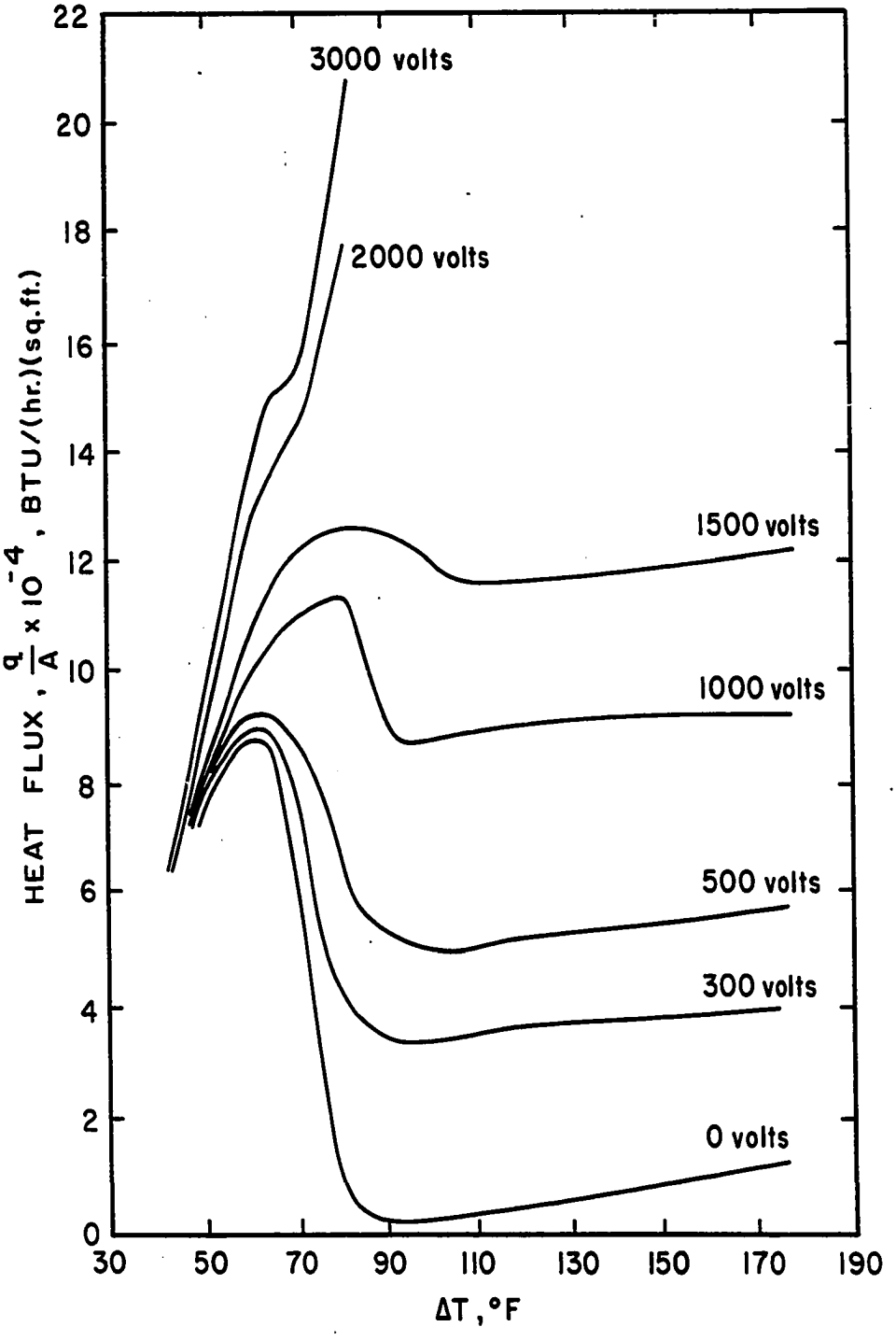

Figure 2. Isopropanol Boiling Heat Transfer Data of Markels and Durfee [13,14] with an Applied Electric Field

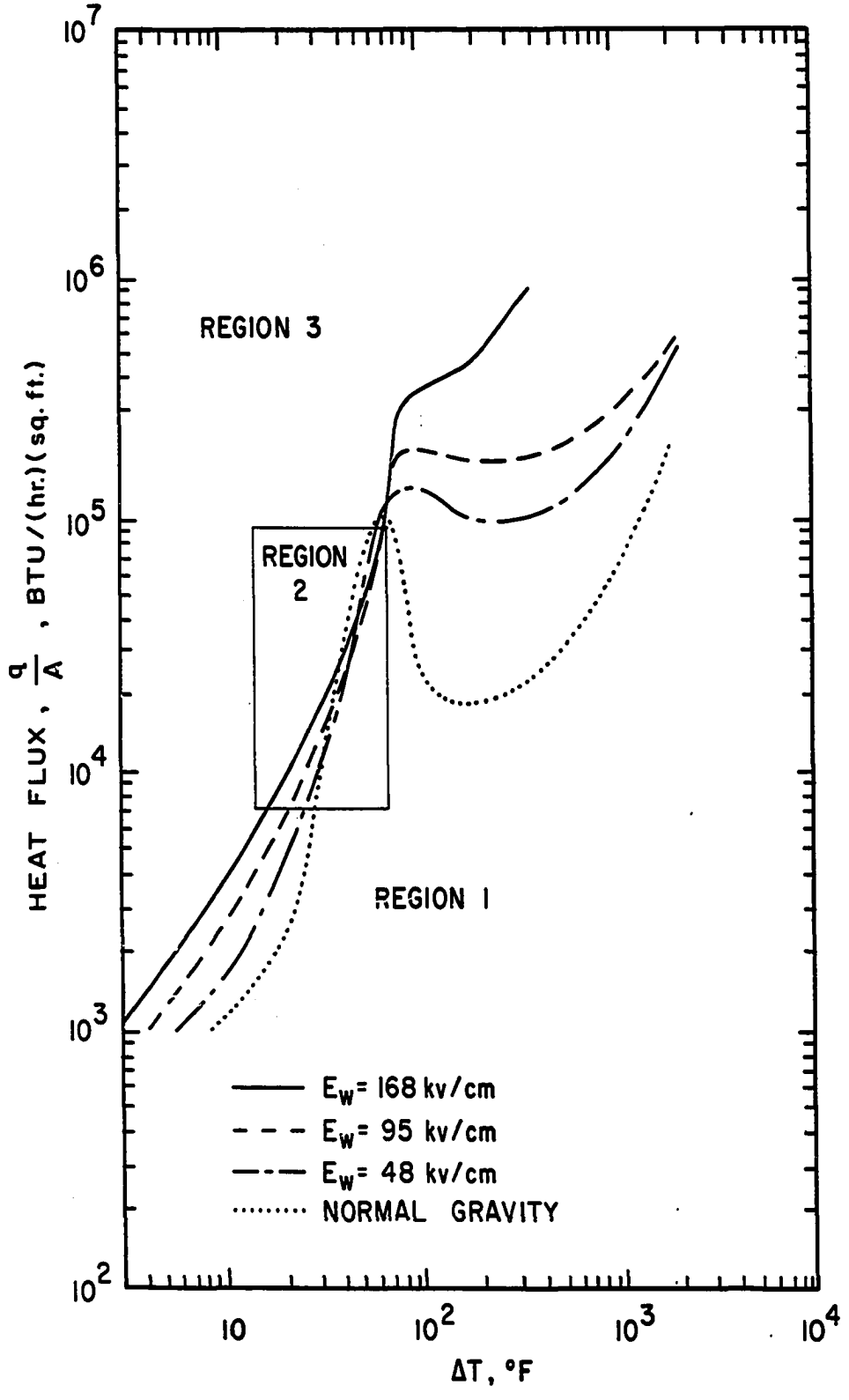

Figure 3. Freon 113 Boiling Heat Transfer Data of Choi [5] with an Applied Electric Field

$$AF = \frac{\frac{q}{A}_{obs} - \frac{q}{A}_{base} + \frac{q}{A}_{VI}}{\frac{q}{A}_{VI}} \qquad (4)$$

$\frac{q}{A}_{obs.}$ = the actual heat transferred with an applied electric field

$\frac{q}{A}_{base}$ = the heat transferred at the same ΔT, but without the presence of the electric field

$\frac{q}{A}_{VI}$ = the heat equivalent of the power dissipated in producing the field, which is given by the product of the applied voltage, V, and the field current drawn, I.

In the area of nucleate boiling, the electric field effects found by the various investigators varied considerably depending on the liquid used. It can be generally stated that the effects of the electric field on nucleate boiling at heat fluxes below the no-field burnout heat flux, Region 2, Figure 3, were considerably less in terms of AF than either above the no-field burnout point, Region 3, or the natural convection boiling region, Region 1. In some instances, the heat transferred at a fixed ΔT in nucleate boiling was even less with an applied electric field than without an electric field, as found by Choi with Freon-113 and shown in Region 2 of Figure 3.

Use of the concepts of electrophoresis and dielectrophoresis in one form or another to explain the electric field effects on boiling heat transfer has been made by all investi-

gators in this area. Kronig and Ashmann [1], whose data was obtained using non-conducting liquids, developed a correlating technique for interpreting electric field effects on convective heat transfer. The technique consisted of defining the Nusselt number for electroconvection in the following manner:

$$Nu = f(Gr\ Pr) + f(El\ Pr) \tag{5}$$

The group (El Pr) is the additional contribution to the Nusselt number caused by the electrical forces. El is a dimensionless group defined as

$$El = \frac{\rho \frac{d\chi}{dT} d_w^2 \Delta T E_w^2}{\tau^2} \tag{6}$$

By use of this group, convective heat transfer data obtained with liquids of high resistivity (hexane, benzene, toluene, liquid nitrogen, etc.) could be correlated. For more conductive liquids, such as water, alcohol, etc., the electrical dimensionless group required redefinition to the following form:

$$El' = \frac{\rho(3s+2t)\epsilon_o d_w^2 \Delta T E_w^2}{\tau^2} \tag{7}$$

Bonjour et al. [5], followed Kronig's work and extended his natural convection correlation to liquids with very diversified characteristics, by obtaining quantitative estimates of the increased thermal exchange due to electrically promoted liquid convection. In this work, as in that of Kronig and

Ashmann, an electrically heated wire strung along the axis of a cylinder was used as the heating element. The high potential electrodes consisted of the heated wire and the surrounding cylinder.

Since the technique developed by Kronig and Ashmann [1] and expanded by Bonjour et al. [5] for correlating natural convection boiling heat transfer data was developed from a consideration of a single medium or phase, it did not serve as a basis for correlating nucleate and film boiling results. The difficulties involved in describing the electrical effects on boiling, when both liquid and vapor are present, arises because of the inhomogeneity of the properties in the two-phase mixture. For example, while the expression shown in Equation (3) could be used to describe the dielectrophoretic effect on a single uniform medium of either vapor or liquid, a problem arises as to how to describe the dielectrophoretic effect on a medium containing both these phases simultaneously.

In 1962 Choi [6] published work in which the effect of a strong non-uniform electric field on atmospheric pressure pool boiling Freon-113 was reported in the convective, nucleate, and film boiling regions. Using the obtained experimental results, Choi developed a technique which could be used to correlate all the Freon-113 boiling results. In the experimental portion of the work, Choi employed the same type of system used by

Kronig and Ashmann [1] and Bonjour et al. [5]. The boiling element was a 0.02-inch diameter electrically-heated platinum wire, which was held in position along the axis of a cylindrical vessel wall, with the wire grounded. In operation, this concentric arrangement was inserted into a tank of the Freon-113. Choi's experimental results with Freon-113 are depicted in Figure 3.

The technique developed by Choi to correlate his results followed an approach similar to that used by Merte and Clark [20] in their work on boiling heat transfer in accelerating systems. The approach was based on defining a new acceleration term as shown by

$$g_t = g + g_o \tag{8}$$

The term g_t is the total acceleration, g the acceleration of gravity and g_o the acceleration from force fields other than normal gravity. This total acceleration term was used in some of the existing correlations for boiling heat transfer. The extraneous acceleration term g_o, due to the applied electric field, was evaluated by Choi by starting with the force equation for dielectrophoresis as shown in Equation (3).* The electric field intensity, $\vec{E}$, in Equation (3) was obtained

*Since Freon is a highly resistive material and since the region in which the phase change occurs is in an area of very strong field gradient, Choi considered only dielectrophoresis to be active.

by first determining the potential from Laplace's equation, shown in Equation (9), using the boundary conditions of the potential at the two electrode surfaces.

$$\nabla^2 V = 0 \tag{9}$$

Using the relationship shown by Equation (10), the electric field intensity, $\vec{E}$, can be easily obtained once the potential is known.

$$\vec{E} = -\vec{\nabla} V \tag{10}$$

The procedure for carrying this out is shown below.

In cylindrical coordinates with only a variation of the potential in the radial direction, Equation (9) becomes

$$\frac{1}{r} \frac{\partial}{\partial r} \left(r \frac{\partial V}{\partial r} \right) = 0 \tag{11}$$

Applicable boundary conditions are:

$V = 0 \quad x = r_w \quad$ (wire radius)

$V = V_o \quad x = r_o \quad$ (outer cylinder radius)

On solution, the potential is found to be

$$V = V_o \frac{\log \left(\frac{r}{r_w}\right)}{\log \left(\frac{r_o}{r_w}\right)} \tag{12}$$

With the potential related to the field intensity by $\vec{E} = -\vec{\nabla} V$, the field intensity is then found to be

$$\vec{E} \frac{V_o}{\log \left(\frac{r_o}{r_w}\right)} \left(\frac{1}{r}\right) \vec{i}_r \qquad (13)$$

where $\vec{i}_r$ is the unit vector in the radial direction. By substitution of this expression for the electric field into the relationship for the volume force from dielectrophoresis, shown in Equation (3), the force on a fluid as a function of radius is obtained for a coaxial cylindrical electrode arrangement as shown by

$$F_V = - \frac{\epsilon_o (K-1)(K+2) V_o^2}{3r^3 \log \left(\frac{r_o}{r_w}\right)^2} \qquad (14)$$

In order to represent the volume force in terms of an acceleration that would be common to both phases, Choi found that the ratio of the dielectrophoretic force on the liquid freon relative to that on vapor freon was approximately in the same ratio as their densities.

$$\frac{(F_V)_{liq}}{(F_V)_{vap}} = \frac{(K_\ell - 1)(K_\ell + 2)}{(K_v - 1)(K_v + 2)} \approx \frac{\rho_\ell}{\rho_v} \qquad (15)$$

The electrical acceleration term, as such, was defined by

$$g_e = \frac{F_V}{\rho} g_c \qquad (16)$$

By evaluating the volume force at the heating wire surface, r_w, the electrical acceleration, shown by Equation (16), was

combined, in accordance with Equation (8), with the acceleration of gravity to obtain the total acceleration. The value for the total acceleration was then used in the Lorentz equation [3] for natural convection boiling, the Bromley equation [25] for film boiling, and the Zuber burnout correlation [25].

Choi's success in interpreting his experimental results by this technique, and his comments and observations about the nucleate boiling data can be summarized as follows:

(1) In natural convection, the classical Lorentz relationship, shown by Equation (17), correlated all of the data (field, non-field, boiling and sub-cooled natural convection) to within $\pm$ 30 percent.

$$Nu = 0.56\ (Gr\ Pr)^{\frac{1}{4}} \qquad (17)$$

(2) In the low heat flux region of nucleate boiling, where a significant fraction of the heat transferred is by natural convection, the effect of the electric field was similar to that in convection, and could generally be correlated in the same fashion as the natural convection data. As the heat flux increased and heat transfer by phase change became a significant mode of heat exchange at the heated surface, the effect of the electric field became less. As shown in Region 2, Figure 3, the heat transferred at a fixed ΔT with an applied field in nucleate boiling actually became less than in the case of no field at all. Visual observation of the bubble motion in this region of heat flux suggested the presence of a

strong radial force field at the wire, as bubble diameters at departure decreased and bubble frequency increased with increasing field strength. These phenomena, which are normally associated with increased heat transfer, were not reflected in the data.

(3) The first critical heat flux data was correlated with the Zuber Equation, shown by

$$(q/A)_{max}/\rho_v H_{fg} = C\left[\frac{\sigma(\rho_\ell-\rho_v)gg_c}{\rho_v^2}\right]^{\frac{1}{4}}\left[\frac{\rho_\ell}{\rho_\ell+\rho_v}\right]^{\frac{1}{2}} \quad (18)$$

While the normal gravity burnout heat flux was quite adequately predicted by this equation, the electric field data deviated considerably from the 1/4 power slope.

(4) In film boiling, the Bromley equation was used to correlate the data.

$$h' = C\left[\frac{k_v^3\rho_v\,(\rho_\ell-\rho_v)\,(H_{fg}+0.4\,Cp_v\Delta T)g}{d_w\mu_v\,\Delta T}\right]^{\frac{1}{4}} \quad (19)$$

Reasonable agreement with the normal gravity data was obtained using a constant of 0.95 as recommended by McAdams [18]. There was some scatter in the electric field data, but Choi pointed out that the agreement was better than expected.

The technique of interpreting electric field effects on boiling heat transfer from an acceleration field standpoint, developed by Choi [6], represented a considerable step forward toward a better understanding and interpretation of electric

field effects on boiling heat transfer. Further substantiation of Choi's approach has been subsequently provided in independent investigations. Costello [7], in a report on an investigation of the effect of a centrifugally-generated acceleration on the burnout heat flux, reports the correlation developed from his data could be used by substitution of Choi's electrical acceleration to correlate the electric field data. The interpretation of electric field effects on boiling heat transfer as given by Choi is, however, not all-encompassing. A fundamental principle to Choi's analysis is the assumption of the equivalence of the electrical acceleration, g_e, in the vapor and liquid phases. Unfortunately, it is not a common property of fluids that this ratio be equal to unity. This fact is shown in Table 1.

TABLE 1

COMPARISON OF THE MAGNITUDE OF THE LIQUID TO VAPOR ELECTRICAL ACCELERATION RATIO FOR FREON-113 AND WATER

Material	$\frac{(F_V)_\ell}{(F_V)_v} = \frac{(K_\ell-1)(K_\ell+2)}{(K_v-1)(K_v+2)}$	$\frac{\rho_\ell}{\rho_v}$	$\frac{(g_e)_\ell}{(g_e)_v}$
Freon-113	1,060	204.5	5.2
Water	75,800	1,603.0	47.2

Further, the decrease in the heat transfer coefficient, with an applied electric field, to values below those with no

applied field, as shown in Region 2, Figure 3, is not consistent with the interpretation given by Choi [6], which predicts increasing heat transfer enhancement with increasing applied voltage.

Markels and Durfee [14,15,16] have to date done the most extensive work using electric fields in boiling heat transfer. Like Choi's work, Markels and Durfee studied the effects of the electric field on boiling heat transfer over the complete boiling curve. The fluids used by Markels and Durfee were water and isopropanol. Since water and isopropanol are partially ionized and, thus, conducting mediums, the work of Markels and Durfee in many respects is very different from Choi's work with freon.

The isopropanol work of Markels and Durfee [14,15] was an atmospheric pressure pool boiling study, which used a horizontal steam-heated, chrome-plated copper tube as a heat transfer surface. The 3/8 inch diameter tube was suspended in a tank of isopropanol with the high voltage being applied between the heat transfer tube and the rectangular tank walls. The results obtained with isopropanol are shown in Figure 2. Resistance measurements between the two electrodes were taken before and during the application of voltage in nucleate boiling, and yielded results which showed that the effective result of the electric field was to increase liquid wetting of the

heated surface. Data was also taken to check the effect of medium conductivity, by doping the isopropanol with ammonium perchlorate. These results showed that, while the heat transfer increases markedly with increasing conductance, the overall effect, as measured by amplification factor, was essentially negligible. Because of the geometry of the electrodes and the largeness of the heated tube, dielectrophoretic effects were thought to be of minor importance in this work in comparison to the effects of electrophoresis.

The boiling water study of Markels and Durfee [15,16] was conducted under forced convection conditions at atmospheric pressure. The apparatus used consisted of two concentric cylinders (inner cylinder 3/8-in. O.D. and outer cylinder 0.96-in. I.D.) mounted in an aluminum shell. In the setup it was possible to boil either from the O.D. side of the inner cylinder, the I.D. side of the outer cylinder, or from both of these surfaces simultaneously. In use, the apparatus was mounted so that the cylinders were operated from a vertical position with AC high voltage being applied to the concentric cylinders with the inner cylinder grounded. For this system Markels and Durfee investigated the three possible modes of boiling. In terms of amplification factors for these three boiling arrangements, results of the type shown in Table 2 were typical in nucleate boiling.

TABLE 2

TYPICAL AF RESULTS OBTAINED BY MARKELS AND DURFEE [14,15] WITH BOILING WATER FOR VARIOUS BOILING CONFIGURATIONS

Configuration	Amplification Factor
Heating from the interior cylinder only	9.5
Heating from the outer cylinder only	4.5
Heating from both sides simultaneously	15.4

In this work Markels and Durfee considered both electrophoresis and dielectrophoresis to be active. For all boiling configurations, the effect of electrophoresis was to enhance the heat transfer. Dielectrophoresis, on the other hand, enhanced the heat transfer only at the inner cylinder, where the electric field intensity, $\vec{E}$, was increasing in the direction toward the heated surface. The dielectrophoretic force was calculated using a form of the volume force equation developed by Pohl [23]. The expression, shown by Equation (20), is for the net force on a spherical dielectric particle of dielectric constant K_2 and radius r_p, in a bulk medium of dielectric constant K_1.

$$\vec{F} = 2\pi r_p^3 K_1 \epsilon_o \frac{(K_2-K_1)}{(K_2-2K_1)} \vec{\nabla}E^2 \qquad (20)$$

The electrophoretic phenomena, which was considered active in this work, was accounted for in terms of a capacitor stress, as given by

$$\frac{F}{A} = \frac{1}{2} \epsilon_o E^2 \tag{21}$$

This relationship is the same expression used to obtain the force per unit area experienced by oppositely charged capacitor plates.

In order to make the calculations for the dielectrophoretic force, as given by Equation (20), and the electrophoretic stress, as given by Equation (21), Markels and Durfee made two sets of assumptions. For the calculation of the force from dielectrophoresis, the following assumptions were made:

(1) The liquid medium was continuous between the electrodes, with the vapor bubbles existing in this bulk medium.

(2) The voltage varied continuously as calculated from Laplace's equation.

For the calculation of the capacitor stress, the assumptions were:

(1) The voltage drop through the liquid was neglected and, as such, the liquid was considered to be one of the conducting plates of the condenser.

(2) The bubbles in nucleate boiling were considered as elements of a continuous vapor film.

The assumptions for these two forces are basically incompatible, since the former assumptions refer to a continuous voltage drop between two electrodes with an insulating material between them, while the latter ignores the presence of the liquid and refers to the plates of a capacitor with vapor between them, where one of the plates is the vapor-liquid interface. While conceding this contradiction, Markels and Durfee [14] believed that the actual variation of voltage between the two concentric cylinders was somewhere between these two extremes. In actuality, an analytic description of the forces arising from a partially conducting system, such as this, is indeed a complex problem.

While proposing the activity of electrophoresis and dielectrophoresis, Markels and Durfee did not attempt to use them as data-correlating tools in the water work, as did Choi in his freon work. Instead, a comparison of the force from dielectrophoresis and the capacitor effect was made for the three boiling configurations. So that equivalent terms could be compared, the dielectrophoretic force (Equation (20)) was converted to a stress by dividing by the bubble projected area, πr_p^2. As such, the two forces exerted

per unit area on a bubble were as follows:

DIELECTROPHORETIC EFFECT:

$$\left(\frac{F}{A}\right) = 4r_p K_1 \epsilon_o \frac{(K_1-K_2)}{(K_2+2K_1)} \frac{V^2}{r^3 \ln\left(\frac{r_i}{r_o}\right)^2} \tag{22}$$

CAPACITOR EFFECT:

$$\left(\frac{F}{A}\right) = \frac{\epsilon_o V^2}{2r^2 \ln\left(\frac{r_i}{r_o}\right)^2} \tag{23}$$

The quantities r_i and r_o are the inner and outer cylinder radii. For boiling from the inner and outer cylinders, the location of the bubbles formed on the heater surface, with respect to r=0, requires that r_p be defined, as shown below, for use in Equations (22) and (23).

$r_p = r-r_i$ inner cylinder boiling

$r_p = r_o-r$ outer cylinder boiling

Calculations for the stresses given by Equations (22) and (23) for three different bubble radii, r_p, and a comparison to the experimental amplification factor results are shown in Table 3.

During the course of their investigations with isopropanol and water, Markels and Durfee [14] also studied the effects of voltage polarity, AC vs. DC, and AC frequency on boiling heat transfer. The results of these investigations

TABLE 3

A COMPARISON OF THE CALCULATED ELECTRICAL EFFECTS TO THE EXPERIMENTALLY DETERMINED AF'S FOR BOILING WATER [16]

Cylinder Being Heated	Calculated Total Force Ratio* and % Total Force due to Dielectrophoresis						Experimental Amplification Factor Ratio*
	r_p = 0.010 in.		r_p = 0.03 in.		r_p = 0.05 in.		
	$\frac{F}{A}$ Total	% $(\frac{F}{A})_{Di.}$	$\frac{F}{A}$ Total	% $(\frac{F}{A})_{Di.}$	$\frac{F}{A}$ Total	% $(\frac{F}{A})_{Di.}$	
Inside	1.01	2.8	1.47	38.3	3.46	71.4	2.32
Outside	1.00	-0.2**	1.00	- 6.3**	1.00	-41.5**	1.00
Inside and Outside	2.01	2.6	2.47	32.0	4.46	29.9	3.76

* The calculated total force and experimental amplification factors are reported relative to the values for outside cylinder heating.

** Negative values indicate that the dielectrophoretic force was acting in a direction opposite to that required for heat transfer enhancement.

are summarized as follows:

(1) From a series of AC voltage frequency tests with isopropanol, which covered AC frequencies from 50 cps to 5000 cps, no effect of AC voltage frequency on the heat transfer was found. These tests included the determination of characteristic, or resonance, frequencies for isopropanol and tests at these characteristic frequencies.

(2) Direct current proved to be substantially more effective in enhancing the heat transfer with isopropanol than AC. With water, AC was considerably more effective.

(3) No difference in the heat transfer was found to be attributable to voltage polarity.

Condensation Studies With An Applied Electric Field

In the area of condensation Velkoff and Miller [25] and Holmes [11] have made significant contributions. The work of Velkoff and Miller was conducted with Freon-113 using a vertical flat plate condensing surface. In the investigation several electrode types, including single wire, an oval wire, a flat plate and several screen grids, were used adjacent to the condensing surface. Electric field effects with a uniform field were studied with the flat plate and screen grids, while the single wire and oval-shaped wire were used to

generate a non-uniform field. The electrode found most effective was a fine grid. With it, it was possible to increase the heat transfer up to 3.0 times that obtained without an electric field with little power dissipation. External effects were observed with all electrodes, but due to ionization with some of them, the power consumption was of such a magnitude that when it was deducted from the increased energy transfer the net increase was too small to be considered of any practical importance. Based on the results obtained and physical observations, Velkoff and Miller hypothesized a mechanism based on corona effects and an electric field generated vapor-liquid interface instability to explain the results.

The condensation heat transfer investigation of Holmes [11] was also made with Freon-113. The heat transfer surface was a vertical flat plate with the other electrode also being a flat plate. Data was taken at several different system pressures and for several plate angles relative to each other. The results obtained were similar to those taken by Velkoff and Miller with the grid electrode. The results were interpreted from the standpoint of including an electrical body force term in Nusselt's analysis for condensation heat transfer on a vertical plate in the presence of gravity.

CHAPTER III

BASIS FOR AND PURPOSE OF PRESENT EXPERIMENTAL ELECTRIC FIELD BOILING HEAT TRANSFER STUDIES

A particularly disturbing fact concerning the previous experimental results and the interpretation it had been given is the large difference in the magnitude of the voltage effect on the critical heat flux and film boiling as compared to nucleate boiling. Such a difference would not be expected from the interpretation given by Choi [6] or Markels and Durfee [14]. Recall that Choi's interpretation was based on an acceleration which was phase independent while Markels and Durfee considered the bubbles themselves to be elements of a vapor layer. This difference, it was felt, strongly suggested that electrical interactions with a vapor layer or film are quite different from the type of interactions with discrete bubbles. Since all the previous work had been done with an external non-uniform electric field* and the results interpreted solely on this basis, it

*An external non-uniform electric field refers to a field which is non-uniform due to the geometry of the electrodes, and as calculated assuming Laplace's equation for potential ($\nabla^2 V = 0$) applies.

seemed quite possible that electrofluid interactions are occurring in the two-phase boiling medium which an analysis based solely on electrode configuration was ignoring. If such two-phase electrofluid interactions were occurring, a basis for possible explanation of the anomaly between nucleate and film boiling could be at hand. As such, the purposes of the experimental investigations carried out in this work were as follows:

(1) To find out if electrofluid interactions not caused by the external electric field non-uniformity were occurring.

(2) To try to characterize the nature of the occurring non-external field-caused phenomena.

To facilitate the first of these objectives, the experimental work was conducted with a parallel plate electrode configuration. Since the electric field generated between such electrodes is uniform, any effects due to external electric field non-uniformity were foregone. To fully investigate the observed effects with the uniform electric field boiling system, provisions were made to study the effects of the electric field intensity magnitude (by making provisions for a variable electrode spacing), direction (by making provisions for operation with both positive and negative polarity), and type (AC or DC). Further, investigations with the above system variables were made with water and freon, fluids which

differ widely in physical and electrical properties and which had been investigated as to electric field effects on boiling in other systems.

The ultimate objective to be achieved from these experimental studies was to use the results to develop and support a more general explanation for electrofluid interactions and, thus, electric field effects on boiling heat transfer.

CHAPTER IV

EQUIPMENT DESCRIPTION

Introduction

In designing the equipment to carry out this investigation, the following criteria were fixed:

(1) The investigation was to involve atmospheric pool boiling from a horizontal flat plate heater facing upwards;

(2) The fluid container was to be transparent so that visual observations could be made of the boiling phenomena;

(3) The heater was to be designed with a heat flux capacity of 1×10^6 Btu/(hr.)(sq.ft.);

(4) The heat was to be electrically generated with the origin of electrical dissipation being electrically isolated from the heat transfer surface;

(5) Water and freon were to be the test liquids in the investigation.

Specifying a heat flux capability of 1×10^6 Btu/(hr.)(sq.ft.) was dictated from a consideration of the heat fluxes attained with applied electric fields by some previous investigators using water. Electrical isolation of the heat transfer

surface from the heater was necessary to assure that the electrical effects on the boiling phenomena were due solely to the applied electric field.

With the above criteria as a basis, the system as described in the following sections was constructed and operated.

Over-all Equipment Description

An over-all view of the equipment is shown in Figure 4. Shown in this picture are the 0-6 kilovolt AC-DC source, the mounting table, the reflux condenser, various instrumentation, and the glass-walled boiling tank assembly containing the heater. As shown the boiling tank projected from a compartment filled with perlite insulation. The compartment and tank-heater assembly were bolted to the aluminum frame table which was mounted on four 8 inch concrete blocks.

Beneath the table an ice bath containing a thermocouple reference junction was stored. The heater power leads, which projected through the aluminum table top, were connected to the power cables from a 20 kw Udylite rectifier. A variable transformer for controlling the power input to four tank auxilliary heaters was also located beneath the table.

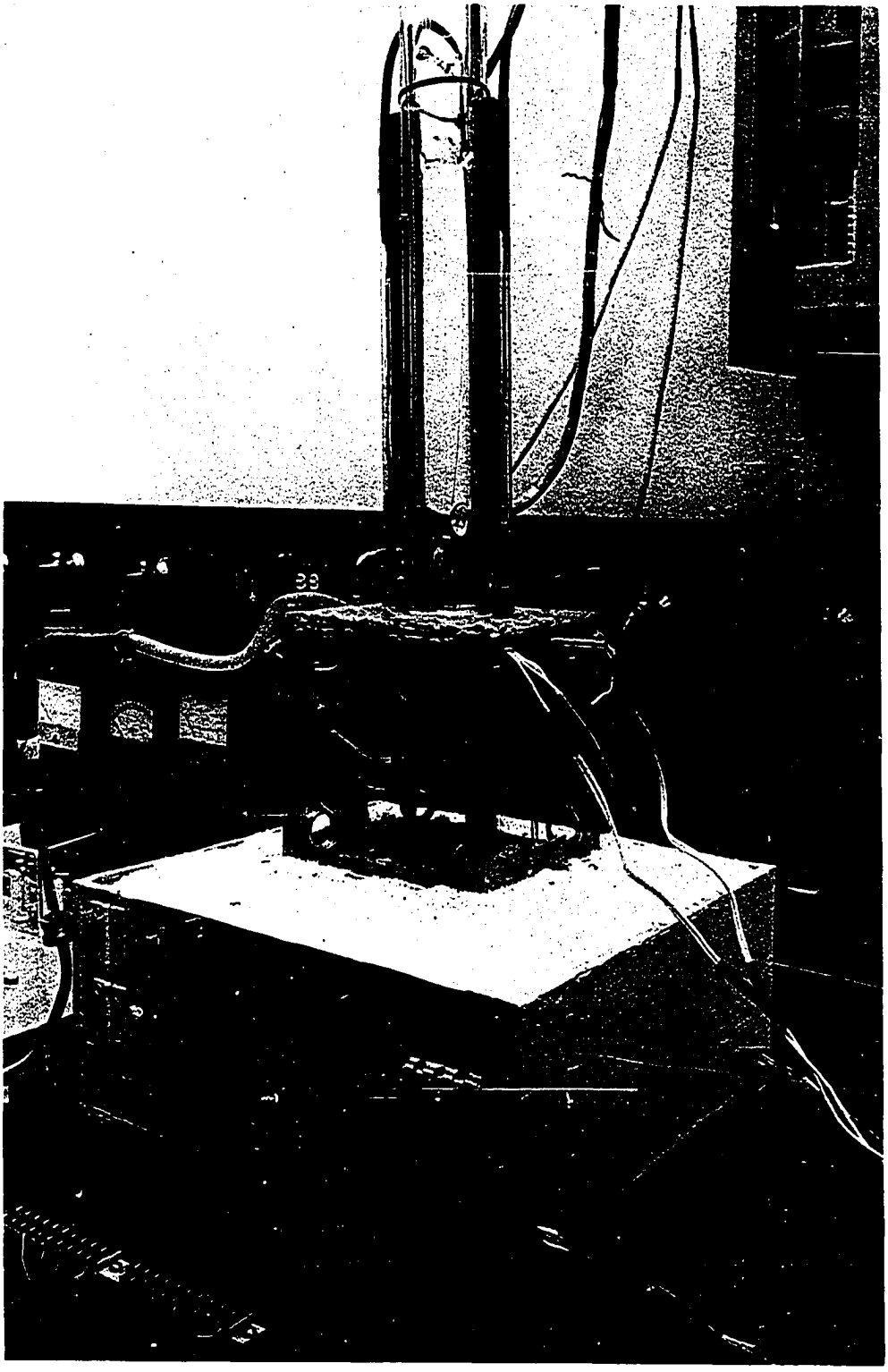

Figure 4. Overall View of Apparatus Used in the Present Investigation

Figure 5 shows a cross-sectional view of the boiling assembly. The tank base and contained heater, the glass tank walls, the tank lid with suspended high voltage electrodes and attached condenser are shown in this sketch. In the following sections, some of the components of this assembly are discussed in greater detail.

The Boiling Tank

The sidewalls of the boiling vessel were 1/4 inch thick Pyrex glass, sealed at the corners with Dow Corning 733 room-temperature vulcanizing (RTV) silastic. As shown in Figure 5, the glass sides were mounted on a 1/8 inch thick aluminum frame which had two grooves machined into it. Into these grooves, 1/16 inch thick upright strips of aluminum were sealed with Emerson and Cumings 2762 epoxy resin. These strips formed a mold into which the glass sides were sealed with RTV silastic.

Figure 6 shows what constituted the bottom of the tank. This base consisted of four pieces of unfired Grade A lava and the heat transfer surface machined to the dimensions shown. The center section of the tank base, consisting of the two vertical lava blocks with the attached heat transfer surface between them, was separated on each side from the horizontal lava side blocks by a 3/16 inch thick Durometer 40 silicone rubber gasket. The assembly was fastened together by means of

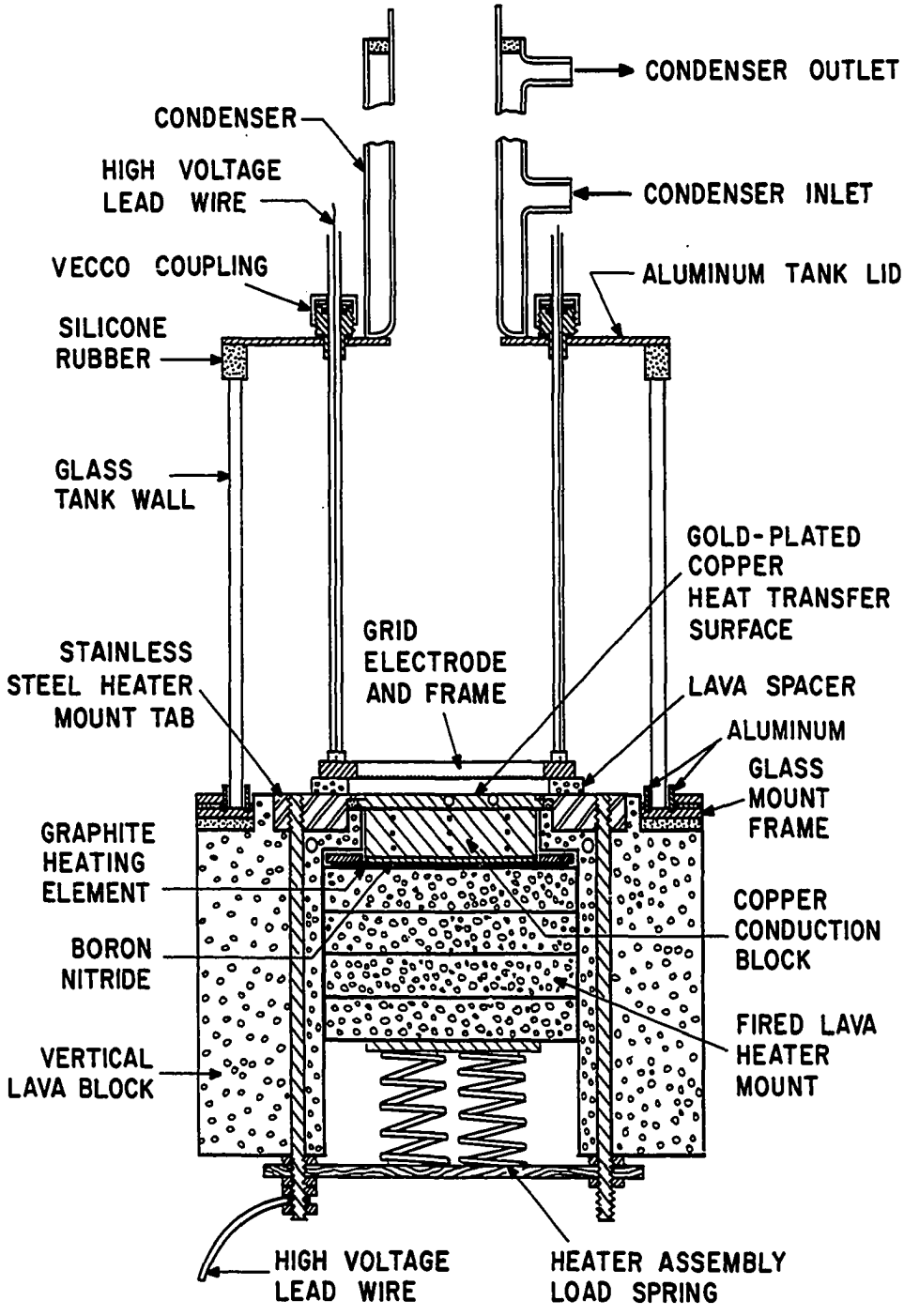

Figure 5. Cross-Sectional View of the Boiling Assembly

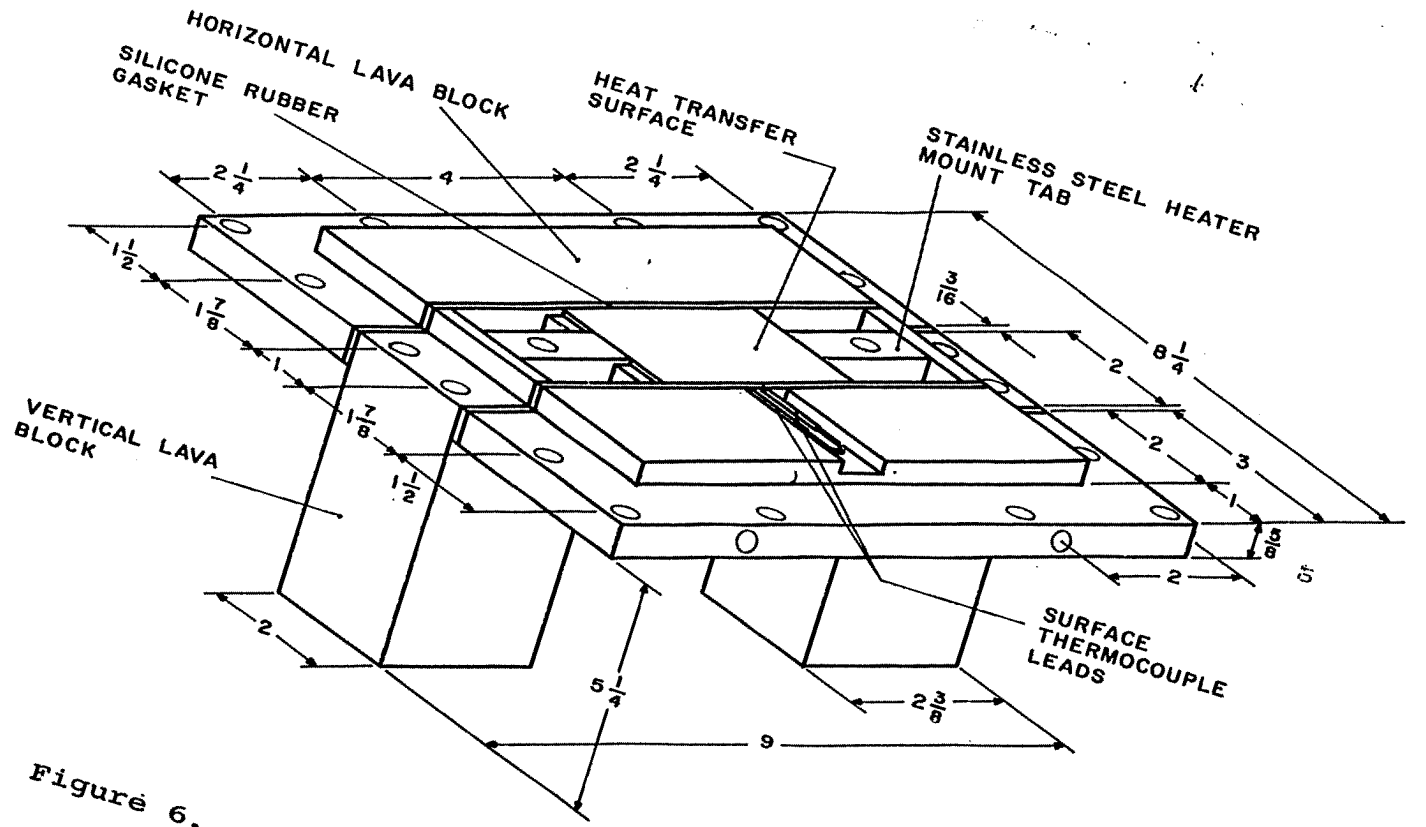

Figure 6. Boiling Assembly Lava Superstructure with Contained Heat Transfer Surface

the two 1/4-inch side bolts extending through the lava assembly and forming a seal between the center section and the side lava pieces. Prior to operation, that portion of the lava tank base contacting the boiling medium was coated with RTV silastic. This provided a more inert tank bottom, allowing a higher electrical resistance to be maintained in the fluid. The region immediately next to the heat transfer surface was sealed with Emerson and Cuming 2762 (or Armstrong A-1) epoxy resin. The epoxy was used in this region because preliminary system testing showed that very small smears of RTV silastic on the heat transfer surface had a very large effect on the heat transfer characteristics of the surface.

In Figure 6, holes are shown for sixteen 3/16-inch bolts which attached the glass tank to the lava base. As shown in Figure 5, a 3/16-inch thick Durometer 40 silicone rubber gasket was placed between the aluminum frame holding the glass tank and the lava. On the top side of the frame, a 1/8-inch gasket of silicone sponge rubber was placed, followed by another 1/8-inch thick aluminum frame. The purpose of this top frame was to insure an even pressure on the aluminum frame holding the glass tank.

Tank Lid Assembly and Tank Auxiliary Components

The glass-tank lid was a 1/4-inch thick aluminum plate with a two-inch center hole over which the glass condenser was sealed with RTV silastic, as shown in Figure 5. A 1/2-inch gasket of Durometer 40 silicone sheet rubber was sealed with RTV silastic between the tank lid and glass tank walls. A fixture for one of the high voltage electrodes was suspended from this lid through two 1/4-inch I.D. Vecco vacuum couplings. Glass tubing (10 mm), encasing the electrode lead wires, entered the lid through the Vecco couplings which acted as the mount for the electrode grid. Thus, the electrode could be raised or lowered at will. A more detailed description of the high voltage system is given in the following section. The condenser consisted of two 4-foot long glass concentric cylinders, of 2-3/4-inch and 2-1/16-inch diameters respectively, fabricated to permit cooling water to run through the annular gap. A one foot coil of 1/4-inch copper tubing was inserted in the vapor space at the top of the condenser, providing additional condenser capacity to insure complete vapor reflux back into the boiling tank.

Inside the boiling tank, four 500 watt immersion heaters were installed to provide auxiliary heating to maintain a saturated liquid condition. The leads of these immersion heaters

were sealed inside Pyrex glass tubing which entered the tank through the 1/2 inch silicone gasket between the tank lid and tank walls. The auxiliary heaters were affixed inside the tank by sealing the Pyrex tubing to the tank walls with RTV silastic. The four heaters were connected in parallel to give a maximum of 3300 Btu/hr of auxiliary heating; a variable transformer regulated the power to the heater circuit.

An aspirator line connected to glass tubing, entered the tank and could be used to withdraw the tank charge. Upon readjustment it was also used as a liquid leveling device during the water runs. During these runs, fresh de-ionized water was continuously fed to the tank at a slow rate through the top of the condenser, so that the water in the boiling tank could be maintained at a high resistance level.

Heater Assembly and Its Mountings

A sketch of the heater is shown in Figure 7. The heater element was a 4 inch by 2 inch by 1/16 inch thick slab of Pure Carbon Co., grade 56HT graphite. Since it was desired to make the bottom side of the heater nearly adiabatic, the graphite slab was mounted on a stack of four 4-1/4 inch by 2 inch by 5/8 inch thick fired Grade A lava slabs, as shown in Figure 7. The fired lava served as a very stable heat resistance refractory. Electrical connection to the graphite was

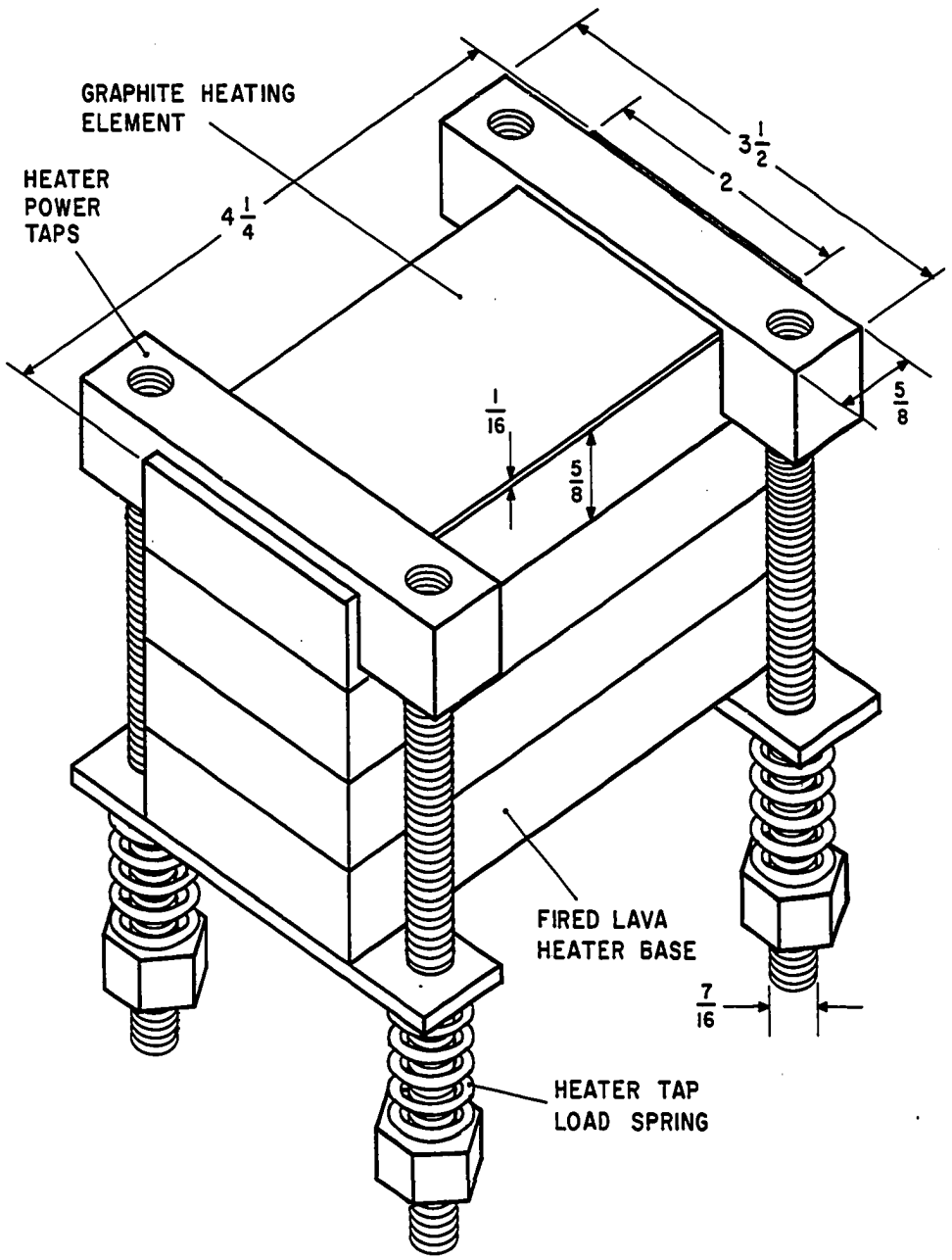

Figure 7. Assembled Heater

made through the copper taps shown in Figure 7. These taps were machined from slab copper to fit snugly on the graphite and around the lava heater mount. A snug fit prevented bowing of the taps when tightening onto the graphite. The leads to each copper tap consisted of two 7/16-inch diameter copper rods, threaded and screwed into the tap, as illustrated in Figure 7. The taps were tightened to the graphite by means of a spring assembly. As shown in the sketch, the copper rods were fixed with a spring and nut below the lava heater mount. With the tap set in place the nut on each rod was tightened to compress the spring against a steel plate on the bottom of the lava heater mount. To insure a good electrical contact between the copper taps and the graphite, that portion of the tap which made contact with the graphite was coated with Handy and Harmon Silpaint No. 2267-01.

The incorporation of the assembled heater in the tank base assembly is shown in the cross-sectional view in Figure 5. The heater assembly consisted of the heater, a 1/16-inch thick slab of boron nitride, a 3/4-inch thick by 2-inch by 3-inch rectangular copper conduction block and the 3/16-inch thick by 2-inch by 3-1/4-inch rectangular heat transfer surface plate. The boron nitride slab, of 3-inch by 2-inch by 1/16-inch dimensions, between the graphite heater and conduction block, served to electrically insulate the graphite heating element from the

copper conduction block. Fifteen thermocouples located in the conduction block measured the temperature profile for determining the heat flux through the heat transfer surface. Figure 9 gives a three-dimensional view of the conduction block and the thermocouple locations. The thermocouples were made from 30-gauge, fiberglass-insulated, iron and constantan thermocouple wires, and were fitted into 1/32-inch diameter holes drilled to the depths shown in Figure 9.

The 3/16-inch thick copper heat transfer surface block had steps 1/16-inch thick and extending 1/8-inch out from the plate edge (See Figure 6). The steps did not serve as part of the heat transfer area but only for mounting the heater assembly in the tank assembly. As such, the dimensions of the heat transfer surface were 3 inches by 2 inches. To provide a good thermal contact between this surface plate and the conduction block, the joining surfaces were machined flat and soldered together with soft solder. Two Mo-Re Model 107 copper-constantan surface thermocouples, which were used to measure the heat transfer plate surface temperature, were silver-soldered in place. One surface thermocouple was located in the center of the heat transfer surface; the other was located 3/4-inch removed from this center along the length axis of the plate (See Figures 5 and 6). As shown in Figure 6, the leads from these thermocouples projected from the 3 inch side of the heat transfer

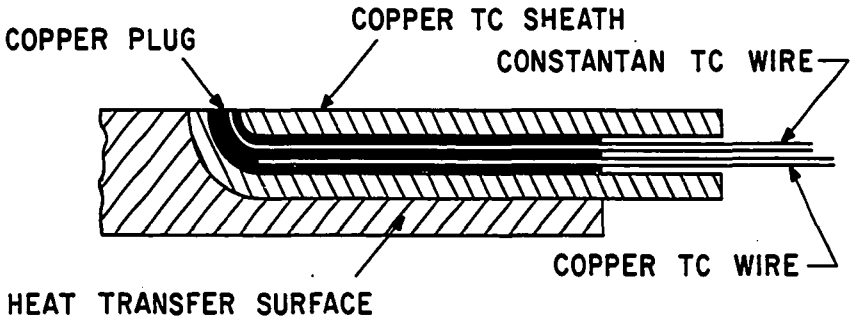

Figure 8. Diagram of Surface Thermocouple Installation

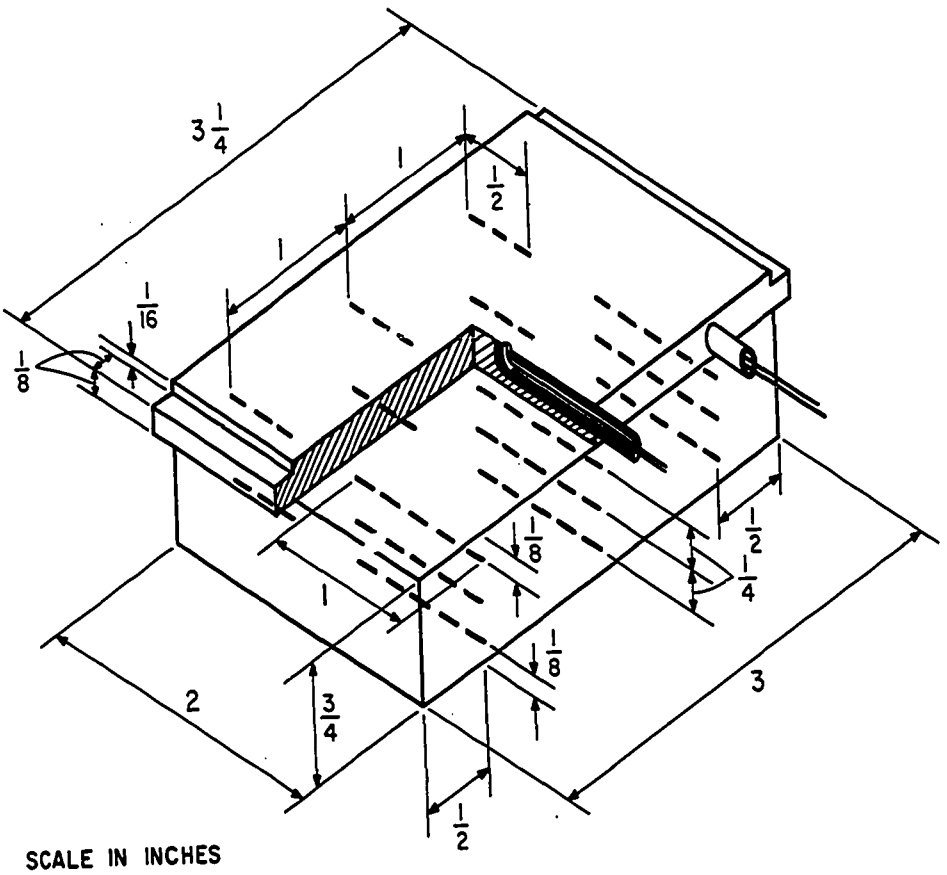

Figure 9. Conduction Block and Heat Transfer Surface Assemblage with Installed Thermocouples

surface plate. Figure 8 shows a cross-sectional view of an installed surface thermocouple. The thermocouple assembly consisted of a 3/16-inch O.D. copper tube swaged over an alumina two-hole sheath, containing the 30-gauge copper and constantan wires. A 1/4-inch long copper one-hole plug, threaded with the constantan wire, was press-fitted into the end of the copper tube as shown in Figure 8. A 0.005 inch thick layer of alumina insulated the constantan wire from the copper. The thermal junction was formed on the surface by copper slivers which bridged the thin insulation on the outside of the constantan wire. After silver-soldering into the heater surface, the surface was machined and finished.

In order to maintain a reproducible boiling surface, the top side of the heat transfer plate was gold plated. This was accomplished by plating a 0.001-inch thick sheet of silver over the copper, and then a 1 to 2 $\times 10^{-6}$ inch thick layer of gold on the silver.

The mounting for the above described heater assembly is shown in Figure 5. The heat transfer surface plate with attached conduction block rested on 1/4-inch wide steps machined in the two vertical lava blocks. Two 3/4-inch wide by 1/2-inch thick stainless steel tabs were machined to fit in the steps on the heat transfer surface plate and served as a means of holding the heater assembly in place. Stainless steel bolts (1/4-inch

diameter), which extended through the vertical lava pieces were tapped into each tab and secured with a nut on the bottom of the vertical lava pieces. The heater was spring-loaded into position as shown in Figure 5. The two springs were loaded by bolting down a piece of plywood on the two bolts extending vertically through the lava blocks.

High Voltage Source and Connection to the Tank Assembly

The high voltage source (HVS) used to generate the electric field across the boiling medium was constructed at the University of Oklahoma. It was designed to deliver up to 6000 volts AC or DC with a maximum current output of 250 milliamperes. The input to this unit was from a 230 volt single-phase AC line, connected to a variable transformer so that the output voltage could be continuously varied from 0 to 6000 volts. From the variable transformer, the voltage was increased through two step-up transformers; in AC operation, the output was taken from these transformers. In DC operation, the AC transformer output was rectified in two mercury vapor tubes and the rectified AC filtered by a bank of capacitors. The DC output contained less than five percent ripple. Switching from AC to DC operation or vice versa involved de-energizing the source and manually switching two 12-inch long 250 milli-

ampere high voltage fuses inside the box which housed the components of the HVS. As a safety precaution, the metal box housing the HVS was grounded. The output of the HVS was taken from two plexiglass enclosed terminals. A circuit diagram showing the external electrical circuitry is shown in Figure 10. The output leads from the HVS was connected to a knife switch, thereby permitting the voltage polarity to be conveniently and quickly reversed. A stabilization resistance of 60,000 ohms was used to maintain a continuous load on the HVS when in operation. Stabilization of the voltage was not possible without some load on the HVS. A calibrated AC voltmeter was connected across 10,000 ohms of the stabilization resistance, while the DC voltmeter was connected in series with 60 megohms directly across the HVS terminals. As shown, the AC and DC ammeters in this portion of the circuit were connected through a circular selector switch enabling AC, DC, or reversed polarity current measurements.

Since it was desired to carry out the investigation with a uniform field, the high voltage electrodes were initially designed to be solid flat plates. In all actual runs, however, the electrodes suspended from the tank lid were flat grid electrodes. The choice of a grid rather than a solid plate electrode was made on the basis of the vapor holdup which was experienced beneath a solid flat plate.

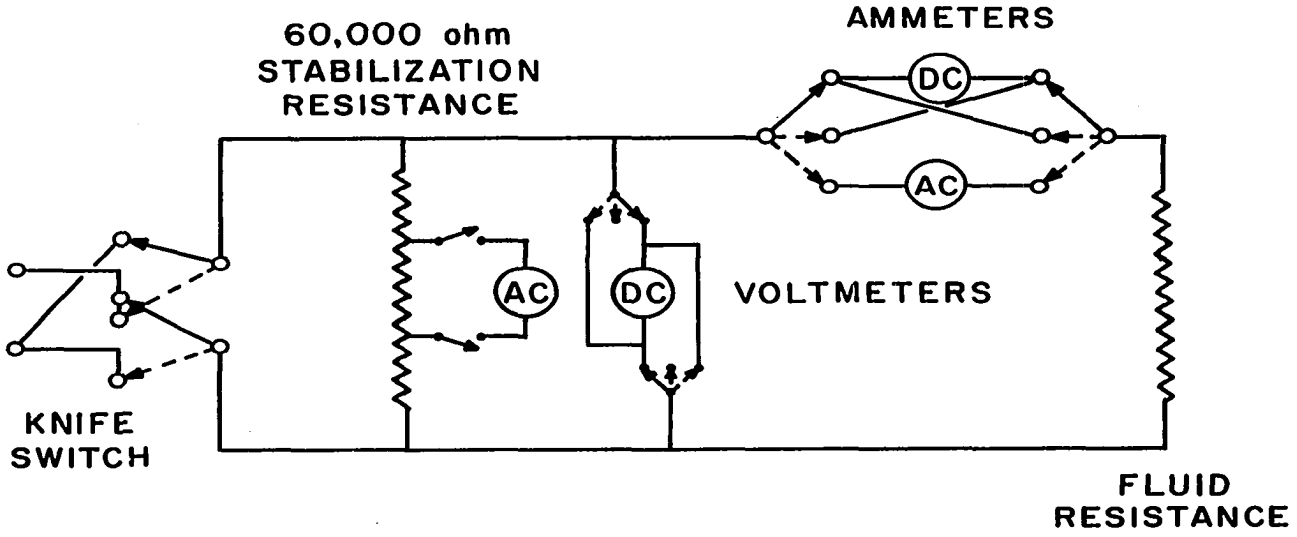

Figure 10. External High Voltage Circuity

In order to estimate the difference in electrical effects introduced by using the grid electrodes, two different sized grids were used. One of the grid electrodes was made of 20-mesh copper wire cloth; the wire cloth was sealed to an aluminum frame with RTV silastic. The other grid electrode was made from 28-gauge Chromel-P wire, woven directly onto an aluminum support frame at 1/4-inch spacing. Figure 11 shows the assembled 20-mesh grid electrode. Electrical connection to this electrode was made by means of the lead wires which entered the tank through two 10 mm glass tubes. The connection between the lead wire and the grid was made by press-fitting a 1/4-inch by 3/4-inch copper tab, which was silver-soldered to the incoming lead wire, to a flap of the grid as shown in Figure 11. With the assembly held in this position, the copper tab was sealed to the grid flap with RTV silastic. The aluminum frame holding the grid, and a portion of the grid itself, were coated with RTV silastic so that only a section of the grid the size of the heat transfer plate was exposed to the fluid medium. Electrical connection to the heat transfer surface plate was made through one of the bolts screwed into the stainless steel heater assembly tab mounts (See Figure 5).

The spacing between the grid electrode and the heat transfer surface was determined by using lava block spacers machined to within .001 inches and set on the stainless steel

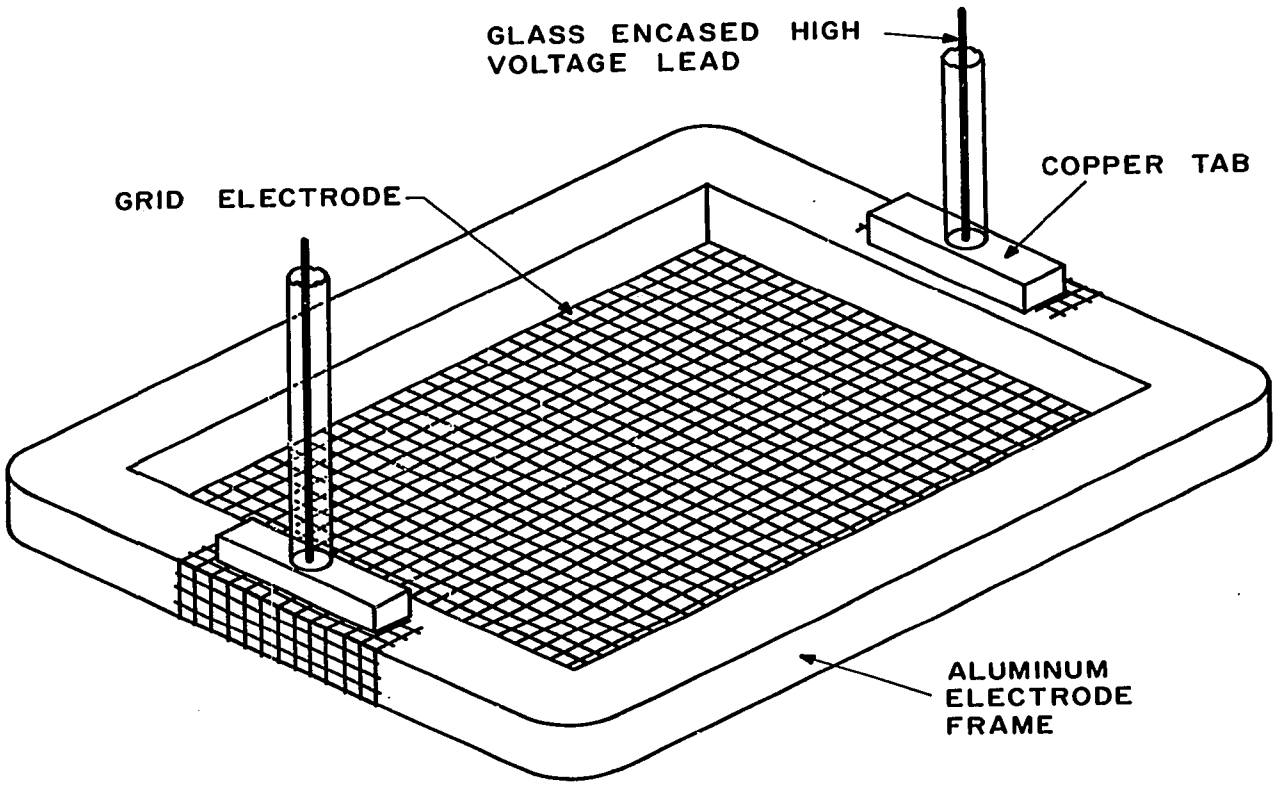

Figure 11. Construction of Grid Electrode

heater assembly tab mounts.

Instrumentation

The instrumentation consisted of four voltmeters, two ammeters, a thermometer, a potentiometer and a Sym-Ply-Trol relay for opening the heater circuit.

The voltage output from the Udylite rectifier was measured on a 10-volt full-scale Tabtron DC voltmeter. The amperage readings in this system were obtained from voltage readings on a General Electric Type DP-9 50 millivolt voltmeter connected across an 800 amp 500 millivolt shunt. These voltage and amperage readings, while not used to calculate the heat flux, were used as a check on the heat flux calculated from the temperature profiles in the conduction block, and also to estimate the heat losses.

The voltage and amperage of the HVS were measured as shown in Figure 10. The AC and DC current readings were made with 0-250 milliamp Triplett Model 330-G meters. The 0-6000 volt DC voltmeter, a Weston Model 741 meter, was connected in series with four 15 megohm 1% Penn resistors. The AC voltage was measured on a 0-300 volt Type AP-11 General Electric AC voltmeter which was connected across 10,000 of the 60,000 ohm HVS stabilization resistance. The thermocouple measurements were made with a Leeds and Northrup Model 8686 potentiometer.

The Sim-Ply-Trol relay was used to automatically shut down the heater power in the event the heater assembly temperature went above a set value. The relay was not used as a data producing piece of instrumentation, but merely as an equipment protection device. It was particularly useful when the burnout point was reached and a very rapid temperature rise was experienced.

CHAPTER V

EXPERIMENTAL PROCEDURE

Run Preparations

The operational methods for the water and freon runs were basically the same with only minor differences. The day before runs were to be made the lid was sealed to the top of the tank with RTV silastic, and the charge prepared. The water used was distilled and then deionized in an Illinois Water Company research-grade ion exchange resin cartridge. The resistivity of this water was about 1×10^7 ohm-cm at room temperature. Water was charged to the tank through the top of the condenser from a five-gallon polyethylene bottle, positioned above the condenser. When the tank bottom was covered, the rectifier was started and set at a low heat flux; auxiliary heaters were started as soon as they were completely submerged. Upon filling the tank to about 2500 ml, the incoming water was shut off and this initial charge boiled one to three hours and then dumped. The removal of the charge was accomplished by means of the aspirator and a glass tube which

projected to the bottom of the tank. Since the surface was cleaned following each run, this initial boiling was used as a surface conditioning period. Another function of this initial boiling was to extract foreign material from the tank, and any acetic acid carrier from fresh Silastic around the tank lid. This charging, boiling, and dumping operation was continued until the resistance of the water in the tank was brought to an acceptable level. The resistance of the water was monitored by measuring the resistance between the grid electrode and the heat transfer surface. From experience, a value of 20-30,000 ohms ($3\text{-}4 \times 10^5$ ohm-cm) between these two conductors, at a low heat flux, was established as a criterion to be satisfied before data-taking runs were begun. When this resistance condition was achieved, a fresh charge was put in the tank and a continuous trickle of water (30-50 cc/min) was allowed to flow into the tank. Since data-taking sessions ran for 12 to 15 hours or more, this slow trickle of water was found necessary to maintain the water at the desired resistance level. The liquid level in the tank was controlled with the aspirator connected to a glass tube which projected into the tank to the desired liquid level.

Basically, the same preparatory procedure was used when freon was the boiling medium, with the exception that the flow through the system was not found necessary as a very high

resistance level could be achieved and maintained throughout the duration of a run period. Charging and dumping of the freon into the tank was done using a vacuum flask. To charge the tank, freon was blown with compressed air from the vacuum flask into the tank, while dumping was accomplished by connecting the flask to the aspirator.

Equipment Operating Procedure

The normal procedure of operation in nucleate boiling consisted of setting a heat flux and varying the voltage applied across the boiling medium. Operation in this manner was found to be superior to operation in which the voltage was fixed and the heat flux varied. The superiority of the former method of operation resulted from the fact that from one data-taking session to the next, the variation in the nonfield ΔTs in nucleate boiling were, in many cases, of the same magnitude as the voltage effects on the ΔT. This irreproducibility of ΔTs at a fixed heat flux was found to occur in nucleate boiling despite extensive care to insure a surface which would be reproducible from one period of operation to the next. With the heat flux at a fixed value, the surface thermocouple and top and bottom thermocouples along the center line of the conduction block were monitored until a steady state condition was obtained. Due to the bulkiness of the heater, the line out time to a

steady state condition in nucleate boiling normally required 50 to 60 minutes. During this time, all the thermocouples and the heater were given a final check to insure that they were functioning properly. A calibration curve of heater voltage drop versus heater current was used to check how the heater was functioning. A deteriorating heater or a bad electrical contact in the heater could quickly be detected by deviations from this curve. The HVS filament circuitry was also energized at this time. Normally, 30 minutes was required to heat up the mercury vapor tubes.

When a steady state condition was achieved a complete set of readings was recorded. The readings taken were the conduction block temperatures, the surface temperature, the bulk fluid temperature, the heater current and voltage, and the fluid resistance as measured between the surface plate and the grid electrode. After these readings were recorded the desired voltage, polarity, and electrode spacing were set. With the voltage applied, the surface plate temperature was recorded as a function of time until steady state was again reached. When steady state with the applied voltage was reached, the desired readings were recorded. This was followed by increasing the applied voltage to the next level and allowing the system to again line out. When all the desired voltage levels had been run at the fixed heat flux, the applied volt-

age was shut off and the resistance between the two electrodes again measured. This resistance measurement was made with a Simpson Model 260 volt-ohm meter and was used to compare with the resistance calculated from the HVS voltage current readings. The heat flux was then increased and allowed to line out and the same procedure of voltage application followed. Initially, a complete set of readings were taken at each applied voltage level. This was not done in all of the runs, as it was found to be unnecessary if, during the time of voltage application, the heater power and HVS voltage and current were kept at constant levels.

For safety purposes one side of the high voltage was initially grounded. When connected in this manner, however, shorting through the auxiliary heaters frequently occurred. With this mode of HVS hookup, thermocouple readings were also difficult to obtain since induced EMF was excessive. As such, the HVS output was left ungrounded, or, floating electrically. Operation in this manner resulted in no measurable current leakage and no measurable induced EMF as measured on the Leeds and Northrup Model 8686 potentiometer.

The saturated fluid temperature for the water runs was measured by means of a thermometer which read from 200 to 220 degrees F. full scale, in increments of 0.2 degrees. The

thermometer was affixed with RTV silastic to the inside of the condenser and projected about 2 inches below the liquid level directly above the heat transfer plate.

The film boiling runs were essentially carried out in the same fashion as those in nucleate boiling. The heat flux in film boiling was set and stabilized. The voltages of increasing magnitude were then applied at the fixed heat flux. As an equipment protection device, a Sim-Ply-Trol electrical relay system was employed to shut the heater power off when film boiling occurred. This relay was connected to one of the thermocouples in the conduction block. Since the whole heater assembly was very bulky, there was never a problem of film collapse when the rectifier power was shut off by the relay. The line out time to reach a stable condition in film boiling was quite lengthy and often took two or three hours. The temperature being quite sensitive to small changes in heat flux, the task of achieving a stabilized condition in film boiling, in many instances, was quite difficult. Small changes or fluctuations in the rectifier output was a constant problem in film boiling, and in some instances, created such a problem that attempts to obtain film boiling data had to be aborted. Since these fluctuations in line power occurred mostly during the day, the problem to a large degree was overcome by obtaining the film boiling information at night.

System Cleanup

Although during the water runs the resistivity could, to a large degree, be controlled by the constant input of a small amount of fresh water, the heat transfer surface in a 12 to 24 hour run normally did pick up some foreign material. As a result, it was standard procedure after each data-taking period to remove the tank lid and clean the gold-plated heat transfer surface. The method used to clean the surface varied depending on the degree of scaling. For run periods in which no difficulties were encountered, a xylene wash and acetone rinse was sufficient to remove any scale. Occasionally, however, the surface required the use of Brasso or similar cleansing agent to remove the scale. Use of such harsh cleansing methods was very hard on the gold-plated surface, and was reluctantly used as a last resort only once or twice.

Operational Limits of System

As originally designed, the system was to be capable of operating up to a million Btu/(hr)(sq.ft). However, due to contact resistance problems at the boron nitride-graphite heating element and boron nitride conduction block interfaces, the temperature limitation of the heater was exceeded at about one quarter of this value. Many techniques were tried, in an attempt to decrease this contact resistance, so operation at

higher fluxes could be achieved, but with very little success. Because of the presence of the silicone rubber gasket next to the heat transfer surface, the maximum continuous operating surface temperature was limited to 550°F. The maximum operating heat flux and temperature limitations of the equipment posed no problem in the freon runs. In the water runs, operation for sustained periods of time at heat fluxes much above the burnout heat flux, for the non-electric field condition, was impossible. Since the second critical flux, or minimum in the boiling curve for water, occurs at a ΔT of about 285°F (495°F surface temperature), it was necessary to operate very near the second critical heat flux in film boiling work with water. These limitations, while considerably more severe in the work with water than with freon, did not present an insurmountable obstacle to the objectives of this work.

CHAPTER VI

RESULTS AND DISCUSSION

Boiling Results Which Yielded Premature Burnout

Before carrying out experiments using an applied electric field, the system was operated to obtain the boiling curve for water. Initial attempts to obtain this data resulted in burnout heat fluxes for water as low as 74,000 Btu/(hr)(sq.ft), which is between one-half to one-sixth the water burnout values reported by a number of investigators [4,7,9,17]. Data for the runs yielding premature burnout are plotted in Figures 12 and 13 and are shown in Table 1-B of Appendix B. Figure 12 shows the time history curves for three of the boiling runs. Figure 13 presents the results of a run in which the heat flux was successively increased to a burnout value of 102,000 Btu/(hr)(sq.ft). A more than adequate period of time was allowed in this run for the heater to come to a steady state condition at each heat flux for, as shown, all lineout times were in excess of 80 minutes. As

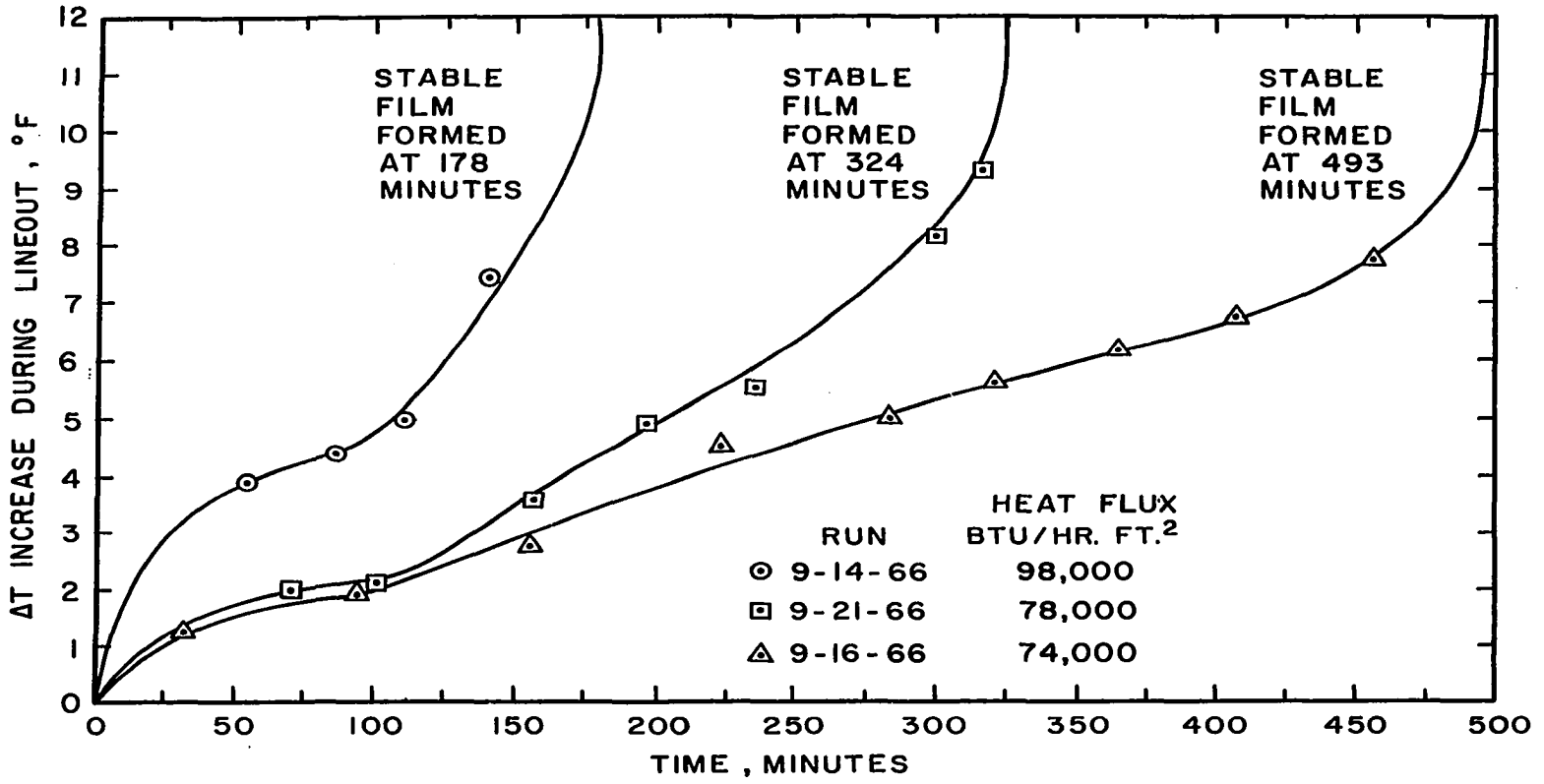

Figure 12. Time History for Premature Burnout Runs with Water

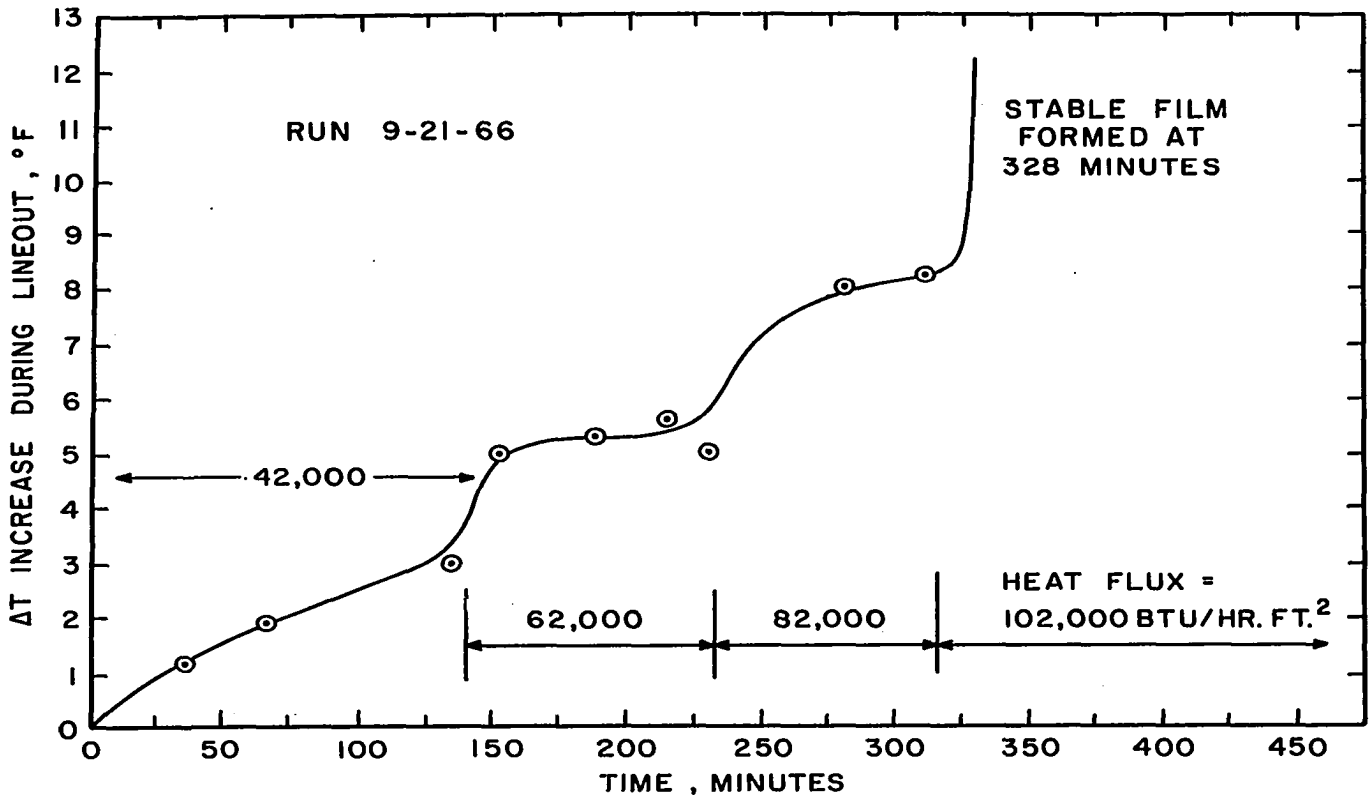

Figure 13. Variable Heat Flux History for Premature Burnout Run with Water

previously stated, a normal lineout time of 50 to 60 minutes was adequate at moderate heat flux levels in nucleate boiling.

On observing the data shown in Figure 12, it is seen that the time required for the stable film to form was dependdent on the heat flux. As the heat flux increased, the time for the film to form decreased. For example, to achieve the stable film boiling condition at a heat flux of 74,000 Btu/(hr)(sq.ft) required 493 minutes, while at 98,000 Btu/(hr)(sq.ft) the time required was 178 minutes. In both cases the length of time was well in excess of the 50-60 minutes necessary for the heater to reach a steady condition. The point to be made here is that the time required for the stabilization of boiling can be quite independent of the calculated lineout time for a particular heater system. As such, an experimental study designed to obtain representative boiling data which unequivocally equates the heater lineout time to a boiling stabilization time could result in erroneous results, or, more drastic, result in a catastrophic failure. This type of situation is depicted in Figure 13 where a burnout heat flux of 102,000 Btu/(hr)(sq.ft) was obtained instead of the 74,000 Btu/(hr)(sq.ft) or lower values as shown in Figure 13. This type of erroneous result could be particularly significant in small electrically-heated systems where the calculated lineout time is quite small.

In an attempt to eliminate premature burnout, tests were carried out using a 3-inch by 2-inch electrically-heated flat stainless steel strip. These tests yielded a burnout heat flux in the vicinity of 300,000 Btu/(hr)(sq.ft) and revealed a marked difference in the observed bubble dynamics from that previously obtained on the gold-plated surface. Suspecting that the gold surface was developing a non-wetting condition during operation, a search of the literature was made to see if a similar problem had been encountered by other investigators. This search led to articles by Gaertner [8] and Young and Hummel [33], in which investigations on the effect of surface coatings were reported. In both articles, considerably lower burnout heat fluxes were indicated when a fluorocarbon or silicone grease coated the surface. Since RTV silastic had been used in the present study in the vicinity of the gold-plated heat transfer surface, a simple test such as described by Gaertner [8] was made in which the boiling characteristics were compared between a clean container and a silastic-coated container. Even though there was no apparent distinction whatsoever between the two test containers, the one coated with silastic differed drastically in the manner the vapor bubbles formed. Visually, the results were identical to those of Gaertner's report [8]. The silastic-coated container had large hemispherical bubbles forming on

the heated surface, as opposed to the formation of small spherical bubbles in the clean container. It was further shown that the silastic-coated container could be restored to a wetting condition (formation of small spherical bubbles) through use of xylene and paint remover on the surface.

As a result of the above findings, all silastic adjacent to gold-plated heat transfer surface was removed and replaced with epoxy resin. The gold-plated surface was scrubbed with paint remover and xylene. Following such treatment, representative boiling heat transfer data were obtained although maintaining a reproducible surface throughout this work was continually a problem.

Boiling Water Heat Transfer Results Without an Electric Field

Figure 14 is a plot of all non-electric field surface wetting data taken for boiling water. A complete tabulation of the data is given in Table 2-B and Table 3-B in Appendix B. The nucleate boiling data shown in Figure 14 resemble the data of Gaertner [9] taken on a horizontal 4/0 polished copper surface. The burnout heat fluxes obtained in this work ranged between 215,000 and 235,000 Btu/(hr)(sq.ft) and were considerably lower than a burnout heat flux of 493,000 Btu/(hr)(sq.ft) as reported by Gaertner.

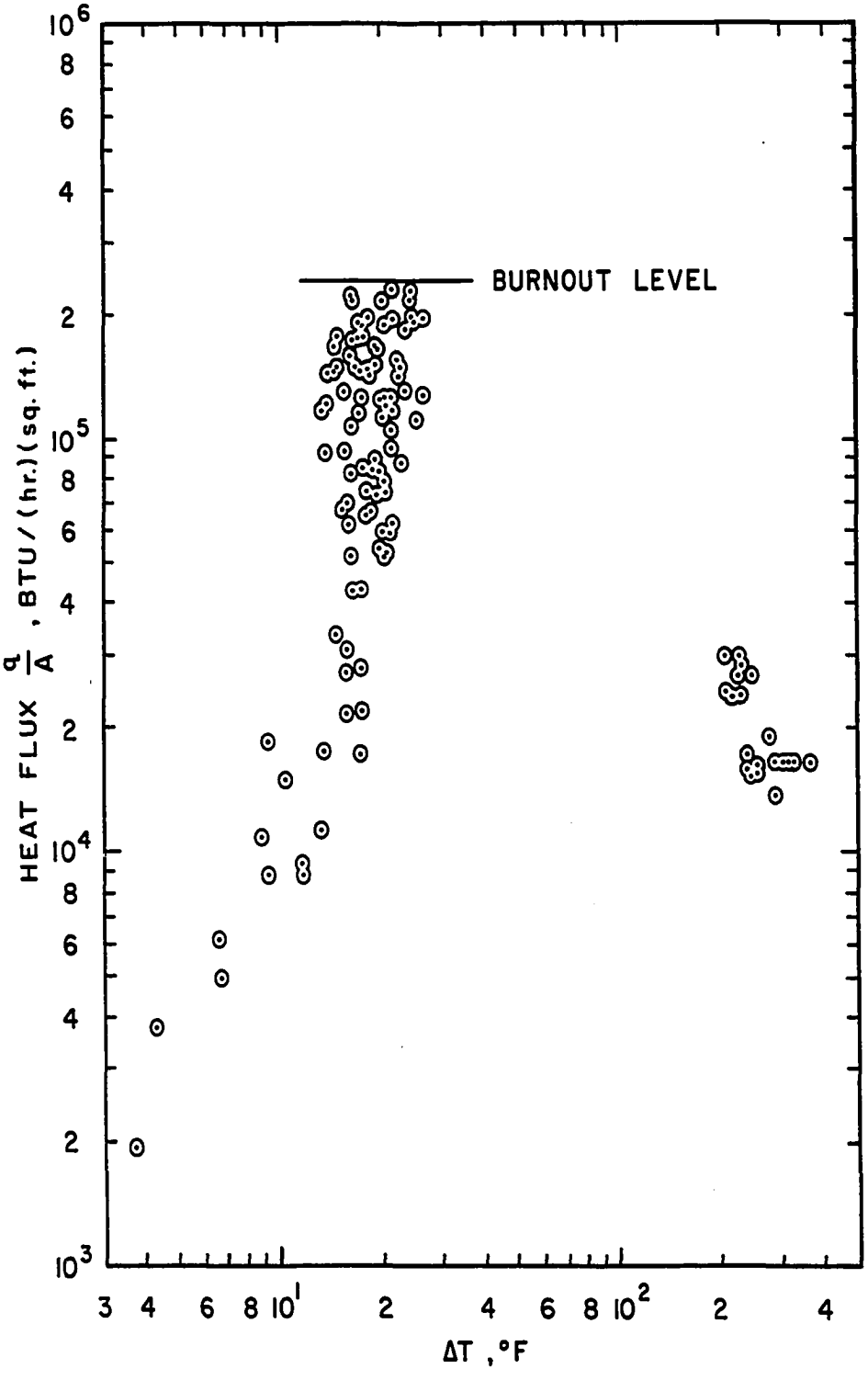

Figure 14. Pool Boiling Water Heat Transfer Data

The film boiling data in Figure 14 shows two clusters of points, one in the heat flux range of 13,800 to 19,000 Btu/(hr)(sq.ft) at ΔTs of 240° to 360°F, and the other in the heat range of 23,000 to 30,000 Btu/(hr)(sq.ft) and ΔTs of 200° to 260°F. The former cluster of points closely corresponds to the second critical heat flux value of 11,000 Btu/(hr)(sq.ft) at a ΔT of 285°, as determined experimentally by Hosler and Westwater [12]. All points in the range of 14,000 to 19,000 Btu/(hr)(sq.ft) appeared visually to be in stable film boiling, whereas those in the range of 23,000 to 30,000 Btu/(hr)(sq.ft) appeared to be in the transitional regime, although a vapor film completely covered the surface. Holding a stable vapor film on the surface was not always achievable because of a temperature limitation on the equipment. The higher surface temperature necessary to drive a transitional boiling condition into stable film boiling could not be tolerated by the equipment. Whether stable film boiling or transitional boiling occurred was very much affected by the condition of the surface. The cluster of points near the Hosler and Westwater second critical data were obtained with the surface in a consistently wetting condition. The points in the range between 23,000 to 30,000 Btu/(hr)(sq.ft) were obtained after the surface had been cleaned with Brasso metal cleaner and polish. Following this surface treatment, a surface condition

existed whereby it was no longer possible to achieve a completely stable vapor film as in the previous run. A further characteristic of this surface condition was the peculiar manner in which the vapor film collapsed on reverting back to nucleate boiling. Instead of a sharp change to nucleate boiling when the film collapsed, as observed in the previous runs, the process involved a gradual transition from a complete vapor film to vapor patches instead of reverting from a vapor film to individual bubbles.

Boiling Water Heat Transfer Results With An Applied Electric Field

It was found convenient to report all electric field results in terms of the following three categories:

(1) Nucleate boiling results with an applied DC voltage

(2) Nucleate boiling results with an applied AC voltage

(3) Film boiling results with an applied voltage.

Measurements recorded for runs in each of the above categories were the applied voltage, the heat flux, the heat transfer surface (HTS) polarity, the electrode spacing (1 inch or 1/4 inch), the type of electrode used (fine grid (FG) or coarse grid (CG)), and the amount of current drawn between the electrodes. All the results obtained are tab-

ulated in Appendix B, Tables 5-B through 15-B.

Prior to any electric field runs, a test was conducted using the fine grid positioned 1/4-inch above the heater surface to determine any effect the presence of the electrode had on the boiling characteristics. No effect on the ΔT was found for heat fluxes up to 125,000 Btu/(hr)(sq.ft). These results are shown in Table 4-B of Appendix B.

Nucleate Boiling Water Results With An Applied DC Voltage

Results obtained consisted of visual observations of the bubble dynamics and measurements of the thermal and electrical parameters of the system. Measurements made on water using DC voltage at various system conditions are shown in Table 5-B of Appendix B. The extent or degree of the voltage effect on the heat transfer is reported in terms of the percent the surface temperature was lowered at a fixed heat flux by voltage application. As such, the term "percent surface temperature lowered" represents a percent increase in the heat transfer coefficient at the specified heat flux.

It was not possible in this work to obtain a set of distinct nucleate boiling curves at the voltages applied, as obtained by some previous investigators [6,14,15]. Nonetheless, distinct DC voltage effects on nucleate boiling water

were apparent. Aside from the heat flux and applied voltage effects, the only other noticeable effect during the DC nucleate boiling water work resulted from voltage polarity. The end result of an applied DC voltage with the heat transfer surface of positive polarity, HTS(+), was in most instances the promotion of film boiling. For the case of the heat transfer surface with negative polarity, HTS(-), at no time did film boiling result, and in most instances the surface temperature at a fixed heat flux was lowered. In all of the HTS(-) runs and in a majority of the HTS(+) runs, the effect of the voltage on heat transfer was consistent with visual observations of the bubble dynamics. When the voltage was initially applied the bubbles forming on the heat transfer surface were observed to be smaller for both HTS(+) and HTS(-). Along with this observation was a measureable lowering of the surface temperature. This phenomena was particularly of note in the runs which ultimately resulted in film boiling. In eleven of the sixteen runs in which temperature histories to film boiling were obtained, an initial lowering of surface temperature was recorded. Typical examples of this phenomena are shown by the runs 5-25-67 and 5-26-67 in Figure 15. The temperature-time record for all DC voltage runs yielding film boiling are given in Table 6-B in Appendix B.

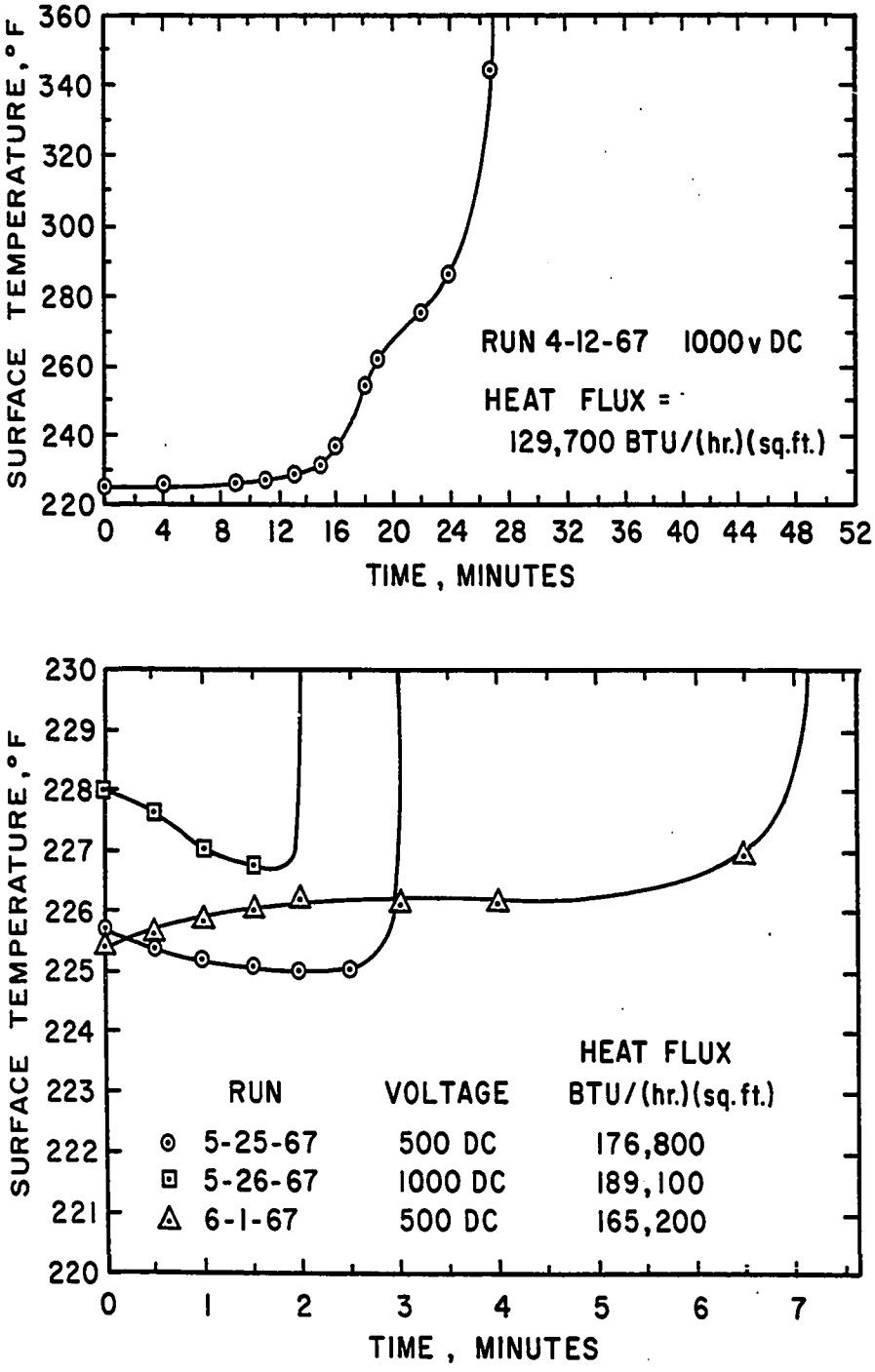

Figure 15. Temperature History for Typical DC HTS(-) Applied Voltage Nucleate Boiling Runs with Water

During the HTS(+) mode of operation the formation of a vapor film after the initial surface temperature lowering was also accompanied by a visual change in the bubble dynamics. In these runs, while the departure bubble size did not appear to be drastically affected, the discrete sites on the surface from which the bubbles generated became larger and larger. This phenomena led to the formation of vapor patches on the heater surface, followed by coalescence of the patches to form a stable vapor film. The observed sequence of this phenomena combined with the manner in which the surface temperature was obtained undoubtedly accounted for the two types of temperature histories, i.e., a continuously increasing temperature and an initial temperature decrease followed by a rapid increase to film boiling shown in Figure 15. Since the surface temperature was measured at only one point on the surface*, the result was completely dependent on what occurred at that particular location. If a vapor generation site began spreading precisely at the thermocouple location, a continuous rise in surface temperature was recorded. This is shown by the runs 4-12-67 and 6-1-67 in Figure 15. On the other hand, if the spreading of the vapor generation sites did not occur

*Although two surface thermocouples were originally installed, only the centrally located one operated during most of the data runs.

in the vicinity of the thermocouple, the cooling effect from smaller bubble formation when the voltage was first applied was more apparent on the thermocouple. This type of result is depicted by runs 5-25-67 and 5-26-67, shown in Figure 15. As such, the two types of runs shown in Figure 15 are felt to represent the two temperature extremes in progressing from the time of the initial voltage application to the ultimate film formation. From visual observations of the bubble dynamics on the entire surface, the apparent overall effect of the applied voltage in these runs was an initial temperature decrease due to the formation of smaller bubbles when the voltage was initially applied, followed by a temperature rise as vapor patch formation and coalescence progressed, until film boiling resulted.

In all the HTS(+) runs yielding film boiling, the total time from voltage application to the formation of a stable film was recorded. Although no distinct trend could be found, there appeared to be a dependence of the film formation time on the heat flux. A plot of this data is shown in Figure 16. This figure includes data taken with both grid electrodes and both electrode spacings. As shown by the line, the basic trend of a shorter time for stable film formation as the heat flux increased is consistent with visual results. With the nucleation site population becoming more dense with

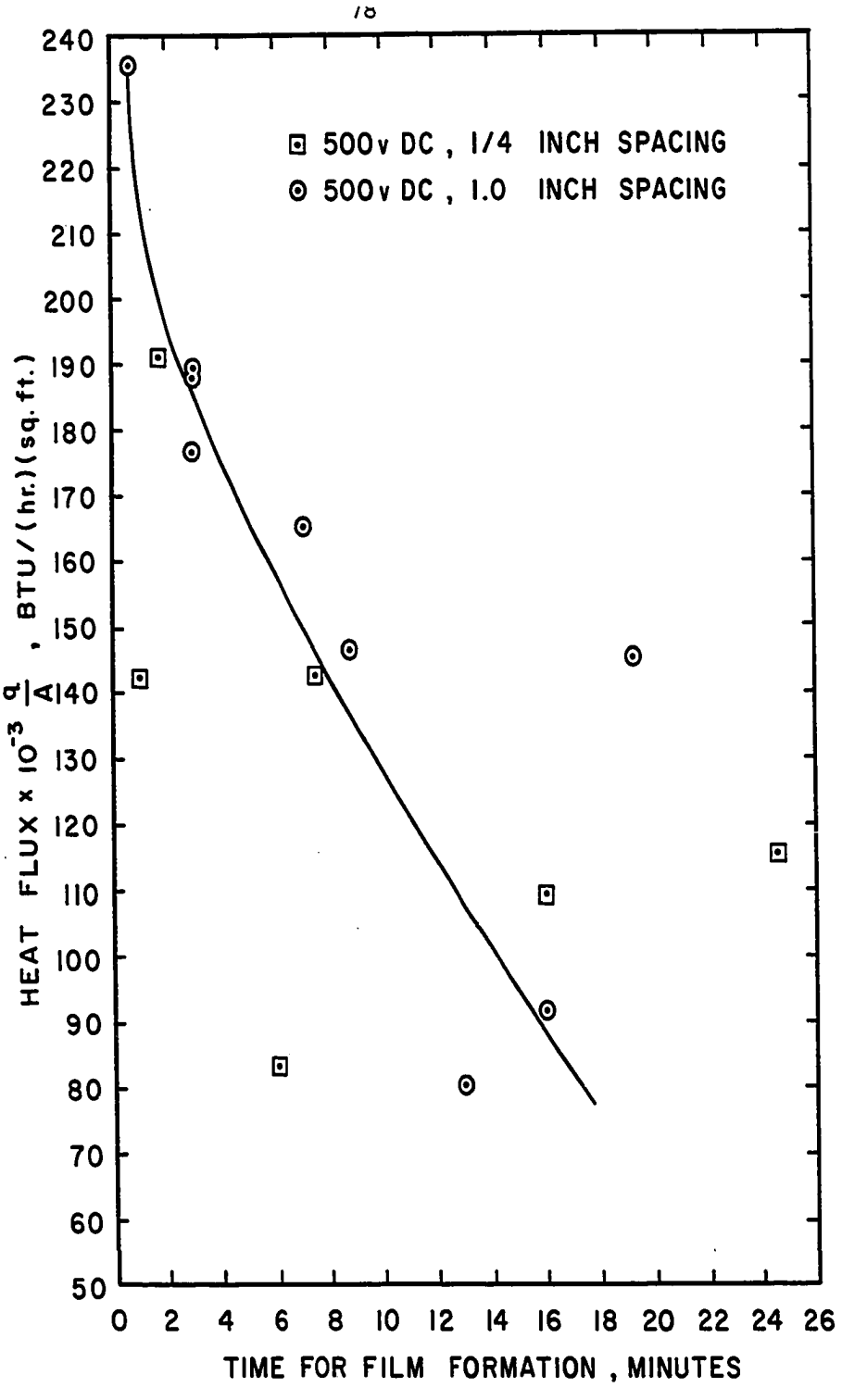

Figure 16. Heat Flux vs Film Formation Time for Boiling Water with an Applied DC Voltage

increasing heat flux, the number of vapor patches formed would be expected to be greater and, as a result, the time for coalescence of vapor patches to form a stable film would be less.

In the water DC HTS(-) applied voltage runs, the effect of the voltage was more difficult to ascertain because a significantly changing heater surface condition occurred during these runs due to a deposition of a precipitate on the surface. Despite various equipment modifications, such as the use of other electrode materials and more adequate isolation of the metallic electrode frame and leads, deposition on the heater surface persisted during this mode of voltage operation. However, in HTS(-) runs in which the current drawn could be maintained at a level comparable to runs in HTS(+) mode of operation at the same applied voltage, a run of significant length of time could be achieved before the changing surface condition gave an appreciable effect. Figure 17 shows the temperature history for two such runs with the HTS(-). The histories for these runs are given in Table 7-B. In both runs, the overall effect of the applied voltage was a decrease in the surface temperature. The significance of this is that the total length of time of voltage application in these runs far exceeded the time for film formation in HTS(+) runs of comparable applied voltage and current draw. A voltage applica-

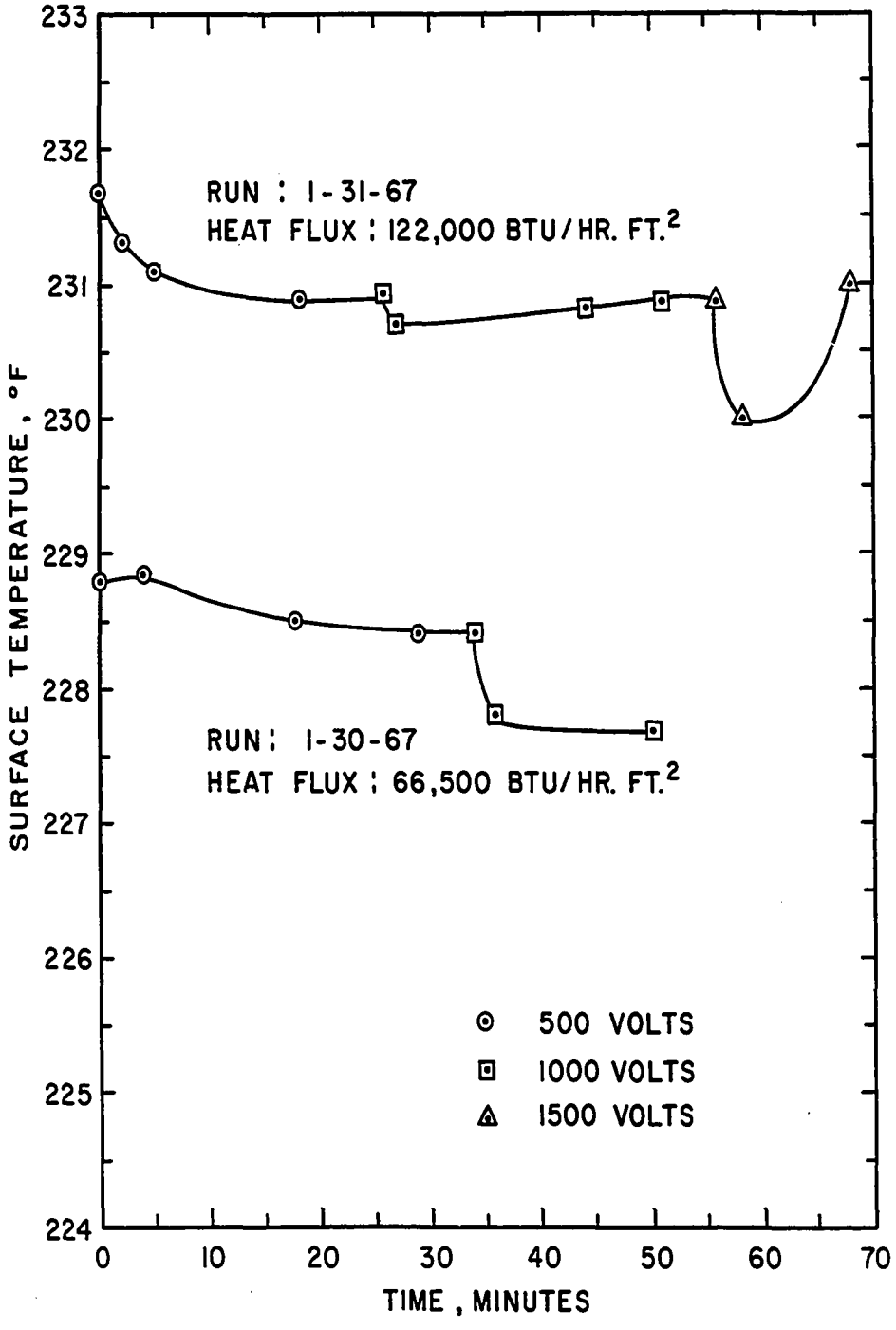

Figure 17. Temperature History for Typical DC HTS(-) Applied Voltage Nucleate Boiling Runs with Water

tion time of fifty minutes in run 1-30-67, and sixty-eight minutes in run 1-31-67, is more than twice the length of time for any of the HTS(+) runs which resulted in film boiling.

In run 1-31-67, while a decrease in the surface temperature was the overall applied voltage effect, an increase in the temperature was apparent during the 1000 and 1500 volt portions of this run. This phenomena, which was observed in varying degrees in all the HTS(-) runs, was accompanied by a visible buildup of deposit on the heater surface. Further, the fact that no visible change in the bubble dynamics accompanied the temperature increase, the increase in temperature during the HTS(-) runs was felt to be a result of deposit buildup on the heater surface and not indicative of a further change in the bubble dynamics as occurred in the HTS(+) runs which promoted film boiling. A test run was devised to substantiate this hypothesis.

In general the test run consisted of initial operation with DC voltage HTS(-) for a length of time to allow a substantial increase in the surface temperature. Careful observation of the bubble dynamics was made during this time. Following this, the system was shut down, dumped, fresh water charged to the tank, and the system lined out to give a surface temperature equal to that before shutdown. The heater surface remained essentially unchanged. Comparison was then made of

the heat flux attained without any voltage to that achieved during the first portion of the run. When the system lined out, the voltgage polarity was reveresed to HTS(+). Measurements and observations of the phenomena occurring on the heater surface were made for this mode of operation. Temperature and current history of this run are shown in Figure 18. A complete documentation of this run is given in Table 7-B. As shown in Figure 18, the initial sixty minutes of the run were with 500 V DC HTS(-) at a heat flux of 172,000 Btu/(hr.)(sq.ft.). Application of the DC voltage resulted in the formation of smaller vapor bubbles and an initial temperature decrease, as shown by the first five minutes of the HTS(-) portion of the run. As the current increased rapidly, the trend of a decreasing temperature reversed and the temperature began increasing sharply. During this time the appearance and buildup of deposit was clearly evident, while the bubble dynamics appeared unchanged from the time of the initial voltage application. For the duration of the HTS(-) portion of the run (13-60 minutes), the current remained in the range of 85-90 milliamperes. A relatively constant current during this time resulted in a constant rate of deposition on the heater surface, which correspondingly showed up as a linear increase in the surface temperature. During this time, the cumulative build-up of surface deposit was clearly apparent. Careful

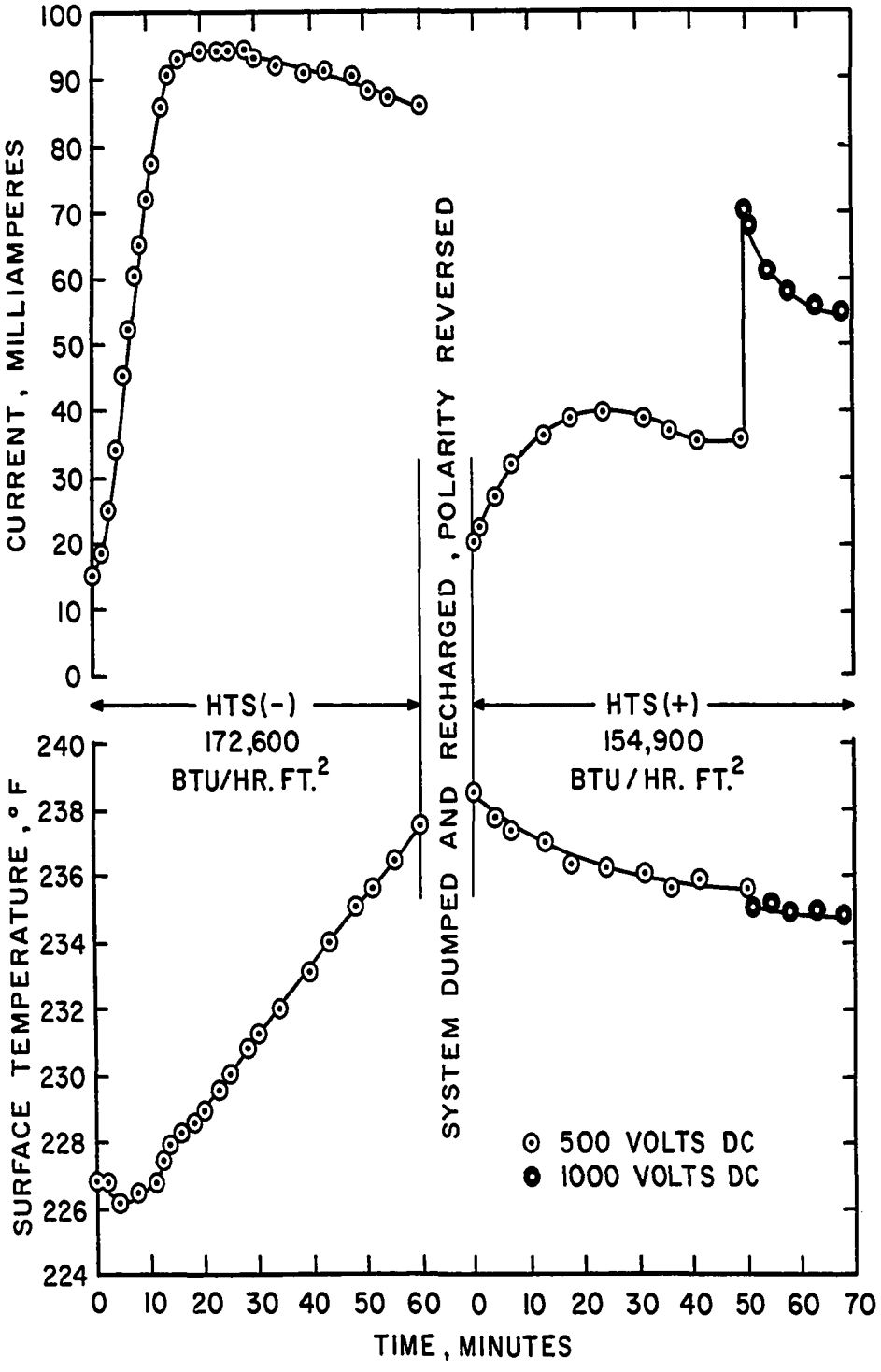

Figure 18. Nucleate Boiling Water Test to Substantiate the Nature of the DC HTS(-) Voltage Effect

observance of the bubble dynamics showed that no change had occurred since the initial voltage application. After sixty minutes of HTS(-) DC voltage application, the system was shut down, recharged with water and lined out at a surface temperature of 238.5°F with a heat flux of 154,900 Btu/(hr)(sq.ft). This compares to a heat flux of 172,600 Btu/(hr)(sq.ft) at a surface temperature of 237.6°F obtained at the end of the sixty minute HTS(-) portion of the run. The higher heat flux at approximately the same ΔT with the applied HTS(-) DC voltage (at a presumably identical surface condition) represented a marked heat transfer enhancement due to the HTS(-) mode of DC voltage operation.

For the HTS(+) portion of the run shown in Figure 18, which followed the system lineout at 238.5°F, the surface temperature was successively lowered during the next seventy minutes of operation. It was visually obvious during this period that the major cause of surface temperature lowering was a result of the surface deposit deplating from the surface. After fifty minutes of 500 volt operation and twenty minutes of 1000 volt DC HTS(+) operation, the system was shut down. At this time an appreciable deposit still adhered to the heater surface.

The results of the test run in Figure 18 are felt to be substantial evidence that the effect of the applied DC

voltage HTS(-) was a lowering of the surface temperature at a fixed heat flux and thus, an enhancement of heat transfer. This conclusion is completely consistent with visual observations of the bubble dynamics. Unlike the HTS(+) case, no change in the bubble dynamics was found to occur during any of the HTS(-) runs.

During the HTS(+) portion of the run shown in Figure 18, no evidence of film formation was observed at either 500 or 1000 volts. A comparison of this portion of the run to the other HTS(+) runs revealed the following two things:

(a) The current levels existing in the 500 and 1000 volt portions of the HTS(+) operation (shown in Figure 18) exceeded the current in all of the HTS(+) runs which resulted in film boiling.

(b) Of all HTS(+) runs made, surface deposition was a factor only in the HTS(+) portion of the run shown in Figure 18.

An inspection of the HTS(+) runs which resulted in film boiling (see Table 5-B) revealed that the highest average currents at applied voltages of 500 and 1000 were 31.5 and 52 milliamperes respectively. These current values were less than during HTS(+) operation at these voltages for the run shown in Figure 18. To provide further evidence of the existence of a current effect on the HTS(+) DC voltage results,

the run whose temperature and current history is shown in Figure 19 was made. This run was identical to the run of Figure 18, except that the voltage was applied over a shorter period, and the water was not changed between the HTS(-) and HTS(+) mode of operation. Since the HTS(-) portion of the run shown in Figure 19 was only of eight minutes duration, appreciable deposition did not occur. As such, during the HTS(+) operation, the current dropped rapidly with time and as a consequence, a film quickly formed, as shown in Figure 19 by the rapid temperature rise.

The dependence of the nucleate boiling water heat transfer results on the current for DC HTS(+) voltage led to a close inspection of all the HTS(+) results (shown in Table 5-B) not resulting in film boiling. Figure 20 demonstrates the significance of this dependence. The points on this plot represent data obtained at 500 and 1000 volts, at both electrode spacings, with both the fine and coarse electrode grids, and for heat fluxes ranging from 51,500 to 167,800 Btu/(hr.)(sq.ft.). The term "percent ΔT lowered" was used for the abscissa in an attempt to eliminate any effect of heat flux level.* The most significant feature of Figure 20 is the

---

*For a constant current drawn, the absolute amount that the ΔT decreased became larger with increasing heat flux. In terms of percent ΔT decreased, however, the quantities were about the same at the same current, irrespective of the heat flux.

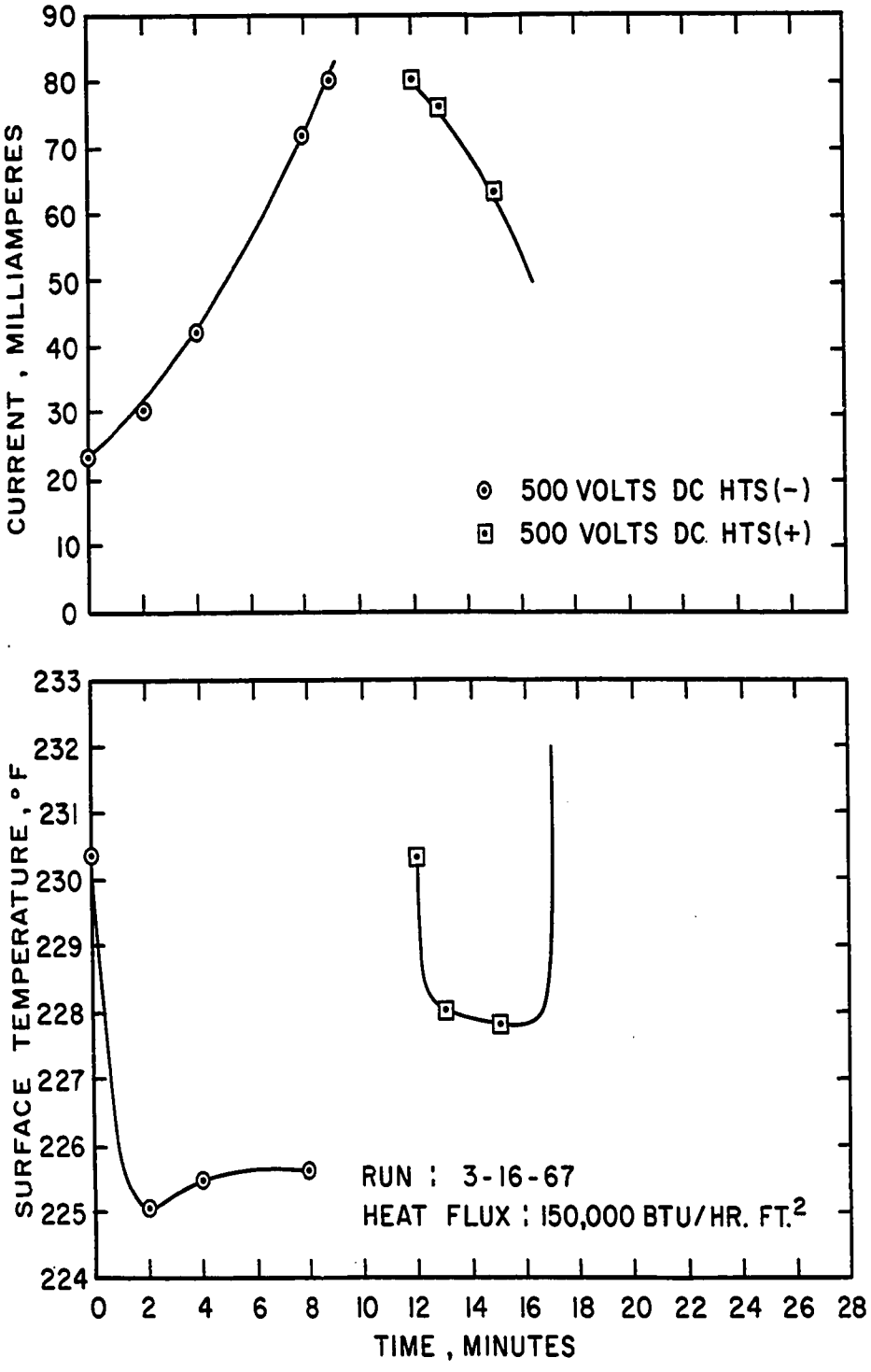

Figure 19. Effect of Current Level on Nucleate Boiling Heat Transfer to Water

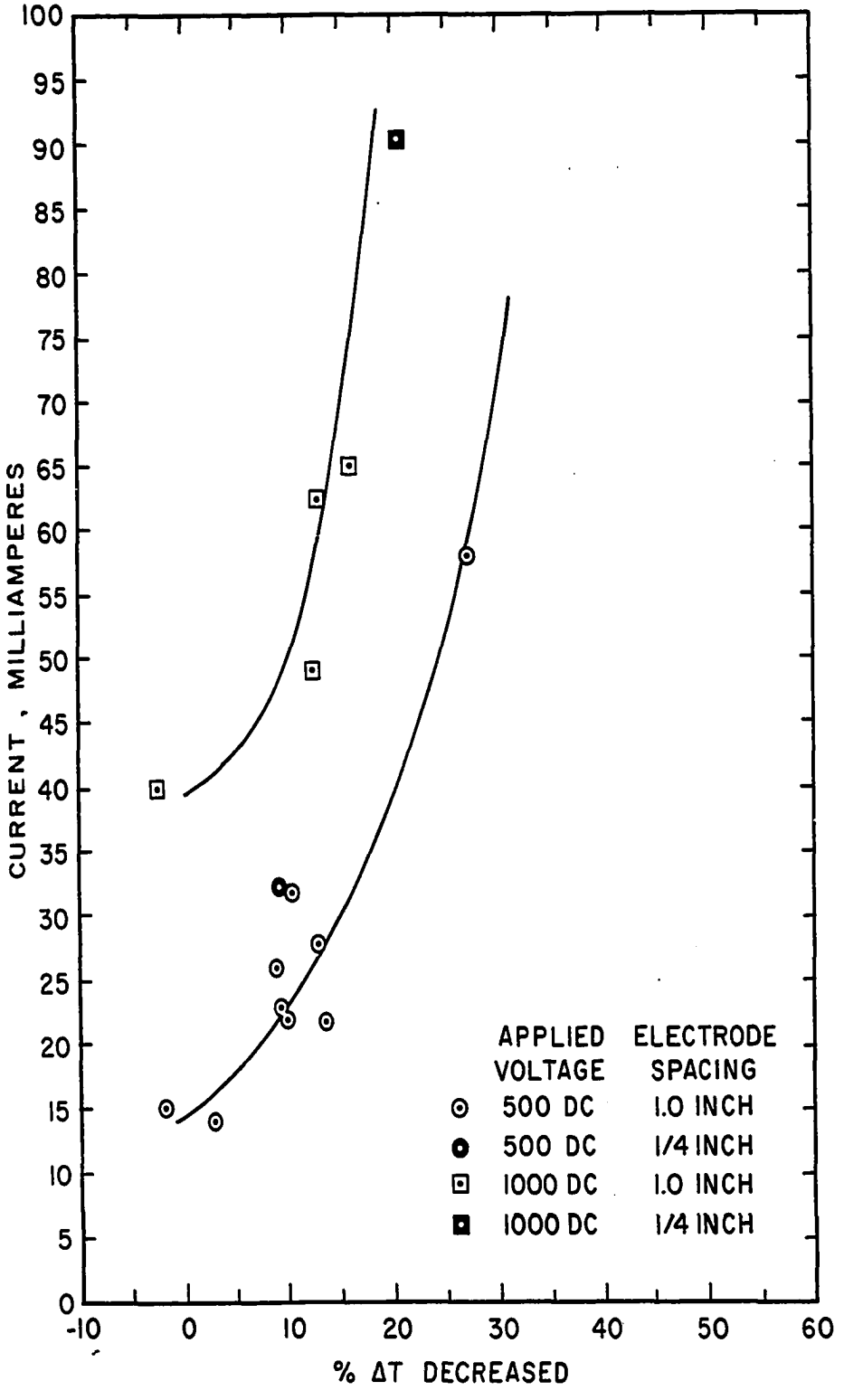

Figure 20. Effect of Current Level on the Heat Transfer to Nucleate Boiling Water During Application of a DC HTS (+) Voltage

nature of the dependence of the "percent ΔT lowered" on current. Ideally, if the current were the only phenomena affecting heat transfer, the "percent ΔT lowered" would be expected to approach zero as the current approached zero, with no ΔT increased, i.e., negative values of ΔT lowered, values observed. As shown by both the 500 and 1000 volt curves, some runs gave no appreciable decrease in ΔT at significant current levels. Although the points are not shown in Figure 20, the phenomena of ΔT reversal at an appreciable current is substantiated by the many runs shown in Table 5-B in which film boiling resulted with DC HTS(+). This dependence of heat transfer on the current for HTS(+) provided a basis for the existence of two simultaneously occurring phenomena. These phenomena, one of which is related to the voltage and the other to the current, have opposite effects on the heat transfer and can be observed or detected from Figure 20. The phenomena arising from current produces an enhancement of the heat transfer coefficient while that arising from voltage promotes film formation and decreases the heat transfer coefficient. As shown in Figure 20, if the current is above a certain value, its effect is dominant and the net observed effect on the heat transfer coefficient is enhancement. If, on the other hand, the current is below a certain level, the effect of voltage is dominant, and the net observed effect is the promotion of film boiling.

The increasing significance of the voltage effect, with higher voltage, is demonstrated by the distinct curves for the data obtained at 500 and 1000 volts.

Although Figure 20 does show a definite value for the limiting current (current value at zero percent ΔT lowered) at both the 500 and 1000 applied voltages, it must be pointed out that these are not quantitative values. As shown in the HTS(+) data resulting in film boiling (see Table 5-B), film boiling occurred at 500 and 1000 volts for current values as high as 31.5 and 52 milliamperes at 500 and 1000 volts respectively. These values are somewhat greater than the limiting values indicated by Figure 20 at the same voltages. There are several reasons for these differences. For the data of Figure 20, it is quite possible that some of the lower current value points on each curve may have ultimately resulted in film boiling if the time of voltage application had been longer. Moreover, it must be realized that the condition of the heat transfer surface, which undoubtedly affected the limiting value of current, could be sufficient reason for the large values of current obtained in some of the runs resulting in film boiling.

Nucleate Boiling Water Results With An Applied AC Voltage

The most extensive data taken in this work was using an applied AC voltage. This data is shown in Table 8-B of Appendix B. The principle reason that more AC data were taken stemmed from the fact that AC voltage effects were small and often masked by other system conditions and variables over which little control could be exercised. Since it was difficult to separate voltage effects from other extraneous effects, a greater quantity of data was taken from which more representative average values could be obtained. The averaged data from Table 8-B are shown in Table 9-B. These data are not quantitative and are merely used to establish the trend of the AC voltage effects on nucleate boiling water. A plot of the average AC data of Table 9-B is shown in Figure 21. It is apparent that the data in the heat flux range from 60,000 to 170,000 Btu/(hr)(sq.ft) for both the 500 and 1000 applied voltages do not show any distinct consistency. An effect is more apparent at 1500 volts for the same range of heat fluxes. Above 170,000 Btu/(hr)(sq.ft) an AC voltage enhancement effect on the heat transfer is clearly apparent for all the voltages.

Despite the inability to obtain unobscured AC voltage

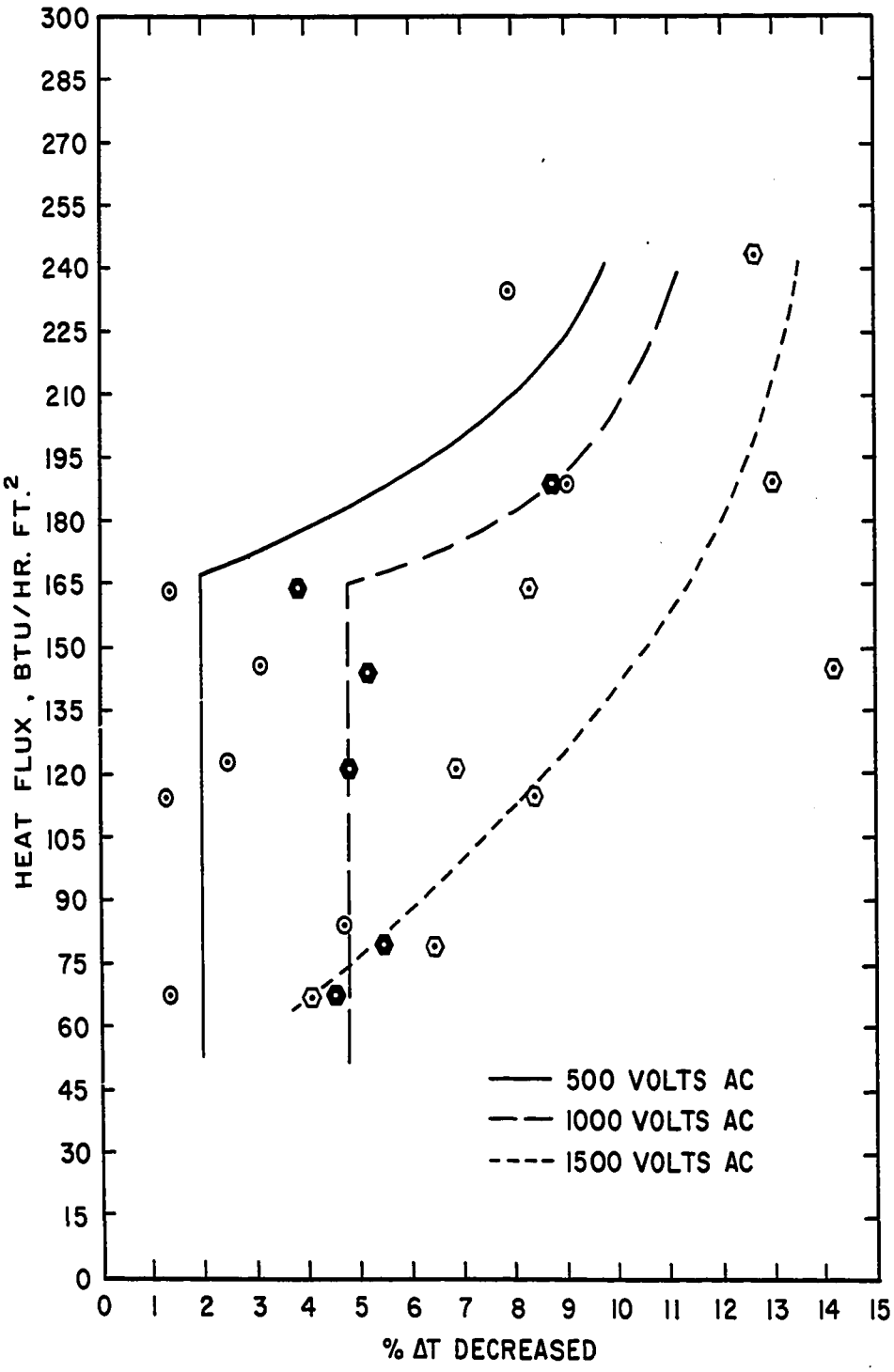

Figure 21. Percent ΔT Decreased vs Heat Flux for Nucleate Boiling Water with an Applied AC Voltage (Averaged Data)

effects for nucleate boiling water, the data obtained provide an amount of significant information. In no instance with an AC applied voltage was there any indication of a film forming. This result was visually verified in that when the voltage was applied the departing bubbles became smaller, with no evidence whatsoever of vapor patch formation. The results obtained with AC voltage are also consistent with the DC results in that the nature and magnitude of the effect on the heat transfer was between that obtained with DC with the HTS(-) and with DC with the HTS(+).

Film Boiling Results With An Applied Voltage

Table 10-B in Appendix B summarizes all the film boiling runs with an applied voltage. These runs consisted of establishing stable film boiling, applying the desired voltage for a specific electrode and electrode spacing, and measuring the surface temperature history. The temperature history results for the individual runs are shown in Table 11-B through 15-B in Appendix B. Because of the temperature limitation of the system, operation with water in film boiling was restricted to a very narrow range of heat fluxes. As opposed to nucleate boiling, it was thus not possible to use heat flux as a variable in the film boiling work. It was

possible, however, to investigate other system variables (i.e., applied voltages, electrode spacings and type of electrode) more extensively than in the nucleate boiling work.

The first of the film boiling results are shown in Figure 22. Plotted are the temperature histories for four DC HTS(+) applied voltage runs in the heat flux range 15,000 to 16,000 Btu/(hr.)(sq.ft.) using the fine grid at 1.0 inch spacing. As shown in this figure, film destabilization (reversion to nucleate boiling) was the end result in each case, with the length of time for film destabilization becoming successively less with increasing voltage. It is interesting to note that all the HTS(+) applied voltage runs in film boiling resulted in a decrease in the ΔT. This result is in contrast to the nucleate boiling results with a DC HTS(+) voltage, in which film boiling resulted if the current was kept below a certain value. Although it was not clearly established what value of the current gave a reversal of the applied voltage effect in the nucleate boiling work, it is significant to note that the final steep downward drop of temperature in the 500 and 1000 volt curves shown in Figure 22 occurred between 15-16 and 29-31 milliamperes respectively. These current values are approximately in the middle of the range at which the current effect was found to dominate the nucleate boiling heat transfer behavior at 500 and 1000 volts. It thus appears that in

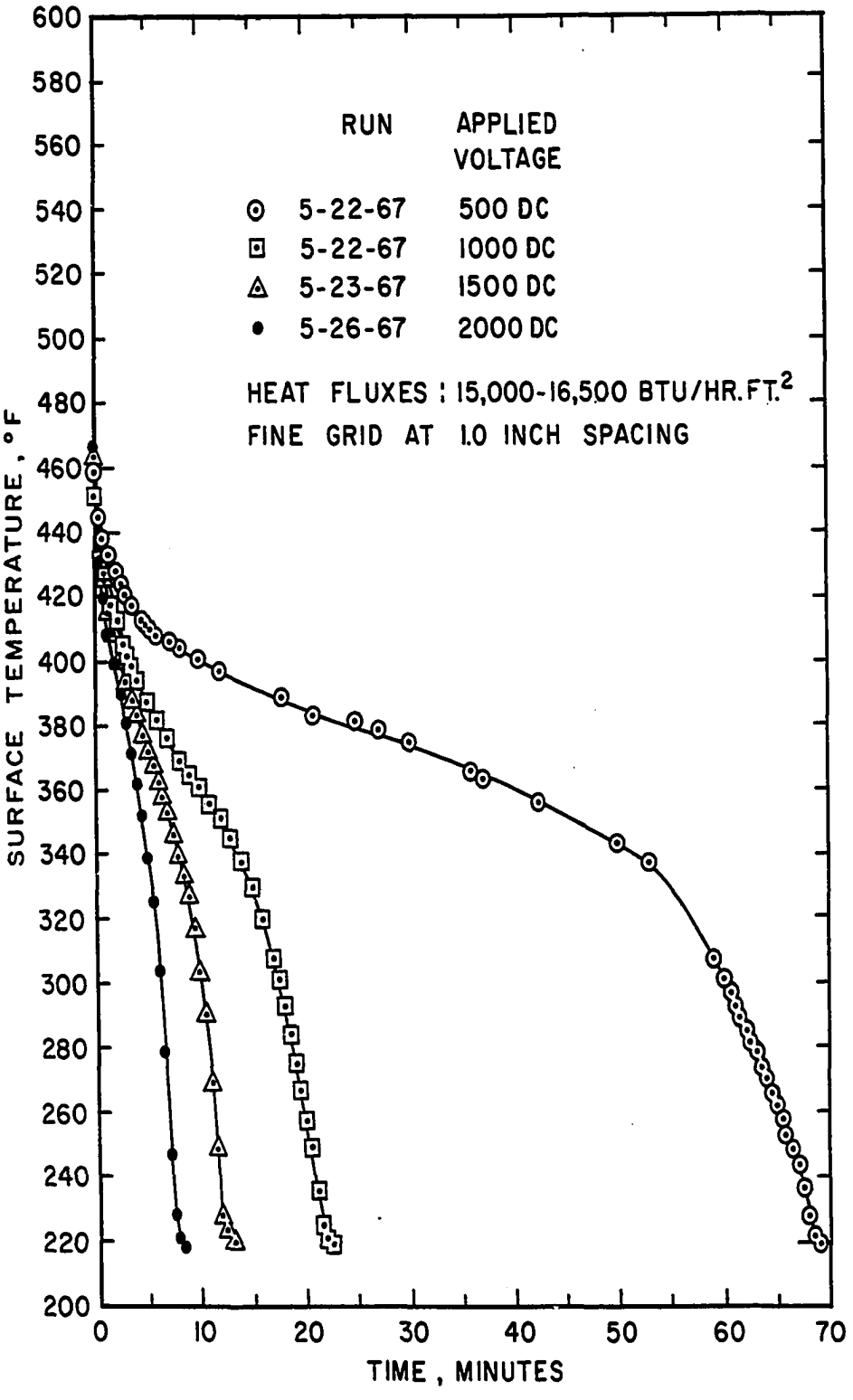

Figure 22. Film Boiling Destabilization Data for Water with an Applied DC Voltage HTS(+)

the DC voltage HTS(+) film data the temperature initially dropped, then attempted to line out. Then as the current gradually increased, due to increased surface wetting, the current effect became significant, causing a further decrease in the surface temperature which ultimately resulted in film destruction and reversion to nucleate boiling. The initially experienced temperature drop, when the voltage was first applied, could be due to the initial current flow; however, the values of current at this time were well below the values at which the current effect was found to be appreciable in the nucleate boiling work. As such, it is possible that the initial temperature drop in the applied voltage HTS(+) film boiling runs is largely an effect of voltage rather than current.

The effect of electrode type and electrode spacing are shown in Figures 23 and 24. The effect of the coarse grid versus fine grid electrode is shown in Figure 23. If the curves shown in this figure were normalized to a common starting temperature, it can be seen that the results at 500 volts, as well as at 1000 volts, would be the same for both electrode grids. A comparison of results obtained for the two electrode spacings, shown in Figure 24, also shows remarkable similarity. Since a decrease in electrode spacing resulted in a decrease in resistance, higher current draw, and an increase in electric

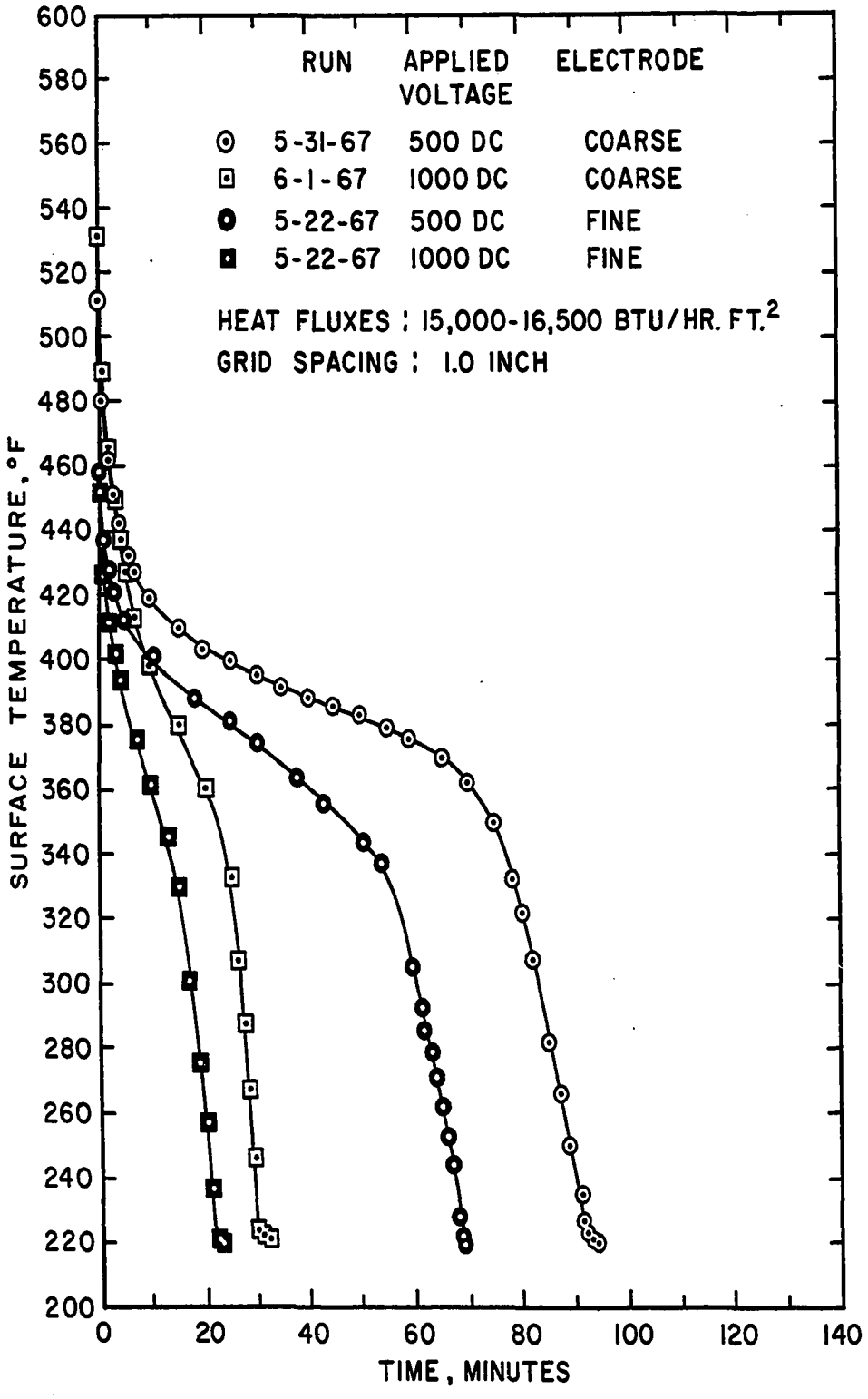

Figure 23. Comparison of Film Boiling Destabilization Data for Water Using Coarse and Fine Grid at 1 Inch Spacing with HTS(+)

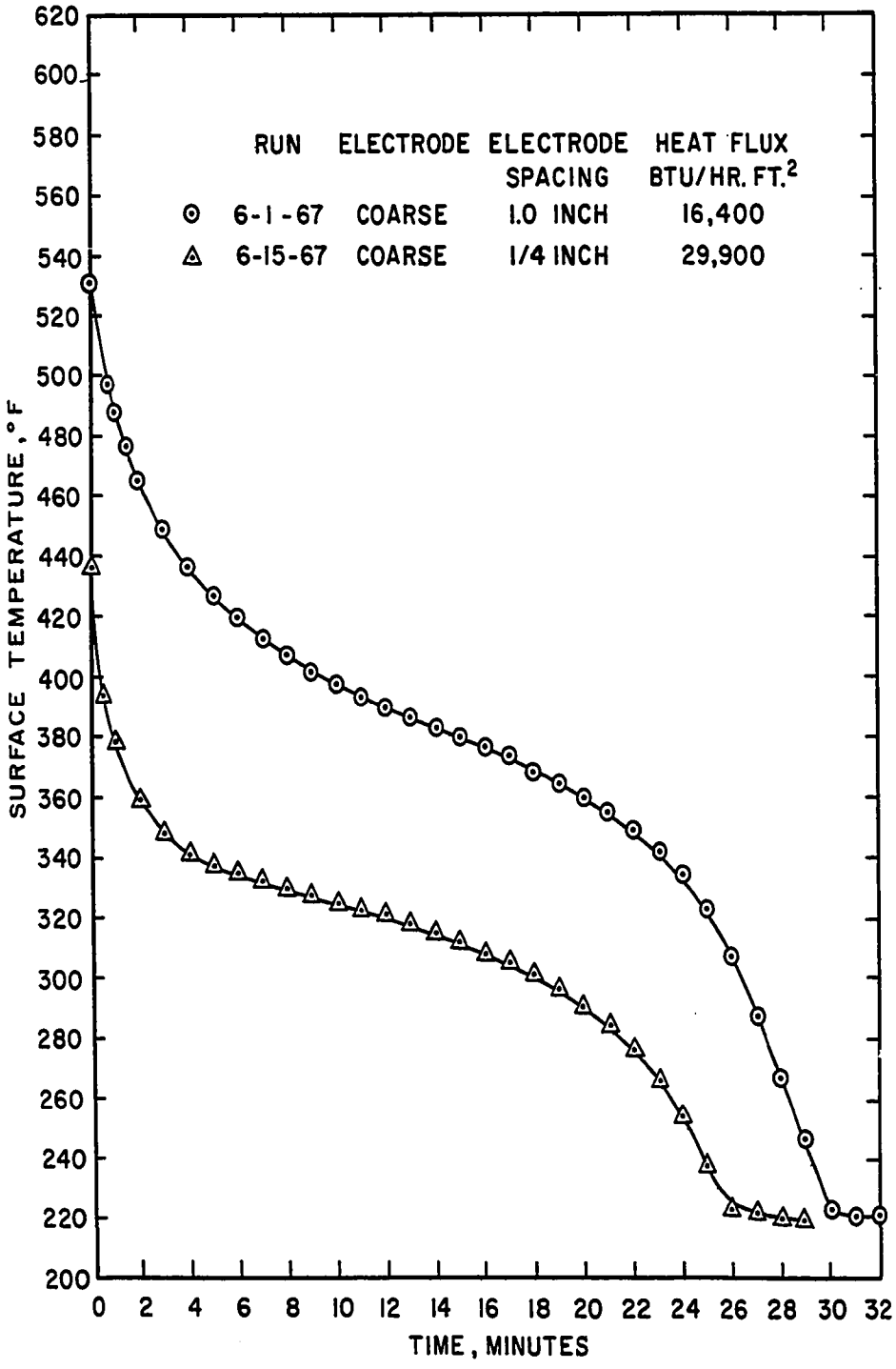

Figure 24. Comparison of Film Boiling Destabilization Data for Water with Two Electrode Spacings at 1000 DC Volts HTS(+)

field intensity (recall that E = V/d for a flat plate electrode configuration), it is possible that the similarity of the two curves in Figure 24 resulted from the fact that the effect on the heat transfer from the increased field strength is matched about equally by the opposite effect of the increased current flow.

Figure 25 shows the AC and DC HTS(-) applied voltage results. From this figure it is apparent that the AC and DC HTS(-) results for both electrodes and electrode spacings are very similar. The large difference in the overall effect of an applied DC voltage with HTS(+) on nucleate boiling, as compared to a DC voltage with the HTS(-) or an applied AC voltage, is also apparent in the film boiling results. A comparison of the results shown in Figures 22 and 25 shows that film destabilization at 500 volts AC or DC HTS(-) was accomplished twice as fast as at 2000 volts DC HTS(+). It is interesting to compare the 500 volt HTS(-) run shown in Figure 25 with the 500 volt HTS(+) results shown in Figure 22, since both runs covered the same range of current. The decay of film boiling for the DC HTS(-) run was so rapid in comparison to the HTS(+) run that there seems little question as to the activity of an opposing electrical phenomenon due to the applied voltage in the latter. This result lends credance to the DC nucleate boiling results in which there was strong evidence that the

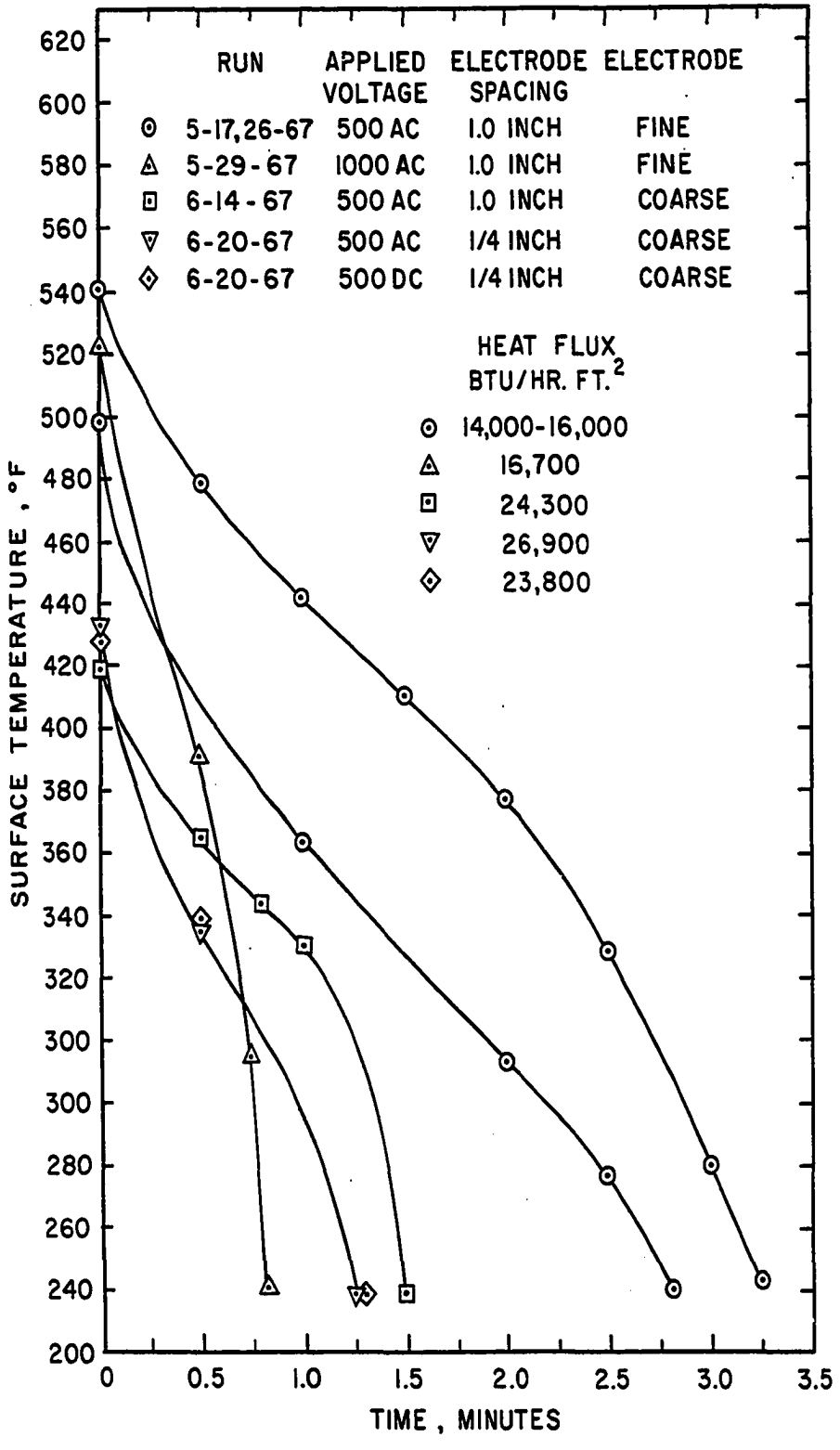

Figure 25. Film Boiling Destabilization Data for Water with AC and DC HTS(-) Applied Voltages

voltage effect was to enhance the heat transfer in HTS(-) operation and was detrimental to heat transfer in HTS(+) operation. In the HTS(-) run of Figure 25, the small current draw (initially 14 milliamps to 24 milliamps when system was totally back in nucleate boiling) and the short time required for film destabilization are both factors which prevented deposit build-up on the heater surface, and further substantiates the fact that deposition on the heater surface, which occurred in the nucleate boiling HTS(-) runs, was not preventing the occurrence of film boiling. Moreover, these factors provide further evidence that the only effect that heater surface deposit had on the results was to cause a rise in the measured surface temperature.

Since operation in the film boiling work was very close to the limiting system temperature, problems were continually encountered. In June of 1967, the system began to leak badly so that the heat transfer surface had to be resealed in place with epoxy. Following this work, extreme surface wetting difficulties were encountered. Although the exact cause of the non-wetting condition could not be found, it was thought to be partially the result of cleaning the surface with Brasso metal cleaner and polish. The nature of the non-wetting condition was similar to that initially encountered in this study (i.e., premature burnout, hemispherical bubble formation, etc.)

except that it could be eliminated by depositing a layer of foreign material on the heater surface. Promoting a wetting condition in this manner was discovered in a nucleate boiling DC HTS(-) voltage run, when it was noticed that as the deposit started forming on the heat transfer surface, the bubbles changed from a hemispherical to a spherical shape. While it was possible to obtain representative non-electric field data by such a surface preparation, extreme difficulty was encountered in attempting to obtain film boiling DC HTS(+) results. In such an operation the deposit on the surface was removed and the non-wetting condition reestablished. Characteristics of the non-wetting condition during the film boiling work were typified by extreme resistance to film destabilization, even with voltage, and the reformation of the vapor film on removal of voltage in runs in which the film had been previously destabilized by a voltage field. Although this problem was alleviated to some degree with time, prolonged operation with a DC HTS(+) applied voltage resulted in a recurrence of a non-wetting condition. This is shown by the two AC runs tabulated in Table 15-B and depicted in Figure 26. Both of these runs were made immediately following 1500 volt DC HTS(+) runs in which the film was destabilized. As shown, achieving a nucleate boiling condition required the use of 1000 and 1500 volts AC. In addition, on completion of these runs, the film

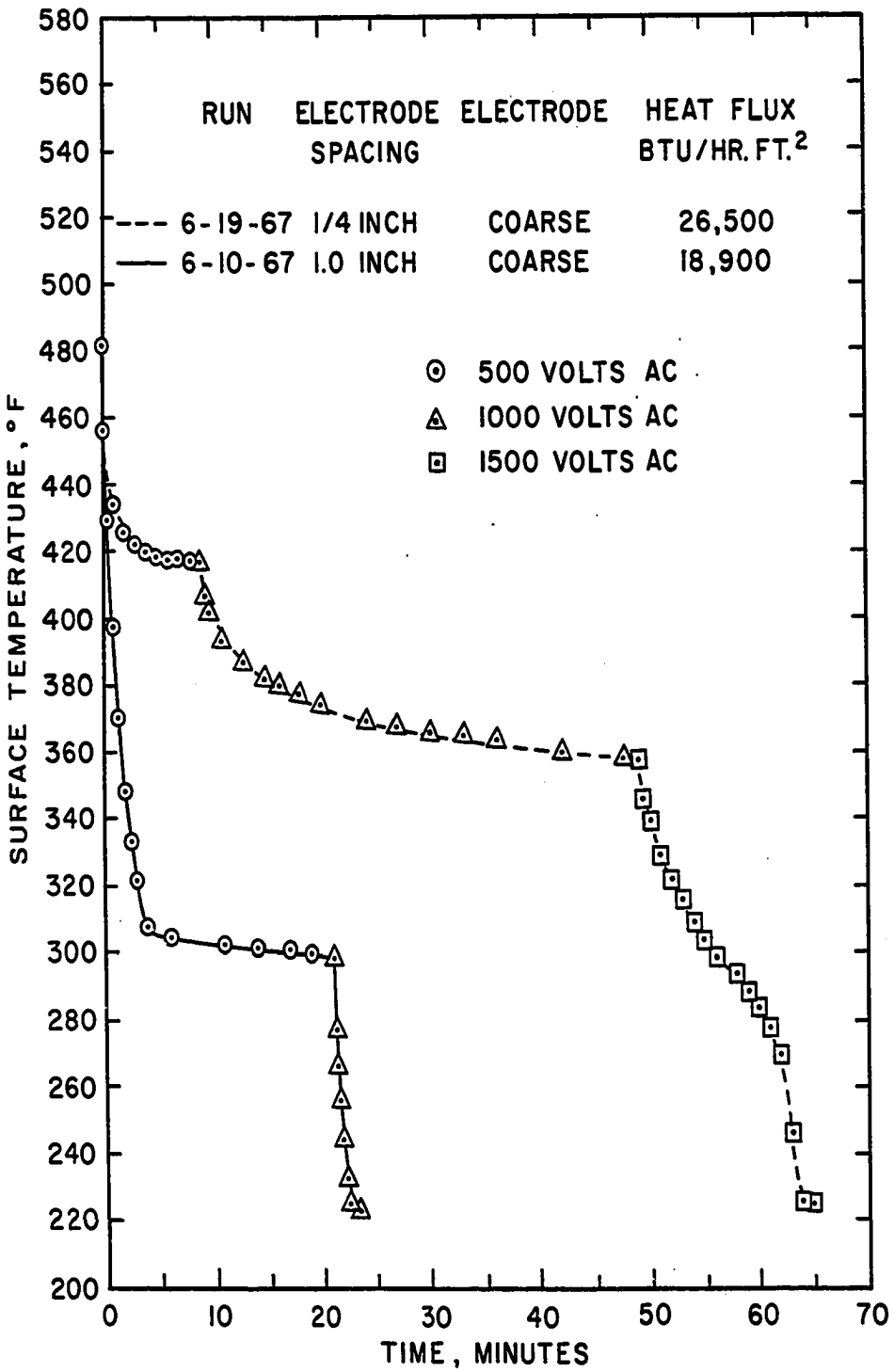

Figure 26. Film Boiling Destabilization Data for Water During AC Runs Showing Condition Affect of Heat Transfer Surface

reformed on removal of the voltage field. These AC runs do not compare favorably to the AC runs shown in Figure 22, which were taken prior to the occurrence of the surface wetting problem. Because of the obvious change in surface condition during this time, the results obtained were not felt to be representative of the actual system performance.

Boiling Freon-112 Heat Transfer Results Without an Applied Electric Field

The boiling data for Freon-112 are shown in Table 16-B of Appendix B and are plotted in Figure 27. Figure 27 includes all of the nucleate boiling data, both field and nonfield. Although no boiling studies with Freon-112 could be located in the literature, the work of Choi [6] with Freon-113 was used to compare the results obtained in the present study. Freon-113 has properties very similar to Freon-112 at its boiling point (BP), as shown in Table 4.

TABLE 4

COMPARISON OF PHYSICAL PROPERTIES OF FREON-112 and -113

Physical Property	Freon-113	Freon-112
ρ_v lbs/ft^3	0.461 at BP	0.438 at BP
ρ lbs/ft^3	95.33 at 104°F	94.51 at 194°F
λ Btu/lb	63.12 at BP	67 at BP
σ dynes/cm	15.3 at 104°F	16.93 at 176°F
BP °F	117.6	199

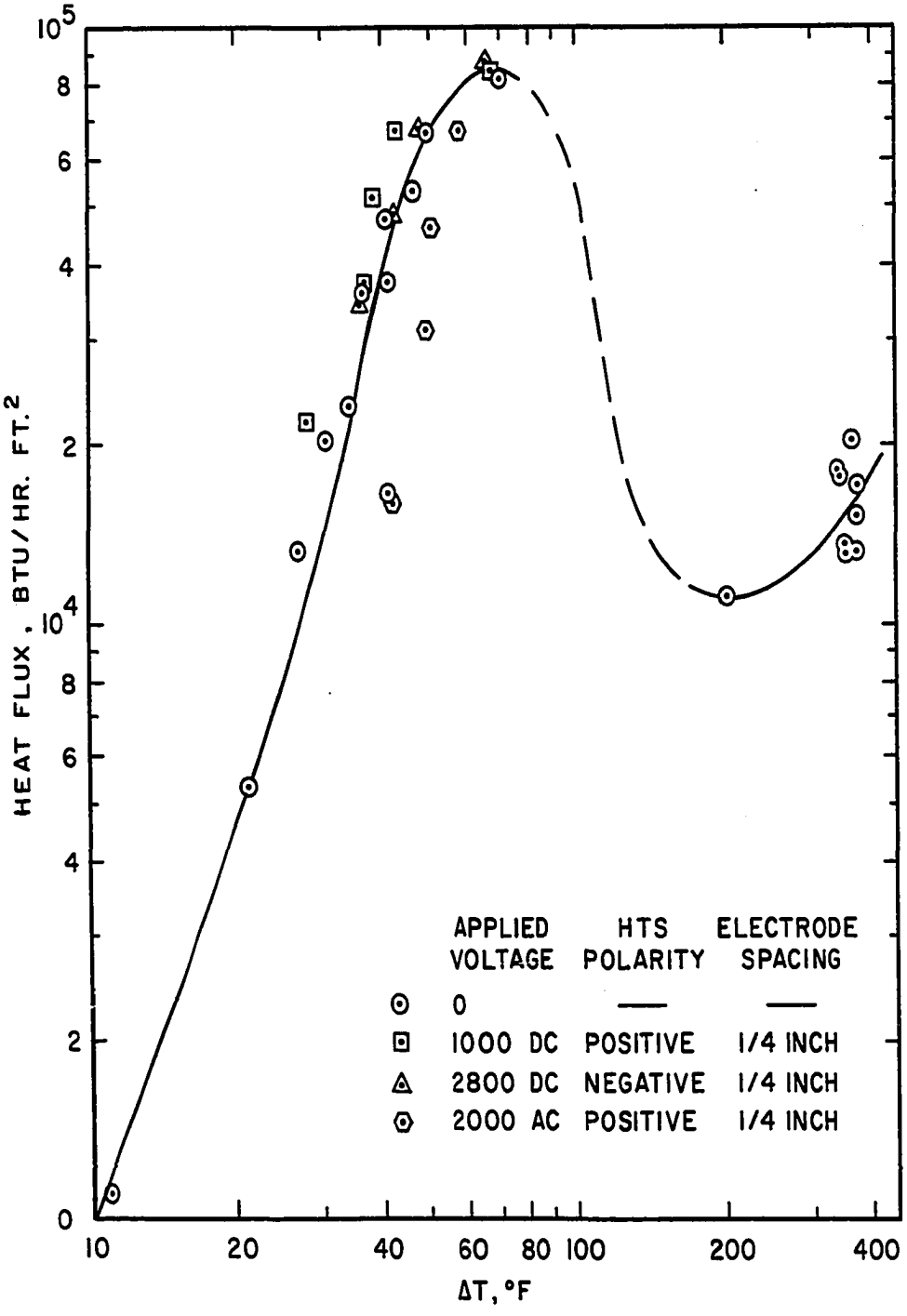

Figure 27. Boiling Heat Transfer Data for Freon-112

Choi [6] reports a burnout heat flux for Freon-113 of about 85,000 Btu/(hr)(sq.ft) at a ΔT of about 65°F. This compares very closely to the Freon-112 burnout heat flux obtained in this work of between 82,500 and 88,000 Btu/(hr)(sq.ft) at a ΔT of 60°F to 70°F. Calculation of the burnout heat flux for Freon-112 using the burnout heat flux prediction of Zuber (Equation (18)) yielded a value of 88,500 Btu/(hr)(sq.ft). Choi reports a second critical flux for Freon-113 of 20,000 Btu/(hr)(sq.ft) at a ΔT between 150° and 200°F. In the present work a heat flux of 11,160 Btu/(hr)(sq.ft) was obtained at a ΔT of 204.7°F. However, the stability of the film was questionable at this condition. At a heat flux from 13,000 to 20,000 Btu/(hr)(sq.ft), a ΔT of about 350°F was obtained and the film was quite stable.

Freon-112 Nucleate and Film Boiling

Applied Voltage Results

The effect of an applied voltage on the heat transfer to boiling Freon-112 was considerably smaller than for a similar voltage in the water work. During nucleate boiling, AC and DC voltages up to 2800 volts were applied to boiling Freon-112. Up to this voltage no major measurable or visible effects on nucleate boiling were apparent.

Although voltage effects were discernable during film boiling, in no case was a stable film destabilized by the application of a voltage. All the applied voltage film boiling data is given in Table 17-B in Appendix B. Figure 28 shows the film boiling results obtained at two different voltages. As is apparent, DC voltage for either polarity was more effective than AC but there is little difference between DC HTS(+) and DC HTS(-), with the former giving the slightly larger effect. Figures 29 and 30 show that the effect of increasing the voltage from 2000 to 2800 volts DC had little effect on the temperature history. However, a difference is apparent in Figure 30 between the 1/4-inch and 1-inch electrode spacing at 2800 volts, indicating that the voltage effects on heat transfer increase with increasing electric field strength.

Summary of Results

The results presented in this chapter may be summarized as follows:

1) Nucleate boiling heat transfer to water was significantly affected by application of a DC voltage whereas application of an AC voltage resulted in essentially no effect.
2) The nature of the DC voltage effect on nucleate

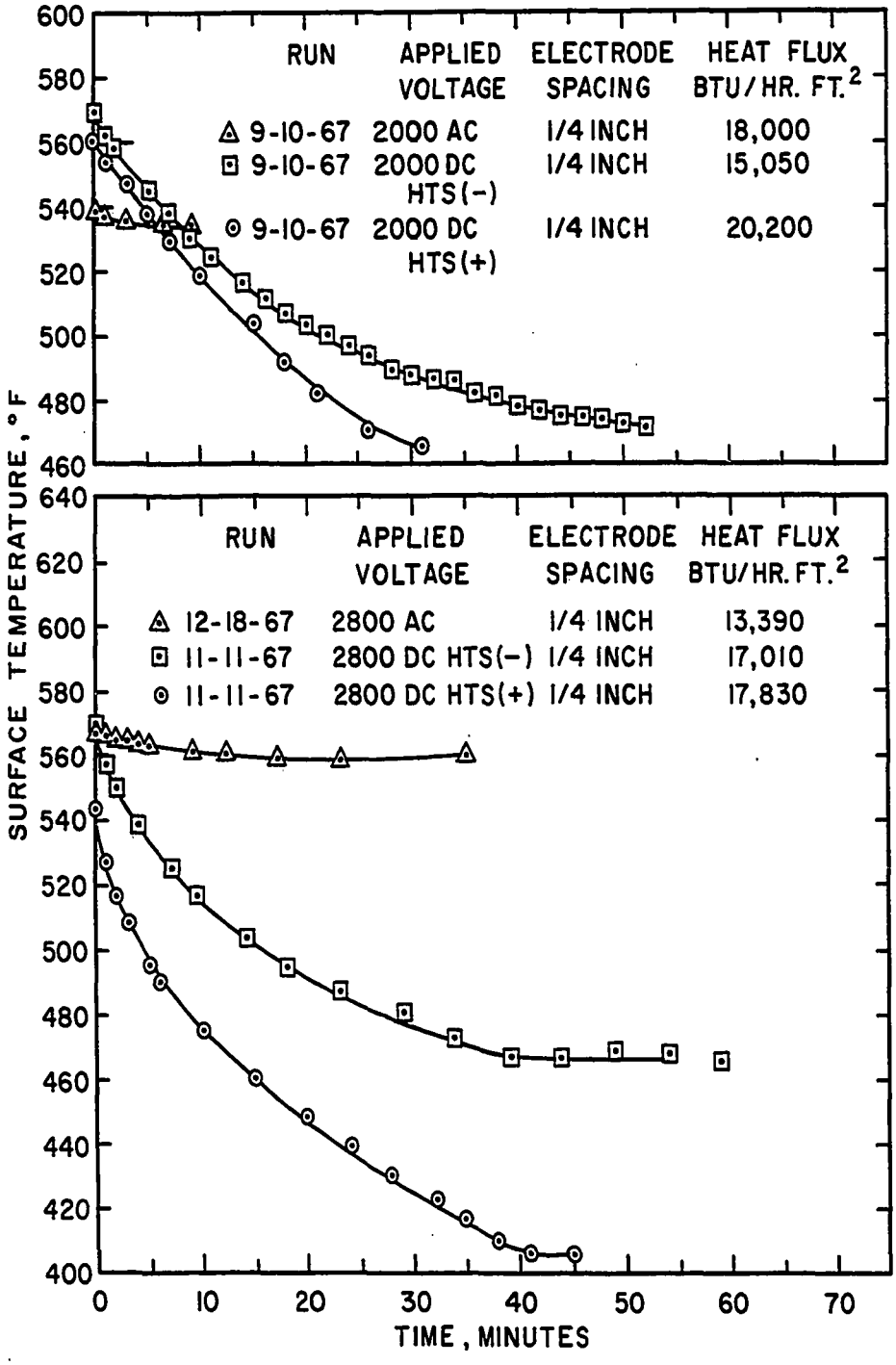

Figure 28. Film Boiling Destabilization Data for Freon-112 Using Coarse Grid

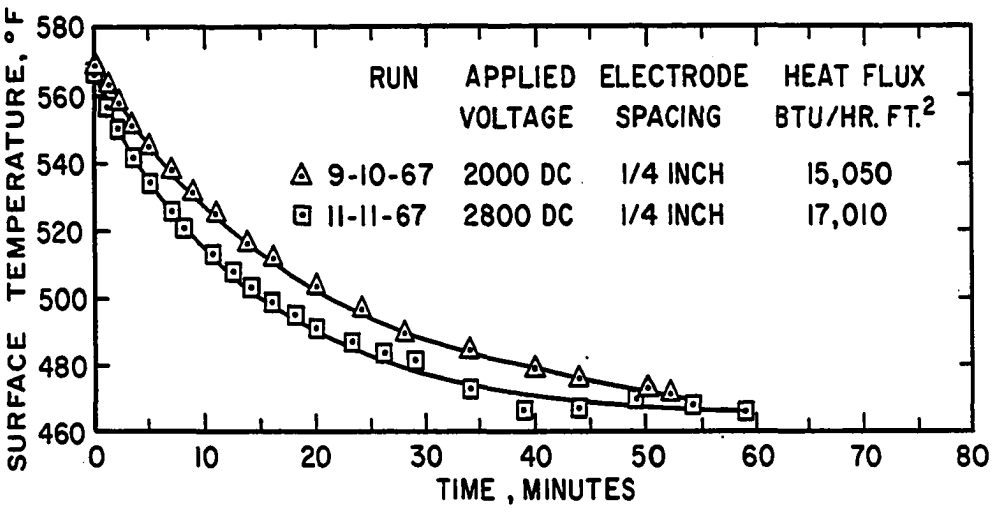

Figure 29. Comparison of DC HTS(-) Film Boiling Destabilization Data for Freon-112 at Two Applied Voltages with the Coarse Grid Electrode

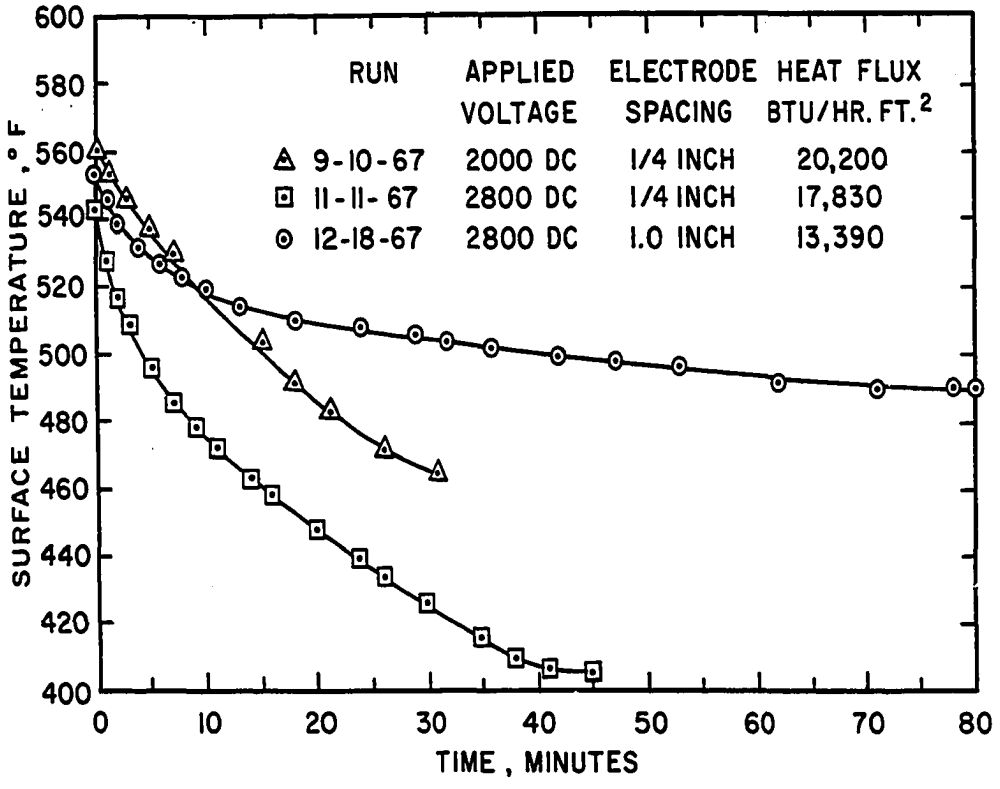

Figure 30. Comparison of DC HTS(+) Film Boiling Destabilization Data for Freon-112 at Two Electrode Grid Electrode

boiling water was dependent on polarity. An enhancement of heat transfer with DC voltage resulted when the heated surface was of negative polarity [HTS(-)]. Operation with a positive polarity [HTS(+)] on the heated surface gave higher ΔT's providing the amperage was below some minimum level. Visual changes in the bubble dynamics were observed for both polarities.

3) Amperage was a factor in the water work with its effect being most apparent in the DC HTS(+) nucleate boiling results.

4) The film boiling results with water differed from the nucleate boiling results in that enhancement of heat transfer resulted for both AC and DC voltage at either polarity. While no detrimental effects of an applied voltage were observed in film boiling for either polarity, the voltage effects on nucleate and film boiling were similar from the standpoint that the DC HTS(+) results were considerably less than HTS(-) results during film boiling.

5) For both AC and DC at the electric field intensity levels studied with Freon-112, there was no apparent or measurable voltage effect on nucleate boiling heat transfer.

6) The Freon-112 film boiling data was affected by both AC and DC electric fields. The DC effect was independent of polarity and resulted in lower ΔTs than during application of AC voltage (cf. Figure 28).

7) Electrode spacing and the type of electrode grid used was of minor effect on the observed results with water for DC HTS(+) and AC voltage application; the water HTS(-) results were inconclusive. For the Freon-112 data electrode spacing for both AC and DC gave a distinguishable effect during film boiling (cf. Figure 30).

8) The present results using uniform electric fields were comparable to the previous non-uniform electric field results of Markels and Durfee [14,15,16] and Choi [6] in a number of ways. Notable similarities were:

   (a) Smaller applied voltage effects were observed during nucleate boiling as opposed to film boiling,

   (b) An applied voltage gave a marked visual change in bubble dynamics during nucleate boiling,

and (c) An increased voltage increased the effect on boiling heat transfer.

9) One striking dissimilarity existed between the past non-uniform electric field boiling studies and the present uniform field work. In the present work, but not in the former studies, DC polarity was found to have an effect on boiling water.

CHAPTER VII

THEORETICAL IMPLICATIONS OF ELECTROFLUIDMECHANICAL INTERACTIONS IN BOILING HEAT TRANSFER

If the electric field intensity existing between the conducting electrodes used in the boiling system is truly uniform the possibility of the activity of dielectrophoretic phenomena is precluded. This is clearly obvious from Equation (16), since if the electric field as generated by the geometry of the electrodes is uniform ∇E^2, and thus F_V, is equal to zero. In the absence of dielectrophoresis the results from the present uniform electric field investigation need to be explained primarily in terms of electrophoresis, or the condenser effect as defined by Markels and Durfee, and given by Equation (21). While Markels and Durfee recognized the condenser effect to be of importance in their work with water, effects of dielectrophoresis were also necessary to render their results meaningful. While it is difficult to compare quantitatively the present results with water to their results, many of the observed phenomena were quite similar (effects on bubble dynamics and relative magnitude of film boiling results to nucleate boiling results). These facts along with the effects observed in film boiling with Freon, an excellent dielectric, strongly imply the existence of electrically generated forces in addition to electrophoresis. In seeking

a basis for such a suspicion, a review of electric field interactions as predicted by electromagnetic theory was undertaken. Since the effects of dielectrophoresis were previously based solely on the electric field as produced by the electrode geometry, without consideration given to the existence of two phases between the electrodes, the review was mainly oriented to electric field interactions with two phase fluids, and directed toward the possibility of electrical activity in two phase media subjected to a uniform electric field.

Review of the Forces in a Two Phase Dielectric Medium Subjected to a Uniform Electric Field as Predicted by Electromagnetic Theory

The volume force (body force) exerted on a continuous dielectric material subjected to an electric field is given by

$$\vec{F}_V = -\frac{1}{2}\epsilon_o \vec{\nabla} K + \frac{1}{2}\epsilon_o \vec{\nabla}\left(E^2 \rho \frac{\partial K}{\partial \rho}\right) \qquad (24)$$

Stratton [26] presents the basic development of this expression along with references to earlier literature where a complete account of the theory is given. This expression is general for dielectrics which do not contain a free charge. The first term of Equation (24) represents a volume force associated with a variation in dielectric constant, whereas the last term is associated with the deformation of the dielectric. The latter

term can be further simplified if a relationship between the density and dielectric constant of the medium is available. For gases, liquids and some solids a very good approximation for this relationship is the Clausius-Masotti law.

$$\frac{K-1}{K+2} = c\rho \tag{25}$$

In this expression c is a constant determined by the nature of the dielectric. Through incorporation of Equation (25) into Equation (24), as shown in Appendix D, Equation (24) can be resolved to the following:

$$\vec{F}_V = -\frac{\epsilon_o}{2} E^2 \vec{\nabla} K + \frac{\epsilon_o}{6} \vec{\nabla} [E^2 (K-1)(K+2)] \tag{26}$$

For the case of a continuous medium of uniform dielectric constant, Equation (26) resolves to Equation (3) which is of the form of the electrical body force, $\vec{F}_V$, used by Choi [6]. By comparison of Equation (26) to Equation (3) it is seen that the analysis used by Choi involved assuming a constant value for the dielectric constant ($\vec{\nabla}K = 0$). In using Equation (26) Choi further assumed that the value and variation of E was dictated by the electrode configuration.

Equation (26) relates the force exerted by an electric field on a unit volume of continuous liquid or gas dielectric. While

variations in medium properties are allowable, an abrupt discontinuity as occurs across a liquid-vapor interface is not permissible. In such an instance the transition layer between liquid and vapor becomes vanishingly small and gives rise to infinite values of the gradient of the dielectric constant. At the same time, however, the volume within the discontinuity also vanishes. As such the total force exerted on the resultant surface of discontinuity is obtained by taking the limit of the force per unit volume as the thickness approaches zero. Stratton [26] gives the development for this situation which is depicted in Figure 31. The resultant force acting on unit area, S, in the direction from medium 1 towards medium 2 as the thickness approaches zero is

$$\vec{S} = [\alpha\vec{E}(\vec{E}\cdot\vec{n})]_2 + [\alpha\vec{E}(\vec{E}\cdot\vec{n})]_1 - [\beta E^2\vec{n}]_2 - [\beta E^2\vec{n}]_1 \quad (27)$$

The subscripts indicate the values are to be taken on the respective sides of the interface, and α and β represent parameters which characterize isotropic dielectric media. In the case of an interface separating two fluids for which the Clausius-Masotti law applies

$$\alpha = K\,\epsilon_o \quad (28)$$

$$\beta = \frac{\epsilon_o}{6}(K^2 - 2K - 2) \quad (29)$$

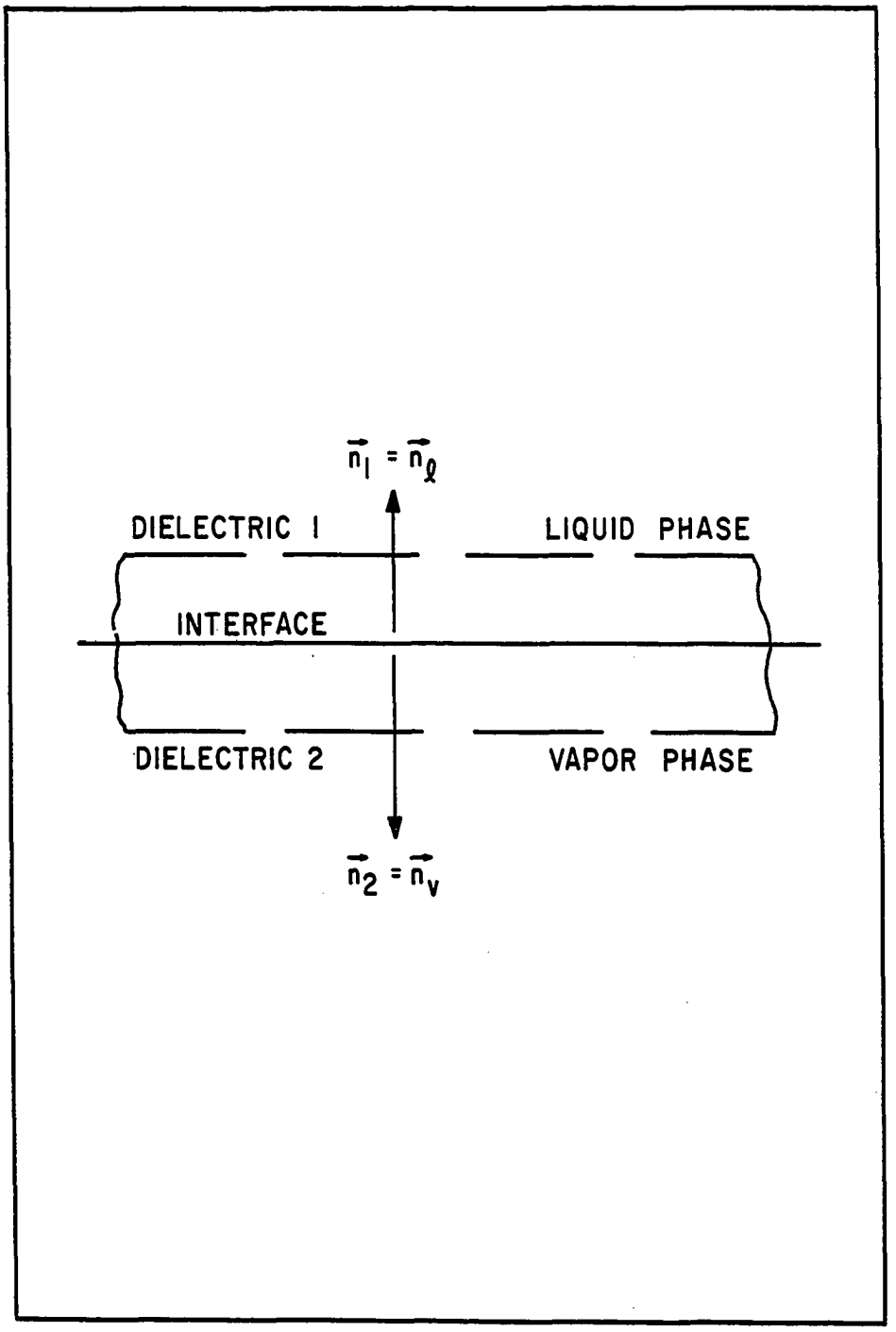

Figure 31. Section of an Interface Separating Two Dielectric Mediums

Substitution of the above relationships for α and β into Equation (27), and by application of the boundary conditions which relate the electric field intensity across a dielectric -dielectric interface,

$$E_{\tan 1} = E_{\tan 2} \tag{30}$$

$$K_1 E_{n1} = K_2 E_{n2} \tag{31}$$

Equation (27) is resolved to

$$\vec{S} = \frac{\epsilon_o}{6}\left\{\frac{1}{K_2}[K_2^2 K_1^2 + 4K_1^2 K_2 - 6K_1 K_2^2 - 3K_1^2 + 2K_1 + 2]E_{n1}^2 + [K_2(K_1-2) - K_1(K_1-2)]E_{\tan 1}^2\right\}\vec{n}_2 \tag{32}$$

If the dielectric fluids are vapor and liquid, Equation (32) can be further simplified by virtue of the fact that the dielectric constants of gaseous or vapor materials are very nearly unity. For region 2 being that of vapor, Equation (32) becomes

$$\vec{S} = \frac{\epsilon_o}{6}(K_\ell - 1)^2 (2E_{n\ell}^2 - E_{\tan \ell}^2)\vec{n}_v \tag{33}$$

This expression states that the stress exerted by the electric field on the vapor-liquid interface is normal to the interface, directed from liquid to vapor, and its value is a maximum when $\vec{E}$ is normal to the surface. If $\vec{E}$ lies in the interface, however, $E_{n\ell}$ is zero and

the stress becomes negative implying a pressure exerted by the electric field in the direction of the liquid. It is worth noting that the interfacial stress is not dependent on an electric field intensity gradient and, thus, its existence is independent of whether the electric field is uniform or non-uniform. As such, even in the case of a uniform field, the interfacial stress as given by Equation (33) is an active phenomenon. In the previous analysis the effect of this interface stress was neglected.

Up to this point no mention has been made of the quantity $\vec{E}$, the electric field intensity, which appears in both Equations (26) and (33). In order to evaluate the magnitude of the electrical body force and the stress across the liquid-vapor interface from these equations, it is necessary to know $\vec{E}$ and its variation. In a two-phase medium $\vec{E}$ is greatly influenced by the geometry of the two phases. If in the two basic regimes of boiling, that is nucleate and film, the geometry of the vapor phase in the bulk liquid medium is approximated by spheres and a flat layer respectively, an expression for the electric field intensity in each phase can be developed for both of these cases. In the case of film boiling where a well-defined layer of vapor separates one of the conductor surfaces (the heated surface) from the liquid, the electric field intensity vectors intersect the vapor-liquid interface perpendicularly. In transgressing the

interface the electric field intensity undergoes a magnitude change as directed by the boundary conditions which apply across such an interface. If the vapor film is considered completely flat, so that the vectors intersect perpendicularly, the field intensity variation on each side of the interface remain as given by the electrode geometry. As such, in the case of a uniform electric field, the electric field intensity in the bulk mediums in the vicinity of the interface remains uniform and no electric field gradient exists parallel or perpendicular to the interface in either of the bulk mediums. On this basis, if the bulk liquid and vapor dielectric constants are assumed constant, i.e., $\nabla K = 0$, each term in Equation (26) is zero and the only dielectrophoretic phenomenon occurring is that of the stress on the vapor-liquid interface. For the case of a vapor sphere embedded in a liquid medium subjected to a uniform electric field, the same cannot be said of the electric field intensity in the bulk liquid medium in the vicinity of the vapor-liquid interface. Expressions for the electric field intensity inside (vapor region) and outside (liquid region) of such a spherical bubble of radius r_1 is given below.

Vapor Region ($r < r_1$)

$$\vec{E}_v = \frac{3K_\ell E_o}{2(K_\ell + K_v)} \vec{r} \tag{34}$$

Liquid Region ($r > r_1$)

$$\vec{E}_{\ell} = E_o \cos\theta\left[1+\frac{2r_1^3(K_v-K_\ell)}{r^3(2K_\ell+K_v)}\right]\vec{r} + E_o \sin\theta\left[\frac{r_1^3(K_v-K_\ell)}{r^3(K_v+K_\ell)} -1\right]\vec{\theta} \tag{35}$$

A formal development of these expressions is given in Appendix E. Equations (34) and (35) show that while the electric field intensity is uniform inside the vapor bubble this is not true on the liquid side of the bubble. As such, a body force as given by Equation (26) exists on the liquid side of the bubble interface, even with the assumption that ∇K is equal to zero. Thus, in the case of a spherical bubble, in addition to the stress on the vapor-liquid interface an electrical body force exists on the liquid in the vicinity of the vapor-liquid interface. Incorporation of Equation (35) into Equations (26) and (33) yields the following expressions for the electrical interfacial stress, and the body force (at $r = r_1$) in the liquid region next to a bubble.

$$\vec{S} = \frac{3\epsilon_o(K_\ell-1)^2E_o^2}{2(K_v+2K_\ell)^2}[2K_v^2\cos^2\theta-K_\ell^2\sin^2\theta]\vec{n}_v \tag{36}$$

$$\vec{F} = \frac{3E_o^2(K_\ell-1)(K_\ell+2)\epsilon_o}{r_1(K_v+2K_\ell)^2}[(K_\ell-K_v)(2K_v\cos^2\theta-K_\ell\sin^2\theta)\vec{r}$$

$$+ \cos\theta\sin\theta(K_\ell^2-K_v^2)\vec{\theta}] - \frac{1}{2}\epsilon_o E_o^2\vec{\nabla}K_\ell \tag{37}$$

A development of Equations (36) and (37) is shown in Appendix F. Equation (37) is the volume force at $r = r_1$ and represents the maximum value of F_v in the vicinity of a bubble. That the maximum value exists at $r = r_1$ is evident from Equation (35) (as r gets large the value of E_ℓ^2 approaches E_o^2 and ∇E_o^2 is zero).

The interfacial electrical stress, as given by Equations (33) and (36), and the electrical body force, as given by Equation (37), are electrical phenomena whose activity is independent of the presence of free charge. In the case where no free charge is present these are the only active electrical phenomena which exist in a two phase media as a result of electric field application. If free charges are present, as with a partially conducting medium, in addition to the existence of forces of the above nature an electrostatic force of attraction exists between the charge carrying fluid and the fixed electrically conducting electrodes. This force is of the same nature as that existing between charged electrodes. Thus for the case where a gas or vapor partially blocks or completely insulates the liquid from the electrode, and some of the free charge accumulates at the vapor-liquid interface, an additional stress of the following magnitude exists on the liquid,

$$F/A = \frac{1}{2} \epsilon_o K_v E_v^2 \approx \tfrac{1}{2} \epsilon_o E_v^2 \qquad (38)$$

where E_v is the electric field intensity in the vapor or gas which separates the liquid from the electrically charged electrode.

Estimation of the Magnitude of the Various Electrically Generated Forces

In an attempt to render more meaningful an interpretation of the water and Freon-112 results of the present investigation, and also in an attempt to tie the present results to those obtained with uniform electric fields, the magnitude of the electrical stress and volume forces involved were calculated. These results are presented in Tables 5, 6, 7, and 8, and are not implied to be of quantitative significance. They are only presented to show relative comparisons and are strictly for qualitative interpretation purposes. Example calculations of the various quantities shown in Tables 5 through 8 are given in Appendix G.

In Table 5 are shown the interfacial stress values calculated for a flat vapor film (film boiling analogy) along with the corresponding electrical acceleration values existing at the vapor-liquid interface. The $\vec{S}$ values were calculated from Equation (33) with E_{tan_ℓ} equal to zero, and the F/A values given for water are the condenser effect stress values as defined by Markels and Durfee [15,16] and shown by Equation (38). Stress values are given for water and Freon-112 from the present investigation and

TABLE 5

ELECTRICAL INTERFACIAL STRESS AND CORRESPONDING ELECTRICAL ACCELERATION VALUES AT A FLAT VAPOR-LIQUID INTERFACE

Material	Electric Field Intensity, Volts/inch	$\vec{S}$* lb_f/in^2	F/A** lb_f/in^2	Total Interfacial Stress, psi	g_e*** Electrical Acceleration $ft/(sec)^2$
Water	500	5.0×10^{-4}	1.4×10^{-2}	1.405×10^{-2}	0****
	1000	2.0×10^{-3}	5.6×10^{-2}	5.8×10^{-2}	0
	1500	4.5×10^{-3}	12.6×10^{-2}	13.05×10^{-2}	0
	2000	8.1×10^{-3}	22.4×10^{-2}	2.32×10^{-1}	0
	4000	1.9×10^{-2}	89.6×10^{-2}	9.28×10^{-1}	0
Freon-113	121,920 (48KV/cm)	1.6×10^{-2}	-	1.6×10^{-2}	3,498
	243,840 (96KV/cm)	7.6×10^{-2}	-	7.6×10^{-2}	13,992
	426,720 (168KV/cm)	2.3×10^{-1}	-	2.3×10^{-1}	42,850
Freon-112	4000	1.9×10^{-5}	-	1.9×10^{-5}	0****
	8000	7.6×10^{-5}	-	7.6×10^{-5}	0
	11,000	1.5×10^{-4}	-	1.5×10^{-4}	0

*$\vec{S} = \frac{\epsilon_o}{3}(K_\ell - 1)^2 E_{n\ell}^2 \vec{n}_v$ **$F/A = \frac{\epsilon_o}{2} E^2$ $F_{V\ell} = \frac{\epsilon_o}{6}(K_\ell - 1)(K_\ell + 2)\vec{\nabla}E_w^2$

***$g_e = \frac{F_{V\ell}}{\rho_\ell} g_c$ ****The values of g_e are zero for Freon-112 and water by virtue of the fact that the electric field is uniform and $\nabla E^2 = 0$.

TABLE 6

INTERFACIAL STRESS VALUES AROUND A VAPOR BUBBLE IMMERSED IN A BULK LIQUID

Material	Angle, θ	Interfacial Stress, $\vec{S}^*$, lb/in^2			
		500 v./in.	1000 v./in.	1500 v./in.	2000 v./in.
Water	0	3.5×10^{-7}	1.5×10^{-6}	3.2×10^{-6}	8.0×10^{-6}
	10	-1.6×10^{-5}	-6.6×10^{-5}	-1.5×10^{-4}	-2.6×10^{-4}
	20	-6.5×10^{-5}	-2.6×10^{-4}	-5.8×10^{-4}	-1.0×10^{-3}
	30	-1.4×10^{-4}	-5.6×10^{-4}	-1.3×10^{-3}	-2.2×10^{-3}
	40	-2.3×10^{-4}	-9.2×10^{-4}	-2.0×10^{-3}	-3.7×10^{-3}
	45	-2.8×10^{-4}	-1.1×10^{-3}	-2.5×10^{-3}	-4.4×10^{-3}
	50	-3.3×10^{-4}	-1.3×10^{-3}	-2.9×10^{-3}	-5.2×10^{-3}
	60	-4.2×10^{-4}	-1.7×10^{-3}	-3.8×10^{-3}	-6.7×10^{-3}
	70	-4.6×10^{-4}	-1.9×10^{-3}	-4.2×10^{-3}	-7.4×10^{-3}
	80	-5.4×10^{-4}	-2.2×10^{-3}	-4.9×10^{-3}	-8.7×10^{-3}
	90	-5.6×10^{-4}	-2.23×10^{-3}	-5.0×10^{-3}	-8.9×10^{-3}
			48 KV/cm	96 KV/cm	168 KV/cm
Freon-113	0		5.1×10^{-3}	2.0×10^{-2}	6.3×10^{-2}
	10		4.5×10^{-3}	1.8×10^{-2}	5.5×10^{-2}
	20		2.8×10^{-3}	1.1×10^{-2}	3.4×10^{-2}
	30		1.9×10^{-4}	7.4×10^{-4}	2.3×10^{-3}
	40		-3.0×10^{-3}	-1.21×10^{-2}	-3.7×10^{-2}
	45		-4.7×10^{-3}	-1.9×10^{-2}	-5.8×10^{-2}
	50		-6.5×10^{-3}	-2.6×10^{-2}	-7.9×10^{-2}
	60		-9.7×10^{-3}	-3.9×10^{-2}	-1.2×10^{-1}
	70		-1.2×10^{-2}	-4.9×10^{-2}	-1.5×10^{-1}
	80		-1.4×10^{-2}	-5.6×10^{-2}	-1.7×10^{-1}
	90		-1.46×10^{-2}	-5.8×10^{-2}	-1.8×10^{-1}

TABLE 6, Continued

Material	Angle, θ	Interfacial Stress, $\vec{S}^*$, lb_f/in^2 4000 v./in.	8000 v./in.	11,200 v./in.
Freon-112	0	5.3×10^{-6}	2.1×10^{-5}	4.2×10^{-5}
	10	4.7×10^{-6}	1.9×10^{-5}	3.7×10^{-5}
	20	3.0×10^{-6}	1.2×10^{-5}	2.3×10^{-5}
	30	0.35×10^{-6}	0.14×10^{-5}	0.27×10^{-5}
	40	-2.9×10^{-6}	-1.2×10^{-5}	-2.3×10^{-5}
	45	-4.6×10^{-6}	-1.85×10^{-5}	-3.6×10^{-5}
	50	-6.3×10^{-6}	-2.54×10^{-5}	-5.0×10^{-5}
	60	-9.6×10^{-6}	-3.83×10^{-5}	-7.5×10^{-5}
	70	-1.2×10^{-5}	-4.9×10^{-5}	-9.6×10^{-5}
	80	-1.4×10^{-5}	-5.6×10^{-5}	-1.1×10^{-4}
	90	-1.45×10^{-5}	-5.8×10^{-5}	-1.4×10^{-4}

$$\vec{S}^* = \frac{3\epsilon_o (K_\ell - 1)^2 E_o^2}{2(K_v + 2K_\ell)^2} [2K_v^2 \cos^2\theta - K_\ell^2 \sin^2\theta] \vec{n}_v$$

TABLE 7

ELECTRICAL ACCELERATION VALUES IN THE LIQUID ADJACENT TO THE VAPOR-LIQUID INTERFACE OF A BUBBLE AS A RESULT OF AN APPLIED UNIFORM ELECTRIC FIELD

Material	Angle, θ	$\tan \Psi = \frac{(F_V)_r}{(F_V)_\theta}$	g_e^*, ft/sec^2 E = 500 volts/in. r_1=.0907 in. (β_o=90°)	g_e^*, ft/sec^2 E = 500 volts/in. r_1=.0193 in. (β_o=20°)	θ	g_e^*, ft/sec^2 E = 1000 volts/in. r_1=.0907 in. (β_o=90°)	g_e^*, ft/sec^2 E = 1000 volts/in. $r_1$0173 in. (β_o=20°)	g_e^*, ft/sec^2 E = 1500 volts/in. r_1=.0907 in. (β_o=90°)	g_e^*, ft/sec^2 E = 1500 volts/in. r_1=.0173 in. (β_o=20°)	g_e^*, ft/sec^2 E = 2000 volts/in. r_1=.0907 in. (β_o=90°)	g_e^*, ft/sec^2 E = 2000 volts/in. r_1=.0173 in. (β_o=20°)
Water	0	+ ∞	0.42	2.21	0	1.7	8.8	3.8	19.9	6.7	35.4
	10	- .0254	2.1	10.8	10	8.2	43.2	18.5	97.1	32.9	172.7
	20	- .2614	4.0	21.0	20	16.0	83.8	36.0	188.6	64.0	335.3
	30	- .5066	5.7	30.1	30	23.0	120.5	51.7	271.1	91.9	481.9
	40	- .7827	7.5	39.4	40	30.1	157.8	67.7	355.0	120.3	631.0
	45	- .9474	8.3	43.5	45	33.2	173.8	74.6	391.1	132.6	695.3
	50	-1.141	9.0	47.1	50	36.0	188.6	80.9	424.3	143.8	754.3
	60	-1.681	10.2	53.5	60	40.8	213.8	91.8	481.0	163.1	855.2
	70	-2.686	11.1	58.1	70	44.4	232.5	99.8	523.2	177.4	930.1
	80	-5.567	11.6	61.0	80	46.6	244.1	104.8	549.2	186.2	976.4
	90	- ∞	11.8	62.0	90	47.3	247.9	106.4	557.8	189.2	991.7

TABLE 7--Continued

Material	Angle, θ	$\tan \Psi = \frac{(F_V)_r}{(F_V)_\theta}$	g_e^*, ft/sec^2 E = 48 KV/cm. r_1=.03878 in. (β_o=90°)	g_e^*, ft/sec^2 E = 48 KV/cm. r_1=.00739 in. (β_o=20°)	θ	g_e^*, ft/sec^2 E = 96 KV/cm. r_1=.03878 in. (β_o=90°)	g_e^*, ft/sec^2 E = 96 KV/cm. r_1=.00739 in. (β_o=20°)	g_e^*, ft/sec^2 E = 168 KV/cm. r_1=.03878 in. (β_o=90°)	g_e^*, ft/sec^2 E = 168 KV/cm. r_1=.00739 in (β_o=20°)
Freon-113	0	+ ∞	676.2	3,548	0	2,705	14,193	8,284	43,466
	10	3.22	662.4	3,475	10	2,650	13,901	8,114	42,573
	20	1.365	624.2	3,275	20	2,497	13,101	7,646	40,123
	30	0.6152	582.7	3,057	30	2,331	12,228	7,137	37,450
	40	0.1119	568.8	2,984	40	2,275	11,937	6,968	36,557
	45	-0.1146	577.9	3,034	45	2,312	12,134	7,080	37,160
	50	-0.3446	598.2	3,139	50	2,636	12,556	7,328	38,451
	60	-0.8799	662.4	3,476	60	2,650	13,903	8,114	42,577
	70	-1.6116	700.5	3,676	70	2,802	14,704	8,582	45,030
	80	-3.959	802.2	4,209	80	3,209	16,836	9,827	51,560
	90	- ∞	807.9	4,240	90	3,232	16,960	9,897	51,940
			E = 4000 V./in.			E = 8000 V./in.		E = 11,200 V./in.	
Freon-112	0	+ ∞	.700	3.68	0	2.80	14.7	5.49	28.8
	10	3.273	.685	3.59	10	2.74	14.4	5.38	28.1
	20	1.389	.644	3.37	20	2.58	13.5	5.04	26.5
	30	0.632	.600	3.14	30	2.40	12.6	4.70	24.7
	40	0.125	.579	3.06	40	2.32	12.2	4.53	23.9
	45	-0.028	.589	3.08	45	2.36	12.3	4.63	24.2
	50	-0.2998	.600	3.15	50	2.40	12.6	4.70	25.6
	60	-0.8695	.671	3.51	60	2.68	14.0	5.25	27.5
	70	-1.709	.743	3.92	70	2.97	15.7	5.83	30.7
	80	-3.87	.801	4.19	80	3.20	16.8	6.27	32.8
	90	- ∞	.821	4.31	90	3.28	17.2	6.44	33.8

$^*g_e = \frac{F_V}{\rho_\ell} g_c$ ** $^{**}\vec{F}_V = \frac{3E_o^2(K_\ell-1)(K_\ell+2)\epsilon_o}{r_1(K_V+2K_\ell)^2}[(K_\ell-K_V)(2K_V \cos^2\theta - K_\ell \sin^2\theta)\vec{r} + \cos\theta \sin\theta (K_\ell^2-K_V^2)\vec{\theta}]$

TABLE 8

ELECTRICAL ACCELERATION VALUES WITHIN THE SUPERHEATED WATER BOUNDARY LAYER ADJACENT TO A HEATED SURFACE RESULTING FROM APPLICATION OF A UNIFORM ELECTRIC FIELD

q/A BTU/hr/(sq.ft.)	E_o $\frac{\text{volts}}{\text{inch}}$	F_V* lbs_f/ft^3	g_e** ft/sec^2
8,840	500	11.17	6.0
	1000	44.75	24.1
	1500	100.7	54.2
	2000	179.1	96.3
100,000	500	51.2	27.5
	1000	205.1	110.3
	1500	461.7	248.3
	2000	820.7	441.3
164,500	500	87.87	47.3
	1000	351.9	189.2
	1500	792.1	426.0
	2000	1408.2	757.3

*$F_V = \frac{1}{3} \epsilon_o E_o^2 \left(\frac{\partial K}{\partial T}\right)_{x=0} \left(\frac{\partial T}{\partial X}\right)_{x=0} (K_\ell - 1)$

**$g_e = \frac{F_V}{\rho_\ell} g_c$

for Choi's [6] Freon-113 work at electric field intensity values representative of those used in the respective experimental investigations. The electric field intensity values used for the non-uniform electric field Freon-113 work of Choi are those which existed at the heated wire surface. These are the field intensity values used by Choi for calculation of F_V in his work. The electrical acceleration values shown in Table 5 are calculated in the manner described by Choi [6] and discussed previously. As such, since there is no electrical acceleration active when a uniform electric field is employed, there are no g_e values for Freon-112 and water. The condenser effect stresses for water are evaluated assuming the full applied voltage exists across the vapor gap. Since the vapor film thickness (which was calculated from the heat conduction equation using the minimum heat flux (13,000 BTU/(hr)(sq.ft.)) and corresponding ΔT ($\Delta T = 285°F$)) was quite small, the electric field intensity values used in the condenser effect calculations were quite large (i.e., 237,600 volts/in. at 1000 volts/in. electrode field intensity). Although unrealistic, this assumption resulted in the maximum value for the stress caused by the condenser effect. At this condition the condenser effect was of predominant importance and comprised approximately 97% of the total electrical activity. For this assumption it is seen from Table 5, however, that the total interfacial stress for water from the present investigation was comparable in magnitude

to those representative of Choi's Freon-113 investigation, while the stress for Freon-112 from the present investigation was probably several orders of magnitude less. In all cases shown, the stress was directed from liquid to vapor.

The results shown in Table 6 are the interfacial stress magnitudes around a vapor bubble as calculated from Equation (36). Positive values of the stress indicate a stress directed toward the vapor, and negative values indicate a stress directed toward the liquid. No stress caused by the condenser effect is reported here since liquid insulated a large percentage of the bubble interfacial area from the electrically conducting heated surface. Only values of θ, which is defined as shown in Figure E-1, from 0° to 90° are presented, since the stress values on the bottom side of the bubble are symmetric with those on the top. Because of the absence of the condenser effect in this case, the Freon-113 and water stress values differ by a greater degree than for the previous situation. A comparison of Choi's Freon-113 and the present water data is not really valid, however, as no condideration is given to the electric field intensity variation in the former stress calculation, and the Freon-113 bubble does indeed extend over a region in which E changes appreciably for the electrode configuration employed by Choi. From comparison of the Freon-112 and water stress results, both of which were run experimentally with a uniform field, a 1.5 order of magnitude difference at most is

evident. The directional distribution of the stress around the bubble for these two cases is, however, considerably different. While the stress direction reverses in going from 0° to 90° around the bubble, its direction is always normal to the bubble vapor-liquid interface.

The values of g_e shown in Table 7 represent the magnitude of the electrical acceleration around a bubble at $r = r_1$, as calculated from Equations (16) and (37), with K_ℓ assumed to be a constant in Equation (37). The two columns of g_e values listed in Table 7 for each value of field intensity correspond to values calculated for two different values of bubble radii. These two bubble radii were calculated from the bubble departure size correlation of Fritz given in Rohsenow [24], for bubble solid contact angles of 20 and 90 degrees respectively. Since bubble radii were observed to be smaller with the applied electric field, the g_e values shown are conservative. Also given in Table 7 is the direction ($\tan \Psi^*$) at which the g_e vector acted at the bubble interface. Unlike the surface stress, which always acted perpendicularly to the vapor liquid interface, the volume

---

*The angle Ψ represents the angle subtended by the interface normal and the respective F_V vector.

force vectors in the liquid adjacent to the vapor-liquid interface acted at angles other than 90°. The variation of g_e magnitude and direction around the bubbles, combined with the fact that the magnitude of F_V, and thus g_e, decreased along any radial line in the liquid away from the vapor liquid interface (cf. discussion on page 120) resulted in an electrical pumping or electrically induced convection in the liquid in the vicinity of the vapor-liquid interface. Further, since the magnitudes and directions of g_e differ from fluid to fluid, the degree and nature of this electroconvection around generated bubbles at a fixed electric field intensity differed. Comparison of the values of g_e for the three fluids under consideration revealed that the Freon-113 values calculated from Choi's electric field intensity conditions are considerably larger than either the water or Freon-112 values corresponding to the conditions of the present investigation. Again it must be recalled that such a comparison is not warranted since the Freon-113 values are based on an electric field intensity value corresponding to the heated wire radius. It is interesting and informative, however, to compare values of g_e around a vapor bubble of Freon-113 calculated totally on the basis of a uniform electric field intensity variation due to field distortion in the vicinity of the vapor-liquid interface, to g_e values calculated on the basis of an external electrode geometry caused non-uniform electric field

intensity. For these two cases values of the square of the electric field intensity and its gradient which existed at Choi's [6] heated wire surfaces were used. The latter values range from 3,498 ft./sec^2 to 42,850 ft./sec^2 for values of E_w of 48 KV/cm and 168 KV/cm respectively. As seen from Table 7 the Freon-113 g_e values for the smaller bubble ($\beta_o = 20°$) are comparable to the above respective values. This implies that the electroconvection currents around a bubble of Freon-113 in a uniform field of the same magnitude as that existing at the heated wire for Choi's electrode arrangement, is of the same order of magnitude as the electroconvection near the heated surface due to the non-uniform electric field. A comparison of the Freon-112 and water g_e values around a bubble revealed that values for water at 500 volts/in., which was the lowest water electric field intensity studied, were comparable to the values obtained at the highest electric field intensities studied with Freon-112. Again, it must be remembered that the effectiveness of the resulting electroconvection is also dependent on the dirrectional distribution of the g_e values around the bubble, which differs from fluid to fluid. As such, an equivalence of the g_e magnitudes for two materials is not a total indication of electroconvection equivalence for these materials.

As previously mentioned, the values of F_v used to calculate the g_e values in Table 7 were formulated from Equation (26)

assuming that the dielectric constant in the bulk liquid medium was constant. Since the dielectric constant is temperature dependent, any place in the liquid where a temperature gradient existed, a variation of the liquid dielectric constant also existed. When such a continuous variation of temperature exists, as between the heated surface and the saturated fluid, the magnitude of the body force generated solely from a dielectric constant variation is of interest. For the case of a uniform applied electric field, the bulk liquid volume force shown in Equation (26), for the one dimensional case, can be resolved to the following form.

$$F_V = \frac{\epsilon_o}{3} E_o^2 (K_\ell - 1) \left(\frac{\partial K_\ell}{\partial T}\right) \left(\frac{\partial T}{\partial X}\right) \qquad (39)$$

In this expression, E_o is the applied uniform electric field intensity, $\partial K/\partial T$ the dielectric constant variation with temperature, and $\partial T/\partial X$ the temperature gradient. Since the latter term approaches zero as the distance from the heated surface increases, the volume force as given by Equation (39) also approaches zero. Table 8 gives values of g_e, the electrical acceleration, for water at three different heat flux levels as calculated using an F_V value determined from Equation (39). The temperature gradients used were obtained using the measured temperature profiles of Bobst [4] at the respective reported

heat flux levels, and the dielectric constant variation with temperature was obtained by taking the derivative of an equation given in Lange [13]. A comparison of the g_e values in Table 8 shows that as the heat flux increases the value of g_e increases. This reflects the steeper surface temperature gradient at the higher heat fluxes. Calculation of similar values of g_e for Freon were not made since there were no thermal layer temperature profiles available. It is suspected, however, that the values would be considerably smaller since both the dielectric constant and dielectric constant variation with temperature are considerably smaller than corresponding values for water.

Discussion of Results in Terms of Electrical Forces in a Two Phase Media Subjected to an Electric Field

The results of the two previous sections can be summarized as follows:

1) A stress exists on any two phase interface subjected to an electric field. The stress exists in both a uniform and nonuniform electric field, with its magnitude being proportional to the dielectric constants of the two phases and the local electric field intensity in either phase at the interface.
2) A variable electrical acceleration, which gives rise to electroconvection, exists within the superheated boundary layer adjacent to the heated

surface and in the liquid region adjacent to the vapor-liquid interface of a bubble.

3) The electrical acceleration in the thermal layer next to the heated surface increases with increasing heat flux resulting in more effective electroconvection at the higher heat fluxes. The magnitude of the electrical acceleration in the vicinity of a bubble vapor-liquid interface varies inversely with bubble radius indicating that electroconvection is greater for smaller radii bubbles.

4) The condenser effect could be of major importance in the water DC film boiling results.

5) For the most optimistic estimate of condenser effect magnitude, the present water stress values at 500, 1000 and 2000 volts/inch uniform electric field intensity were comparable to Choi's [6] 48, 96 and 168 KV/cm nonuniform field intensity calculated stress values with Freon-113.

6) The interfacial stress values around a bubble were in general an order of magnitude smaller than the flat film values.

7) The electrical acceleration values in the vicinity of a bubble vapor-liquid interface calculated for Freon-113 at conditions representative of Choi's operation, results in values several orders of

magnitude greater than for water and Freon-112 at conditions representative of the present investigation.

To determine what manner the above items affect heat transfer in a pool boiling system, it is well to first recall that in all cases with an applied electric field there is a marked observable effect on the system hydrodynamics. In nucleate boiling a change in bubble size and dynamics is a consistent observation, while in film boiling a marked effect on the stability of the vapor film is a recurring observation. It thus seems quite logical that the manner in which the applied electric field affected the heat transfer in the present study was through an affect on the hydrodynamics, particularly at burnout, in transitional boiling and in film boiling. The importance of hydrodynamics in determining the burnout heat flux and the onset of the stable film boiling regime is well recognized. Expressions, whose development are based on a Helmholtz and Taylor instability criterion, provide the basis for a number of existing general burnout and minimum film boiling heat flux correlations. The problem to consider is thus how the electrical forces might be included with hydrodynamic considerations so that an appropriate expression will be available for predicting burnout heat fluxes and minimum film boiling heat fluxes for the appropriate applied electric field situation. Zuber [35] and others did much of the earlier analytical work to develop general burnout and minimum film

boiling heat flux correlations. A general description of the development can be found in most texts containing a treatise of boiling heat transfer [24, 25, 27]. A more detailed description of the development can be obtained from Zuber's [35] original work, and a publication by Pennington and Bellman [21] on the surface tension and viscosity effects on the Taylor instability. The development basically consists of writing the momentum and continuity equations for both phases which form the interface. The interface itself has an oscillatory motion associated with it which is described by an arbitrary function. The problem is to solve the set of equations with the appropriate boundary conditions and determine under what conditions the associated interface oscillation or disturbance will grow with time. The conditions under which this occurs provides the basis for predicting the occurrence of the instability. Using the hydrodynamic stability criterion developed in this manner, Zuber [35] proceeded on to develop expressions of the following nature for the burnout heat flux and minimum stable film boiling heat flux.

$$(q/A)_{max} = \rho_v h_{fg} C \left[\frac{\sigma(\rho_\ell - \rho_v) g g_c}{(\rho_v)^2}\right]^{\frac{1}{4}} \left[\frac{\rho_\ell}{\rho_\ell + \rho_v}\right]^{\frac{1}{2}} \tag{40}$$

$$(q/A)_{min} = \rho_{vf} h_{fg} \left[\frac{g(\rho_\ell - \rho_v)}{(\rho_\ell + \rho_v)}\right]^{\frac{1}{2}} \left[\frac{g_c \sigma}{g(\rho_\ell - \rho_v)}\right]^{\frac{1}{4}} \tag{41}$$

For the normal gravity pool boiling situation, the term g in the above expression represents the body force due to gravity acting on the fluids. Merte and Clark [20] in their investigations in induced gravity fields found that a peak heat flux expression of

the above nature could be modified by appropriately adjusting the value of g to correlate their data. Choi [6] in his work did essentially the same thing, using the electrical acceleration g_e as defined in Equation (16). As reported by Choi, the data deviates from the one quarter power slope which would be expected from a log plot of Equation (40). If such an approach were used with the uniform electric field work with water and Freon-112, both $(q/A)_{max}$ and $(q/A)_{min}$ would be the same with use of an electric field as without, since for such an arrangement there is no body force. Although no substantial burnout data was taken in this work, it has been demonstrated that $(q/A)_{min}$ is substantially affected by a uniform electric field. The interfacial stress being the only active electrical phenomena, it must be responsible for the effects on the hydrodynamics which caused the observed heat transfer changes.

The idea that interfacial traction or stress is a source of interfacial instability is not actually a new concept. Melcher [19] showed theoretically and experimentally, and Young [32] showed experimentally that a vapor-liquid interface instability could be obtained by application of a uniform electric field. Although the experimental work was not conducted for the boiling heat transfer situation, in view of the importance of hydrodynamics in determining burnout and stabilized film boiling, the implications of the results are also valid in conjunction with the boiling heat transfer process. In the analytical work,

Melcher [19] formulated the surface dynamics in terms of the electrohydrodynamic surface traction or stress, and analyzed the effects of an applied electric field on the stability of the interface for the following cases.

1) An interface stressed by a normal electric field
   a) For no free charge on the boundary
   b) For free charge on the boundary
2) An interface stressed by a tangential electric field.

The conclusions at which Melcher [19] arrived can be summarized as follows:

1) Electrohydrodynamic waves result from the electric field produced interface traction or stress. These waves are fundamental in determining the unstable behavior of a gas-liquid or liquid-liquid interface.
2) The effect of the electrohydrodynamic waves is to slow down the existing surface wave of a given wavelength until the effective phase velocity vanishes and the interface becomes unstable.
3) For the case in which the electric field is perpendicular to the interface, the electric field intensity can always be made large enough to produce an unstable interface. This result is not affected by the absence of boundary charge.
4) An instability occurs for some wavelength for

either electric field-interface configuration
if the lower density material is on the bottom
(e.g. film boiling situation).

Melcher et al [19] conducted a number of experiments to verify some of these results. Young's [32] work also provides a qualitative verification of Melcher's results. Young [32] in addition investigated qualitatively the nature of the instability resulting from use of AC or DC voltage, different types and sizes of electrodes, and the effect of a variable electrode spacing. These results show that the nature and extent of the instability is greatly influenced by some of the parameters which were varied. Thus, while being able to provide a basis for the occurrence of electric field effects on some aspects of boiling heat transfer, being able to predict what effect a given type and magnitude voltage with a given electrode arrangement will have on the heat transfer is impossible.

The effect of the electrohydrodynamic waves, their unique character, and their influence on critical heat flux and stable film boiling was recognized by Choi [6]. He pointed out that the term g in the Zuber correlations represented only the body forces acting on the fluids, and could in no way account for the destabilizing influence of the electrohydrodynamic waves discussed by Melcher [19]. He further reasoned that in the presence of a uniform electric field only the influence of the extraneous electrohydrodynamic waves are apparent, whereas nonuniform electric field

boiling heat transfer results represent a combination of the effects of the electrical body force due to field nonuniformity and the electrohydrodynamic waves. On this basis there is a plausible explanation for the deviation of Choi's burnout results from the 1/4 power dependence on g, and also a basis for interpreting some of the results from the present investigation with a uniform electric field. Since the effect of the electrohydrodynamic waves are of a different nature than the electrically generated body force, and since the effect of the EHD waves differ from fluid to fluid, however, there is no basis for comparison of either calculated values of volume force to stress for the same fluid, or of calculated traction or stress values between fluids unless the fluids to be compared are very similar. An instance of exceedingly similar fluids is that of Freon-112 and Freon-113. As such, a comparison of the interfacial stress values for these two fluids from the data in Table 5 seems justified. As previously discussed, the mean values of interfacial stress shown in Table 5 are for conditions corresponding to the present uniform electric field work with Freon-112 and Choi's nonuniform electric field investigation with Freon-113. As such the Freon-112 experimental results obtained represent the effect of the electrohydrodynamic waves, while the Freon-113 experimental results represent the effects of both electrohydrodynamic waves and an electrical body force. Although the voltages at which the values in Table 5 were calculated are quite different, and thus the stress

values quite different, it should be recalled that a definite surface temperature lowering and film destabilizing influence was observed experimentally with Freon-112. If it were assumed allowable to scale up this experimental phenomena to a corresponding level indicative of the stress value shown in Table 5 for Freon-113, it could be visualized that the electrohydrodynamic wave phenomena, and not the electrical body force, was the major factor in film destabilization in Choi's non-uniform electric field Freon-113 investigation.

In view of some of the calculated results of the previous section, the nucleate boiling data obtained presently and in the past with an applied electric field do not seem unreasonable. As discussed, the effects resulting from the applied electric field on nucleate boiling are:

1) to create an interfacial traction or stress,
2) to induce convection in the vicinity of the heated surface and,
3) to induce convection in the vicinity of the vapor-liquid interface of a forming bubble.

In the film boiling situation a very reasonable and well-documented interpretation of the effect of the interfacial stress is available. An interpretation of the effect of the interfacial traction in terms of electrohydrodynamic waves in nucleate boiling is rather void of meaning, however, since bubble formation

and growth is envisioned more as a thermal problem than as a hydrodynamic stability problem. As such, if promotion of a hydrodynamic instability were the only effect of the interfacial stresses they would probably be of little consequence in nucleate boiling at heat fluxes below the burnout value. The two convective phenomena do, however, have an important interrelated effect on the mechanism of heat transfer in nucleate boiling. Before considering their interrelation it is well to first consider each individually. The electrically induced convection in the thermal boundary region next to a heated surface tends to enhance the heat transfer by actual circulation of superheated fluid away from this thermal layer. As a result of this circulation, the transition region in which the temperature progresses from its heated surface value to the saturated fluid value becomes smaller and the temperature gradient is increased. This condition further enhances heat removal by increasing the heat flow by conduction to the bulk fluid. As seen from the results of Table 8 in the previous section, the electroconvection in the thermal layer from a uniform electric field can be appreciable for water at relatively low electric field intensity values. For many other fluids, while phenomena of the same magnitude can occur, much greater electric field intensity values are required. For such fluids a comparable

degree of thermal layer electroconvection can be achieved much easier by use of a non-uniform electric field as was used by Choi with Freon-113.

The electroconvection which occurs in the vicinity of the liquid-vapor interface of a bubble is very similar in nature to that in the thermal boundary layer, but there are some very important differences. When a bubble of vapor forms at the heated surface the thermal boundary layer is believed to be pushed away from the heated surface in front of the forming bubbles. Substantiation is given to this model of occurrences in bubble growth by the remarkable agreement between experimentally measured bubble growth rates and predicted growth rates developed assuming such a model, as is pointed out by Zuber [35]. From the agreement of this model with experimental measurements it can be concluded that the superheated thermal layer pushed ahead of a bubble makes an important contribution to the total vapor generated during bubble growth. As such, if the superheated layer surrounding the forming bubble is disturbed or destroyed, the vapor generation and bubble growth process are seriously affected. The electrically induced convection in the vapor-liquid interface region of a bubble does precisely this. Further, since the entire liquid thermal layer around the vapor bubble can move, by transport of momentum to

the vapor in the bubble, the convection process around the bubble is much more effective in destroying the thermal layer than in the vicinity of the heated surface where a zero velocity boundary condition is fixed at the stationary solid surface. From this analysis the effect of the electrically induced convection around a bubble is seen to be an increase in the transport of heat in boiling by convection with a corresponding decrease in heat transport by a change of phase. Since smaller bubble size was an observed effect in the electric field boiling work, it is desirable to know if the above description of the effect of an electric field on the heat transfer to bubbles is consistent with this observation. Although no effective model for predicting bubble departure sizes is presently available, the maximum size to which a bubble will grow represents an upper limit for departure size. If the only way the superheated layer is cooled is by evaporation, when equilibrium is established (rate of growth is zero and $T_v = T_\ell = T_{sat}$) more vapor generation has occurred, and a larger bubble size is achieved, than in the case where the thermal layer is cooled by convection as well as vaporization. As such, it is quite logical to expect a smaller bubble size with the applied electric field. Since much agitation and convection is generated by the vapor produced in the boiling situation, the above comparison of degree of convection with and without an applied

electric field occurring in nucleate boiling is really not a valid one. It might more accurately be said that in the case of an applied electric field in addition to the normal convection associated with bubble agitation an electrically induced form of convection also occurs.

The net result of the electroconvection in nucleate boiling is indeed complex. From most experimental results obtained it appears that an applied voltage has little effect on nucleate boiling except at heat fluxes in the vicinity of burnout. A bit of reflection on this matter, however, does lead one to a reasonable explanation for these occurrences. First, at low heat fluxes where the vapor generation is relatively small, and the thermal layer electroconvection next to the heated surface is small, the effects of vapor agitation are probably predominant. The larger bubbles formed without the applied electric field are probably much more effective agitators of the liquid than the smaller bubbles produced with the applied electric field. As such, the increased agitation achieved without the field compensates for the electroconvection which occurs with the electric field. As the heat flux is increased electroconvection in the thermal layer adjacent to the heated surface increases (cf. Table 8), and continues to be of major importance as a mechanism for removing heat from the heated surface. In addition, electroconvection in the vicinity of the vapor bubbles

also becomes more effective. This is a consequence of the inverse dependence of the magnitude of the electrical body force, and thus g_e, in the vicinity of a bubble on the bubble radius. Since at the higher heat fluxes the degree of superheat in the vicinity of the heated surface increases, the initial voids from which bubbles can and will grow becomes smaller. As such, the distribution of voids from which bubbles grow shifts to the smaller size* and bubble electroconvection is enhanced. For the cases of boiling without the applied voltage the effectiveness of increased agitation in promoting convection reaches a maximum and then decreases as the flux is increased. This phenomena, which results from interference of the generated vapor with the flow of liquid to the heated surface, and leads to the boiling crisis (burnout), also occurs in the case of boiling with an applied electric field, but because of the simultaneous occurrence of increasing electroconvection the heat flux at which this condition occurs is forestalled.

From the above discussion, and the results of the analysis and calculations in the previous sections, it thus seems that extension of the nucleate boiling regime to higher heat fluxes, when an electric field is applied, is a result of both electro-

---

*The relationship for the minimum radius from which a bubble can grow is $r=2\sigma/\Delta p$. Since the Δp here can be related to the superheat through the Classius-Clapeyron equation, it is clearly seen that as the superheat increases, r decreases.

convection, which forestalls the vapor crisis, and of an electrically generated interfacial disturbance, which decreases the stability of the vapor film adjacent to the surface and extends the onset of stable film boiling to a much higher heat flux. These phenomena are consistent with the experimental results of the present investigation with a uniform electric field, and the previous non-uniform electric field experimental work. In general, it might be said that the occurrence of electroconvection and electrohydrodynamic waves is independent of the nature of the applied electric field (whether it be uniform or non-uniform), but the extent of these phenomena does depend on the nature of the applied electric field as well as on the dielectric constant of the fluid.

Possible Explanation of DC Polarity Effect on Boiling Heat Transfer to Water

The foregoing analysis provides a basis for explaining many of the observed phenomena in the present as well as past boiling investigations using an applied electric field. The interpretation thus far, however, fails to provide an answer to one very important observation of the present investigation, namely the dependence of DC voltage polarity on the heat transfer result to boiling water. All of the electrical phenomena thus far discussed are independent of polarity. In view of this,

it is well to consider what effect the applied voltage and its polarity might have on some of the known phenomena on which heat transfer in nucleate boiling and the burnout heat flux depend. Two such phenomena which deserve consideration are effects due to the electrolysis of water, and the effects of changes in liquid wettability of the surface as a result of an applied voltage. Should appreciable electrolysis of water have occurred during the voltage application, the hydrogen or oxygen gas generated could have had a tendancy to block or blanket the surface causing premature burnout, as observed with HTS(+) operation with water. However, from applied voltage tests in the boiling system with heated water, but without boiling from the heat transfer surface, there was no visual evidence of electrolysis or gas generation at the heat transfer surface for either polarity. As a result, electrolysis was <u>not</u> considered to be a primary cause of promoting film boiling.

The idea of the occurrence of changes in wettability, basically results from the fact that the experimental water results showed a consistent difference in the manner in which the bubbles nucleated for DC HTS(+) and HTS(-). In particular, the wettability, as evidence by contact angle, was directly related to the polarity. This was consistently observed when the heat transfer surface was otherwise reproducible. The importance of contact angle and wettability on the heat transfer to nucleate

boiling, and in determining the critical heat flux, are unmistakable from this work. An expression relating the contact angle to other physical paramters is provided by the following,

$$\sigma_{sv} - \sigma_{s\ell} = \sigma_{\ell v} \cos \beta \qquad (42)$$

where σ_{sv}, $\sigma_{s\ell}$ and $\sigma_{\ell v}$ are the surface free energies per unit area of the solid-vapor, solid-liquid, and liquid-vapor interfaces (i.e., their surface tensions). The contact angle in this expression relates the adhesion of the liquid to the solid, to the cohesion of the liquid to itself. When the adhesion, $(\sigma_{sv} - \sigma_{s\ell})$, is less than the self-cohesion there is a contact angle which increases as the adhesion decreases ($\beta_o \rightarrow 90°$). When the adhesion is equal to or greater than the cohesion, the angle is zero. Thus, any change in the system which affects any or all of the surface free energies could also bring about a change in the contact angle. While it is impossible to predict how the presence of the electric field will affect the contact angle, which is interrelated to the three surface energies, the existence of interfacial forces due to the electric field undoubtedly affects some of these energies. Since predicting how these energies change for various conditions of applied voltage is a complex problem, predicting how the contact angle changes for an applied electric field and, then, its relation to the heat transfer is

almost an impossible task. Instead of approaching this problem from the standpoint of changing surface energies it is good to consider these effects from the standpoint of the heat transfer surface environment.

In this regard, consider what happens in the fluid when an electric field is applied. Since a fluid is composed of many small dipoles, when an electric field is applied to the fluid these dipoles tend to align themselves with the electric field. This is particularly true of the fluid immediately adjacent to the charge carrying electrical conductor, one of which in the boiling situation is the heated surface itself. This alignment of molecules in the vicinity of the heated surface gives rise to a unique surface situation for each of the two voltage polarities, and for the no voltage situation. Thus, if bubble dynamics are controlled by the surface environment, the fluid at the surface for these three cases is likely different, and as far as the surface is concerned, the situations correspond to boiling three different fluids. While this hypothesis cannot be substantiated at present, the voltage polarity effects observed with water can be satifactorily interpreted from this type of analysis. In the case of boiling water with an applied DC HTS(+) voltage, the effect of the applied voltage is to decrease the wettability of the surface. The effect of the current in the HTS(+) water runs, on the other hand, is to produce an

increased charge accumulation in the vicinity of the surface which tends to destroy or counteract the dipole alignment of molecules and, thus, the non-wetting condition at the heated surface. As the applied voltage is increased, a greater current or charge is required to retort the increased alignment effect of the applied voltage. These facts are clearly shown by the data shown in Figure 19. The DC HTS(+) water film boiling results further substantiate this by also demonstrating a similar current effect. The effects on film stability in these runs appeared the same as with HTS(-) with the only difference being in the wettability characteristics. In DC HTS(+) operation the electric field caused an unstable vapor film situation, however, due to the non-wetting character of the liquid, film collapse could not occur. As the quantity of current was increased the non-wetting nature of the liquid was alleviated and film collapse resulted. While changes in the wettability occurred as a result of DC HTS(-) voltage application with water, the changes were of such a nature as to not cause an obvious result. On this basis, therefore, all electrical phenomena which affect the heat transfer in HTS(+) and HTS(-) operation with water are considered to be the same, except that with HTS(+) the nature of the fluid in the vicinity of the heated surface is such as to cause a problem in terms of surface wetting.

With Freon-112 the electric field effects were not of a magnitude to establish the effects of wettability.

CHAPTER VIII

CONCLUSIONS

The significant conclusions of this work may be summarized as follows.

1) It was experimentally demonstrated that boiling heat transfer behavior could be significantly affected by the presence of a uniform electric field.

2) In the boiling work with water for applied electric field intensities from 500 volts/inch to 2,000 volts/inch it was shown that:

   a) heat transfer in the nucleate boiling regime was significantly affected by application of a DC field but not an AC field,

   b) heat transfer in the film boiling regime was significantly affected by application of both AC and DC electric fields,

   c) the DC voltage effect on the heat transfer in both the nucleate and film boiling regimes was polarity dependent,

   and d) the amperage accompanying the applied DC electric field had an important effect on the heat transfer.

3) In the boiling work with Freon-112 for applied electric field intensities from 2,000 volts/inch to 11,200 volts/inch it was shown that:

   a) neither an AC nor DC electric field affected the heat transfer in the nucleate boiling regime,

and b) both AC and DC electric fields affected the heat transfer in the film boiling regime, but the effects were considerably less than in the water work.

4) Applying a uniform electric field to boiling water or Freon-112 caused visual changes in bubble dynamics and in vapor film stability.

5) The applied uniform electric field results of this investigation are similar in nature to previous non-uniform field results except for the DC polarity effect observed with water in the present investigation.

6) Results of the present investigation cannot be explained on the basis of interpretations set forth to explain previous non-uniform field boiling work.

7) On the basis of past and present experimental electric field boiling results, and electromagnetic and electrofluidmechanic theory, a mechanism of electrofluid interactions in boiling was proposed. This mechanism allowed for a common interpretation of all applied electric field heat transfer results in both nucleate and film boiling regimes.

CHAPTER IX

RECOMMENDATIONS FOR FUTURE WORK

In view of the qualitative nature of the present results it is recommended that continued work be oriented toward quantitative evaluation of the hypothesis put forth. Such studies would include an investigation of bubble dynamics (bubble growth rates, frequencies and departure diamters), a measurement of the temperature profiles in the vicinity of a heated surface, and a study of the wetting characteristics of a boiling fluid all while the boiling fluid is subjected to an electric field.

The results of this work also suggest extension of electrofluidmechanics to other physical operations. The effects of an interface instability and electroconvection due to a changing dielectric constant are particularly suited to be advantageous in mass transfer operations. Within the general area of mass transfer, the phenomena of electroconvection and interface instability would be particularly beneficial in gas-liquid contacting operations, such as wetted walled columns and distillation columns. In such contact operations the concentration gradient would serve as a driving force for electroconvection with a uniform electric field in the same fashion as the temperature

gradient did in boiling. With appropriate contactor design, column efficiency could be improved without the disadvantages of operation at high gas velocities. Further, it may be possible to forestall column flooding in the same way that the burnout heat flux is forestalled in boiling. As far as is known there has been no work initiated along these lines.

BIBLIOGRAPHY

1. Ashmann, G., and Kronig, R., "The Influence of Electrical Fields on the Convective Heat Transfer in Liquids," Appl. Sci. Res., A2, 235-244 (1951).

2. ASTM Designation: 230-36. "Temperature-Electromotive Force (EMF) Tables for Thermocouples," ASTM Standards, 30, 672 (1965).

3. Bird, R. B., Steward, W. E., and Lightfoot, E. N., Transport Phenomena. New York: John Wiley and Sons, Publishers, pp. 330-333 (1963).

4. Bobst, R. W., "Temperature Profiles in the Superheated Boundary Layer Next to a Horizontal Heating Surface in Nucleate Pool Boiling Water," M. S. Thesis, University of Oklahoma (1967).

5. Bonjour, E., Verdier, J., and Weil, L., "Electroconvection Effects on Heat Transfer," Chem. Engr. Prog., 58, No. 7, 63-37 (July 1962).

6. Choi, H. Y., "Electrohydrodynamic Boiling Heat Transfer," Ph.D. Thesis, Massachusetts Institute of Technology (1957).

7. Costello, C. P., and Adams, J. M., "The Interrelation of Geometry, Orientation and Acceleration in the Peak Heat Flux Problem," Mechanical Engineering Department, University of Washington, Seattle, Washington (1962).

8. Gaertner, R. F., "Effect of Surface Chemistry on the Level of Burnout Heat Flux in Pool Boiling," G. E. Research Laboratory Report No. 63-RL-3449C, Schenectady, N. Y. (September 1963).

9. Gaertner, R. F., "Photographic Study of Nucleate Pool Boiling on A Horizontal Surface," Trans. ASME, J. Heat Trans., 17-29, (February, 1965).

10. Hayt, W. H., Jr., Engineering Electromagnetics, New York: McGraw-Hill Book Company (1958).

11. Holmes, R. E., "Condensation of a Dielectric Vapor in the Presence of a Non-Uniform Electric Field," Ph.D. Thesis, Rice University (1967).

12. Hosler, E. R., and Westwater, J. W., "Film Boiling on a Horizontal Plate," ARS Journal, 553-558 (April 1962).

13. Lange, N. A., Handbook of Chemistry, Sandusky, Ohio: Handbook Publishers, Inc. (1949).

14. Markels, M., Jr., and Durfee, R. F., "Effects of Electrical Fields on Boiling Heat Transfer," Summary Report (1960-1963), Atlantic Research Nuclear Corporation, Alexandria, Virginia (1963).

15. Markels, M., Jr., and Durfee, R. F., "The Effect of Applied Voltage on Boiling Heat Transfer," Preprint 157, A.I.Ch. E., 55th Annual Meeting, Chicago (December 1962).

16. Markels, M., Jr., and Durfee, R. L., "Studies of Boiling Heat Transfer with Electrical Fields, Parts I and II." Preprint 38a, A.I.Ch.E., 57th Annual Meeting, Boston (December 1964).

17. McAdams, W. H., Heat Transmission, New York: McGraw-Hill Book Company, 368-410 (1954).

18. McAdams, W. H., Addams, J. H., Rinaldo, P. M., and Day, R. S., "Heat Transfer from Single Horizontal Wires to Boiling Water," Chem. Engr. Prog., 44, 8, 639-647 (August 1948).

19. Melcher, J. R., "Plasma Magnetohydrodynamics and Energy Conversion: Electrohydrodynamic and Magnetohydrodynamic Surface Waves and Instabilities," Quarterly Progress Report No. 61, Research Laboratory of Electronics, MIT, Cambridge, Mass. (April 1961).

20. Merte, H., and Clark, J. A., "Pool Boiling of an Accelerating System," Trans. ASME, J. Heat Transfer, 233-242 (August 1961).

21. Pennington, R. H., and Bellman, R., "Effects of Surface Tension and Viscosity on Taylor Instability," Quarterly Appl. Math. 12, 2, 151-162 (1951).

22. Pohl, H. A., "The Motion and Precipitation of Suspensoids in Divergent Electric Fields," J. Appl. Phys. 22, 7, 869-872 (July 1951).

23. Pohl, H. A., "Some Effects of Non-Uniform Fields on Dielectrics," J. Appl. Phys., 29, 8, 1182-89 (August 1958)

24. Rohsenow, W. M., Developments in Heat Transfer, Cambridge, Mass.: The MIT Press, pp. 169-253 (1964).

25. Rohsenow, W. M., and Choi, H. Y., Heat, Mass and Momemtum Transfer, Englewood Cliffs, N. J.: Prentice-Hall, Inc., pp. 211-236 (1961).

26. Stratton, J. A., Electromagnetic Theory, New York: McGraw-Hill Book Co., Inc. (1941).

27. Tong, L. S., Boiling Heat Transfer and Two Phase Flow, New York: John Wiley and Sons, Inc. (1965).

28. Velkoff, H. R., "Electrofluidmechanics: A Study of Electrokinetic Action in Fluids," Propulsion Laboratory Technical Report, No. ASD-TR-61-642, Wright-Patterson Air Force Base, Ohio (February 1962).

29. Velkoff, H. R., and Miller, J. H., "Condensation of Vapor on a Vertical Plate with a Transverse Electrostatic Field," Paper No. 64-HT-13, Trans. ASME, J. Heat Transfer (1964).

30. Von Hippel, A. R., Dielectrics and Waves, New York: John Wiley and Sons, Publishers (1954).

31. Whitmer, R. M., Electromagnetics, New York: Prentice-Hall, Inc. (1954).

32. Young, J., B.S. Thesis, Mechanical Engineering Department, Tufts University (1960).

33. Young, R. K., and Hummel, R. L., "Improved Nucleate Boiling Heat Transfer," Chem. Engr. Prog., 60, 7, 53-58 (July 1964).

34. Zisman, W. A., "Contact Angle, Wettability and Adhesion: Relation of the Equilibrium Contact Angle to Liquid and Solid Constitution," ACS Advances in Chemistry Series, No. 43 (1964).

35. Zuber, N., "Hydrodynamic Aspects of Boiling Heat Transfer," Ph.D. Thesis, University of California, Los Angeles (1959).

APPENDIX A

INSTRUMENT CALIBRATION, DATA REDUCTION, AND ERROR LIMITS ON EXPERIMENTAL WORK

INSTRUMENT CALIBRATION, DATA REDUCTION, AND ERROR LIMITS ON EXPERIMENTAL WORK

Instrument Calibration

The instruments requiring calibration were the AC and DC voltmeters for the high voltage source, the heater ammeter and voltmeters, conduction block thermocouples and the heat transfer surface thermocouples.

The DC voltmeter for the high voltage source was calibrated with a Fluke Model-885-AB standard differential voltmeter. The heater voltmeter and ammeter were also calibrated against the Fluke standard differential voltmeter. The high voltage AC voltmeter had to be calibrated in place, since it was connected across a portion of the stabilization resistance. Calibration was made with a Simpson Model 260, Series 3, volt-ohm-milliammeter which had been factory-calibrated to one percent. A calibration curve was obtained up to 1000 volts using the 1000 volt scale on the Simpson meter. This calibration was reproduced on the 5000 volt scale on the Simpson meter. The AC meter was calibrated up to 4000 volts. The 0-250

milliampere DC ammeter used in the high voltage circuitry was calibrated with a Leeds and Northrup Model K-3 potentiometer. The corresponding AC ammeter was calibrated against a 0-500 milliampere AC ammeter which had been calibrated to one percent accuracy.

All thermocouples were calibrated in place at room temperature, 170 and 300°F. The 170 and 300°F calibrations were accomplished by covering the heater surface with perlite and by regulating the system heater. At room temperature all thermocouples read within 0.5°F of a thermometer which was graduated in 0.1°F increments. At 170°F and 300°F no standard was used, so that the exact temperature was not known, but all the thermocouples read within 1.0°F of each other. Since it was only necessary to obtain temperature differences from the conduction block thermocouples, it was not necessary to know the exact absolute temperature of these thermocouples. The heat transfer surface thermocouples were calibrated at the boiling temperatures of Freon-112 and water and at room temperature. Standard table values were subsequently used since agreement was within 1°F.

Data Reduction

A computer program was utilized to reduce the raw data. The input consisted of readings from the fifteen conduction

block thermocouples, the bulk phase thermocouple, the two heat transfer surface thermocouples, and the bulk liquid thermometer temperature as well as the power dissipated in the heater as obtained from the heater current-voltage measurements. The thermocouple EMFs were converted to temperatures by means of a Lagrangian interpolation [2]. Six temperature differences (each referred to as ΔT_{CB}) were obtained from the temperatures in the conduction block. These temperature differences were between the top and botoom thermocouples at six different locations in the conduction block. The distance between thermocouples was ½ inch as is shown in Figure 9.

The boiling surface heat flux was calculated from Fourier's Law using an average conduction block temperature difference and a thermal conductivity for copper at the average conduction block temperature. Deviations of the individual temperature differences from the average value were calculated and served as some indication of the uniformity of heat flux over the heat transfer surface. The surface ΔT was the difference between the heat transfer surface temperature and the bulk phase temperature.

Error Limits on Experimental Work

The accuracy of the high voltage source (HVS) electical

measurements reported in this work can be summarized as follows:

a.) The AC and DC voltages were accurate to within ±5 percent.

b.) The DC amperage readings were accurate to within ±3 milliamperes of the value reported.

c.) The AC amperage readings were accurate to within ±5 milliamperes of the reported values.

The accuracy of the reported heat flux values* was affected by two factors, namely, the accuracy of the conduction block thermocouple calibration and the degree of uniformity of the heat flux over the complete heat transfer surface. While it is difficult to evaluate the individual effect of these two factors the maximum percent deviation of the six conduction block temperature differences (ΔT_{CB}s) from the average value represented a lumped value for both of these effects. For the nucleate boiling work, the maximum percent deviation of the ΔT_{CB}s ranged from 4 to 15 percent with the lower limit being obtained at the higher heat fluxes. In

---

* The reported value of the heat flux was in all cases the value calculated from Fourier's Law using the average of the six conduction block temperature differences, $(\Delta T_{CB})_{avg}$.

film boiling, where the conduction block temperature differences were of the order of 2 to 4°F, the maximum percent ΔT_{CB} deviation ranged as high as 30 percent. At these low conduction block temperature differences, the 1°F difference which was found to exist between all the conduction block thermocouples in the calibration work was the significant effect on the ΔT_{CB} variation. This same situation occurred at a low heat flux in nucleate boiling. If it is assumed that the conduction block thermocouple calibration error is random (equally distributed about a mean value), as should be the case, the reported average value of the heat flux in the film boiling and low nucleate boiling runs are of considerably greater accuracy than indicated by the percent ΔT_{CB} deviation value.

The accuracy of the temperature difference between the heat transfer surface and the saturated fluid, ΔT, was dictated by the error in the surface thermocouple readings, which were used for the reported ΔTs in all cases. In the low nucleate boiling and the film boiling regions the accuracy of the ΔTs was basically that of the surface thermocouple calibration, that is within one degree of the reported values. In these regions of boiling, the surface temperature extrapolated from the conduction block thermocouple located

directly beneath the surface thermocouple was also within one degree of the surface thermocouple reading. In the main portion of the nucleate boiling region, the surface thermocouple readings were at times five to eight degrees lower than the value extrapolated from the conduction block thermocouple. Since this phenomena was not consistently experienced, system changes over which little control could be exercised (i.e., surface condition) were felt to be responsible. The occurence of this phenomena undoubtedly accounted for some of the scatter in the nucleate data obtained in this work.

APPENDIX B

TABLES OF DATA

B-1

TABLE 1-B

TIME HISTORY PREMATURE BURNOUT RUNS WITH WATER

Date of Run	Heat Flux Btu/(hr) (sq.ft.)	Time, Minutes	Surface Temp., °F	Temperature Increase
9-14-66	98,000	0	224.5	0
		26	--	--
		58	228.4	3.9
		87	228.9	4.4
		111	229.5	5
		141	231.9	7.4
		178	Film	--
9-22-66	78,000	0	228.2	0
		70	230.2	2
		100	230.3	2.1
		155	231.8	3.6
		198	233.1	4.9
		245	233.7	5.5
		300	236.3	8.1
		315	237.5	9.3
		324	Film	--
9-16-66	74,000	0	228.1	0
		38	229.3	1.2
		93	230.0	1.9
		153	230.8	2.7
		223	232.6	4.5
		283	233.1	5.0

TABLE 1-B--Continued

Date of Run	Heat Flux Btu/(hr) (sq.ft.)	Time, Minutes	Surface Temp., °F	Temperature Increase
9-16-66	74,000	316	233.7	5.6
		364	234.3	6.2
		408	234.8	6.7
		458	235.8	7.7
		493	Film	
9-21-66	31,000	0	226.2	0
	42,000	5	--	--
		35	227.5	1.3
		65	228.1	1.9
		135	229.2	3.0
	62,000	140	--	--
		155	231.2	5.0
		188	231.5	5.3
		215	231.8	5.6
		230	231.2	5.0
	82,000	235	--	--
		250	232.7	5.5
		280	234.2	8.0
		310	234.4	8.2
	102,000	315	--	--
		328	Film	Film

TABLE 2-B

NUCLEATE AND FILM BOILING HEAT TRANSFER DATA FOR WATER (INITIAL SYSTEM TEST DATA)

Date of Run	Heat Flux Btu/(hr) (sq.ft.)	ΔT °F	Surface Temp., °F	Line Out Time, Minutes	Maximum % Deviation of Heat Flux From the Avg. Value
11-1-66	8,800	11.8	222.7	68	13.15
11-1-66	9,100	11.8	222.7	123	15.92
11-1-66	9,200	11.8	222.8	41	16.98
11-2-66	17,500	17.1	228.1	95	11.07
11-23-66	17,800	13.8	224.1	115	13.97
10-29-66	21,900	17.7	228.7	79	12.89
10-31-66	27,700	17.2	228.7	105	9.88
10-29-66	42,100	16.7	227.6	72	10.17
11-1-66	51,600	20.3	231.4	112	7.86
11-22-66	52,400	20.3	230.6	100	6.59
12-15-66	59,000	21.2	232.1	73	12.25
1-5-67	59,100	20.1	230.1	97	13.79
12-5-66	59,800	21.3	231.5	120	5.28
12-10-66	60,300	21.8	233.0	75	10.33
10-31-66	65,100	18.2	228.6	160	7.65
10-29-66	65,400	17.7	228.7	61	14.20
10-18-66	74,200	20.7	231.2	85	14.67
10-13-66	78,300	20.4	230.2	120	5.71
12-19-66	86,800	23.4	234.0	130	13.01
1-5-67	87,000	22.7	233.1	150	12.61
10-29-66	89,600	19.4	230.4	71	8.36
11-17-66	94,300	21.4	231.9	120	8.58

TABLE 2-B--Continued

Date of Run	Heat Flux Btu/(hr) (sq.ft.)	ΔT °F	Surface Temp., °F	Line Out Time, Minutes	Maximum % Deviation of Heat Flux From the Avg. Value
11-1-66	105,000	21.5	232.6	61	5.93
10-13-66	108,200	21.4	231.2	90	5.86
11-22-66	112,500	25.8	236.2	81	4.94
10-29-66	116,200	20.5	231.5	45	6.19
12-10-66	128,900	27.0	238.2	110	9.77
10-18-66	130,600	23.9	234.3	74	9.59
11-1-66	131,100	23.3	234.3	42	6.74
10-29-66	248,600	22.9	233.9	102	6.43
10-31-66	153,000	22.3	232.7	62	7.71
11-1-66	163,600	24.0	235.0	47	5.37
10-31-66	183,700	23.6	234.0	52	7.63
10-18-66	191,700	24.9	235.3	57	4.04
12-5-66	193,500	21.9	231.9	85	3.44
11-1-66	195,900	24.3	235.3	35	4.73
10-13-66	196,000	26.8	236.7	75	10.66
12-5-66	212,900	20.0	230.0	40	11.02
10-31-66	218,000	24.5	234.9	61	5.75
10-31-66	222,500	24.6	235.0	61	8.57
11-17-66	29,700	259.8	470.3	60	26.73

TABLE 3-B

NUCLEATE AND FILM BOILING HEAT TRANSFER DATA FOR WATER (DATA TAKEN PRIOR TO VOLTAGE APPLICATION IN ELECTRIC FIELD RUNS)

Date of Run	Heat Flux Btu/(hr) (sq.ft.)	ΔT °F
5-20-67	2,000	3.7
5-23-67	3,770	4.3
5-20-67	4,980	6.6
5-23-67	6,100	6.6
5-20-67	9,100	8.7
5-25-67	10,750	8.9
5-18-67	11,210	13.2
5-20-67	14,800	10.5
5-18-67	18,400	9.1
9-16-66	21,230	15.9
10-29-66	21,900	17.7
9-21-66	26,820	15.7
10-31-66	27,700	17.2
9-15-66	31,400	15.9
9-23-66	33,700	14.7
10-29-66	42,100	16.7
9-18-66	43,200	17.3
3-15-67	51,500	16.4
11-1-66	51,600	20.3
11-22-66	52,400	20.3
5-17-67	61,000	16.2
1-30-67	66,400	18.9
1-31-67	66,500	18.9
2-13-67	66,700	15.4

TABLE 3-B--Continued

Date of Run	Heat Flux Btu/(hr) (sq.ft.)	ΔT °F
2-13-67	69,100	15.9
1-23-67	73,500	19.4
1-23-67	74,000	18.1
3-16-67	81,100	16.2
3-7-67	82,800	19.9
3-14-67	83,300	19.0
3-14-67	84,300	17.7
10-29-66	89,600	19.4
10-29-66	89,600	19.4
5-17-67	91,300	13.7
3-15-67	92,000	15.6
10-13-66	108,200	21.4
6-20-67	109,300	16.2
6-15-67	116,100	17.3
1-23-67	117,600	21.7
6-9-67	118,100	14.3
1-31-67	120,300	21.0
6-1-67	120,700	14.8
1-31-67	122,000	20.8
1-31-67	122,000	21.5
1-25-67	122,700	20.4
2-13-67	123,500	21.6
12-10-66	126,900	17.7
3-7-67	127,000	20.8
4-12-67	129,700	15.7
10-18-66	130,600	23.9
3-6-67	142,000	22.7

TABLE 3-B--Continued

Date of Run	Heat Flux Btu/(hr) (sq.ft.)	ΔT °F
6-19-67	142,700	18.9
5-29-67	145,000	14.9
5-22-67	145,200	17.4
5-19-67	145,400	18.1
5-31-67	146,500	14.3
5-22-67	147,100	15.0
3-14-67	148,000	15.0
10-29-66	148,600	22.9
6-15-67	148,600	17.1
6-9-67	149,100	14.8
5-23-67	149,900	16.3
3-16-67	150,000	19.3
10-31-67	153,000	22.3
4-26-67	159,700	16.6
5-17-67	164,200	19.6
6-1-67	165,200	14.6
6-19-67	167,800	19.4
6-13-67	172,600	16.6
5-26-67	174,600	17.1
5-26-67	176,200	16.8
5-26-67	176,200	17.1
5-25-67	176,800	15.1
10-31-66	183,700	23.6
5-19-67	186,800	20.6
6-10-67	188,000	17.8
4-26-67	189,100	17.1

TABLE 3-B--Continued

Date of Run	Heat Flux Btu/(hr) (sq.ft.)	ΔT °F
6-20-67	191,100	18.3
10-18-66	191,700	24.9
12-5-66	193,500	21.9
11-1-66	195,900	24.3
10-13-66	196,000	26.8
12-5-66	212,900	20.0
5-26-67	215,000	16.6
5-29-67	217,100	16.4
10-31-66	222,500	24.6
5-19-67	229,300	21.4
5-22-67	15,200	248.1
5-23-67	16,100	255.9
5-31-67	16,160	301.7
6-1-67	16,400	320.8
6-10-67	16,460	275.3
6-13-67	17,000	238.1
6-15-67	29,900	206.6
6-19-67	28,000	228.9
6-20-67	23,800	226.8
5-17-67	13,800	287.7
5-26-67	16,230	333.0
5-29-67	16,740	312.5
6-10-67	18,900	271.6
6-14-67	24,300	209.3
6-19-67	26,500	244.6
6-20-67	26,900	222.5

TABLE 4-B

DATA TAKEN TO TEST THE EFFECT OF THE GRID ELECTRODE ON THE HEAT TRANSFER

Heat Flux Btu/(hr) (sq.ft.)	ΔT °F	Electrode and Electrode Spacing
121,000	22.27	No Electrode
116,200	20.47	No Electrode
67,800	19.95	No Electrode
78,300	20.38	No Electrode
65,100	18.18	No Electrode
66,400	18.88	Fine Grid at ¼-Inch Spacing
65,000	18.12	Fine Grid at ¼-Inch Spacing
122,200	21.53	Fine Grid at ¼-Inch Spacing
120,300	21.00	Fine Grid at ¼-Inch Spacing

TABLE 5-B

DC-VOLTAGE NUCLEATE BOILING WATER DATA

A. Data Taken With HTS(+)* Which Did Not Result In Film Boiling

Date of Run	Applied Voltage	Heat Flux Btu/(hr.)(sq.ft.)	Non-Field ΔT, °F	Grid Spacing, Inches	Grid**	% Surface Temp. Lowered	Field Current Milliamperes	Voltage Duration, Minutes
1-29-67	500	74,000	18.1	1	FG	8.8	26	30
1-23-67	500	120,000	21.7	1	FG	26.8	58	27
3-14-67	500	84,200	17.7	1	FG	9.1	23	14
4-12-67	500	81,000	17.1	1	FG	12.9	28	19
6-14-67	500	155,000	28.1	1	CG	10.4	32	50
6-19-67	500	167,800	19.8	¼	CG	9.5	32.5	9.5
3-15-67	500	51,500	16.5	1	FG	9.7	22	16
3-16-67	500	90,000	16.2	1	FG	13.6	22	20
4-12-67	500	128,700	15.7	1	FG	2.6	14	20
5-17-67	500	61,500	16.2	1	FG	-1.8+	15	6
5-17-67	1000	61,500	16.2	1	FG	-2.5+	40	8
2-13-67	1000	68,000	15.9	¼	CG	21.4	90.5	22
3-14-67	1000	84,200	17.7	1	FG	12.4	49	15
4-12-67	1000	81,000	17.1	1	FG	15.8	65	20
6-14-67	1000	155,900	28.1	1	FG	12.9	62.5	18

TABLE 5-B--Continued

B. Data Taken With HTS(+)* In Which Film Boiling Resulted

Date of Run	Applied Voltage	Heat Flux Btu/(hr.)(sq.ft.)	Non-Field ΔT, °F	Grid Spacing, Inches	Grid**	% Surface Temp. Lowered	Field Current Milliamperes	Voltage Duration, Minutes
6-20-67	500	109,200	17.1	¼	CG	F±	26.5	16.0
6-15-67	500	116,100	17.3	¼	CG	F	31.5	24.5
6-19-67	500	142,700	18.7	¼	CG	F	26	7.5
6-20-67	500	191,100	18.3	¼	CG	F	18.5	1.75
1-31-67	1000	122,000	21.5	¼	FG	F	52	2.0
3-7-67	500	80,000	20.5	1	CG	F	22	13
3-14-67	500	83,300	19.0	1	FG	F	17	6
5-17-67	500	91,300	13.7	1	FG	F	12	16
5-22-67	500	145,200	17.4	1	FG	F	17	19.2
5-31-67	500	146,500	14.3	1	CG	F	16.5	8.67
6-1-67	500	165,200	14.5	1	CG	F	7.5	7.12
5-25-67	500	176,800	15.1	1	FG	F	10.5	3.0
6-10-67	500	188,000	16.2	1	CG	F	11	3.0
4-26-67	500	189,100	17.1	1	FG	F	10	3.0
6-13-67	500	235,500	14.8	1	CG	F	16	0.75
4-12-67	1000	129,700	15.7	1	FG	F	35	28
5-22-67	1000	147,100	15.0	1	FG	F	22.5	3.4
5-26-67	1000	174,600	16.8	1	FG	F	20.5	2.0

TABLE 5-B--Continued

Date of Run	Applied Voltage	Heat Flux Btu/(hr.) (sq.ft.)	Non-Field ΔT, °F	Grid Spacing, Inches	Grid**	% Surface Temp. Lowered	Field Current Milliamperes	Voltage Duration, Minutes
5-23-67	1500	149,900	16.3	1	FG	F	37.5	5.1
5-26-67	1500	176,200	17.1	1	FG	F	28	0.67
C. Data Taken With HTS(-)*								
12-5-66	60	59,000	21.3	1	FG	55.9	95	20
12-10-66	220	60,300	21.8	1	FG	16.1	30	20
12-10-66	220	128,000	27.0	1	FG	9.2	29	13
1-30-67	500	66,500	18.9	¼	FG	3.2	20	34
1-31-67	500	122,000	21.5	¼	FG	3.7	19	25
3-15-67	500	92,000	15.6	1	FG	26.3	40	5
3-16-67	500	150,000	19.3	1	FG	19.3	35	10
1-30-67	1000	66,500	18.9	¼	FG	6.9	39	19
1-31-67	1000	122,000	21.5	¼	FG	4.2	36	30
1-31-67	1500	122,000	21.5	¼	FG	8.4	70	12

* HTS(+) = Heat transfer surface of positive polarity
HTS(-) = Heat transfer surface of negative polarity

** FG = Fine grid and CG = Coarse Grid

\+ A negative percent surface temperature lowering represents an increase in the surface temperature.

± F = Indication that film boiling resulted. The time stated for duration of applied voltage represents the length of time the voltage was applied till film boiling resulted.

TABLE 6-B

TEMPERATURE HISTORY FOR DC-HTS(+) FILM BOILING
PROMOTED RUNS SHOWN IN TABLE 5-B

Date of Run	Time From Voltage Application, Minutes	Surface Temp., °F	Field Current Milliamp.	Applied Voltage	Heat Flux Btu/(hr.) (sq.ft.)
4-12-67	0	225.2	33	1000 DC	129,700
	4	225.55	34	1000 DC	129,700
	9	226.7	34	1000 DC	129,700
	11	227.8	35	1000 DC	129,700
	13	228.9	35	1000 DC	129,700
	15	231.1	35	1000 DC	129,700
	16	235.8	35	1000 DC	129,700
	18	253.3	35	1000 DC	129,700
	19	261.5	35	1000 DC	129,700
	22	274.4	35	1000 DC	129,700
	24	286.0	35	1000 DC	129,700
	27	343.7	35	1000 DC	129,700
	28	Film	--	1000 DC	129,700
5-22-67	0	228.9	14	500 DC	145,200
	0.5	228.3	14	500 DC	145,200
	1	228.3	14	500 DC	145,200
	2	228.0	14	500 DC	145,200
	3	227.9	14	500 DC	145,200
	4	227.7	14	500 DC	145,200

TABLE 6-B--Continued

Date of Run	Time From Voltage Application, Minutes	Surface Temp., °F	Field Current Milliamp.	Applied Voltage	Heat Flux Btu/(hr.) (sq.ft.)
5-22-67	5	227.6	14	500 DC	145,200
	6	227.6	16	500 DC	145,200
	8	227.6	16	500 DC	145,200
	9	227.4	16	500 DC	145,200
	11	227.1	18	500 DC	145,200
	13	227.0	19	500 DC	145,200
	15	226.8	20	500 DC	145,200
	17	227.0	20	500 DC	145,200
	19	227.6	21	500 DC	145,200
	19.16	Film	--	500 DC	145,200
5-23-67	0	227.1	26	1500 DC	149,900
	1	226.2	31	1500 DC	149,900
	2	226.0	35	1500 DC	149,900
	3	225.8	38	1500 DC	149,900
	4	225.8	44	1500 DC	149,900
	5	229.6	49	1500 DC	149,900
	5.1	Film	--	1500 DC	149,900
5-22-67	0	225.7	22	1000 DC	147,100
	1	225.3	23	1000 DC	147,100
	2	225.4	23	1000 DC	147,100
	3	225.7	23	1000 DC	147,100

TABLE 6-B--Continued

Date of Run	Time From Voltage Application, Minutes	Surface Temp. °F	Field Current Milliamp.	Applied Voltage	Heat Flux Btu/(hr.) (sq.ft.)
5-22-67	3.4	Film	--	1000 DC	147,100
5-25-67	0	225.7	10	500 DC	176,800
	0.5	225.4	10	500 DC	176,800
	1	225.2	11	500 DC	176,800
	1.5	225.1	11	500 DC	176,800
	2	225.0	11	500 DC	176,800
	2.5	225.0	11	500 DC	176,800
	3	Film	--	500 DC	176,800
5-26-67	0	228.0	20	1000 DC	174,600
	0.5	227.6	20	1000 DC	174,600
	1	227.0	21	1000 DC	174,600
	1.5	226.8	21	1000 DC	174,600
	2	Film	--	1000 DC	174,600
5-31-67	0	223.1	15	500 DC	146,500
	0.5	223.3	14	500 DC	146,500
	1	223.3	14	500 DC	146,500
	1.5	223.5	14	500 DC	146,500
	2	223.7	14	500 DC	146,500
	2.5	223.7	14	500 DC	146,500
	3	223.7	14	500 DC	146,500

TABLE 6-B--Continued

Date of Run	Time From Voltage Application, Minutes	Surface Temp., °F	Field Current Milliamp.	Applied Voltage	Heat Flux Btu/(hr.) (sq.ft.)
5-31-67	4	223.7	14	500 DC	146,500
	6	223.7	16	500 DC	146,500
	7	223.7	19	500 DC	146,500
	8	224.2	19	500 DC	146,500
	8.67	Film	--	500 DC	146,500
6-1-67	0	225.4	8	500 DC	162,500
	.5	225.5	8	500 DC	162,500
	1	225.8	8	500 DC	162,500
	1.5	226.0	7	500 DC	162,500
	2	226.2	7	500 DC	162,500
	3	226.1	7	500 DC	162,500
	4	226.1	7	500 DC	162,500
	6.5	226.9	7	500 DC	162,500
	7.1	Film	--	500 DC	162,500
6-15-67	0	226.3	41	500 DC	116,100
	2	226.1	41	500 DC	116,100
	5	226.2	35	500 DC	116,100
	7	226.6	35	500 DC	116,100
	11	227.0	35	500 DC	116,100
	17	228.3	31	500 DC	116,100
	20	229.5	31	500 DC	116,100

TABLE 6-B--Continued

Date of Run	Time From Voltage Application, Minutes	Surface Temp., °F	Field Current Milliamp.	Applied Voltage	Heat Flux Btu/(hr.) (sq.ft.)
6-15-67	22	230.9	26	500 DC	116,100
	23	232.1	26	500 DC	116,100
	24	240.5	26	500 DC	116,100
	24.5	Film	--	500 DC	116,100
6-19-67	0	229.3	20	500 DC	142,700
	1.5	228.9	21	500 DC	142,700
	2	229.2	26	500 DC	142,700
	4	228.9	33	500 DC	142,700
	6	227.75	32	500 DC	142,700
	7	232.7	32	500 DC	142,700
	7.5	Film	--	500 DC	142,700
3-7-67	0	230.4	22	500 DC	80,000
	8	229.1	22	500 DC	80,000
	11	230.95	22	500 DC	80,000
	13	Film	--	500 DC	80,000
3-14-67	0	229.45	16	500 DC	83,300

TABLE 6-B--Continued

Date of Run	Time From Voltage Application, Minutes	Surface Temp., °F	Field Current Milliamp.	Applied Voltage	Heat Flux Btu/(hr)(sq.ft.)
3-14-67	1	227.9	17	500 DC	83,300
(cont.)	5	228.7	17	500 DC	83,300
	6	Film	--	500 DC	83,300
5-17-67	0	224.55	10	500 DC	91,300
	1	225.1	10	500 DC	91,300
	3	224.95	10	500 DC	91,300
	7	224.7	13	500 DC	91,300
	10	224.7	14	500 DC	91,300
	16	Film	--	500 DC	91,300
6-10-67	0	226.2	11	500 DC	188,000
	0.5	226.2	11	500 DC	188,000
	2	226.8	11	500 DC	188,000
	3	Film	--	500 DC	188,000
6-20-67	0	228.35	18	500 DC	191,000
	1	227.8	19	500 DC	191,000
	1.75	Film	--	500 DC	191,000

TABLE 6-B--Continued

Date of Run	Time From Voltage Application, Minutes	Surface Temp., °F	Field Current Milliamp.	Applied Voltage	Heat Flux Btu/(hr) (sq.ft.)
6-20-67	0	227.45	24	500 DC	109,200
	0.5	227.3	24	500 DC	109,200
	4.5	226.6	24	500 DC	109,200
	9.5	226.4	29	500 DC	109,200
	16	Film	--	500 DC	109,200
6-13-67	0	223.9	16	500 DC	235,500
	0.75	Film	--	500 DC	235,500
1-31-67	0	231.5	52	1000 DC	122,000
	2	Film	--	1000 DC	122,000
4-26-67	0	227.9	10	500 DC	189,100
	3	Film	--	500 DC	189,100
5-26-67	0	227.8	28	1500 DC	176,200
	0.67	Film	--	1500 DC	176,200

TABLE 7-B

PERTINENT DC-HTS(-) NUCLEATE BOILING HISTORY DATA

A. Temperature History for Typical DC-HTS(-) Runs (Electrode Spacing = ¼ inch, Coarse Grid)

Date of Run	Time, Minutes	Surface Temp., °F	Field Current Milliamp.	Applied Voltage	Heat Flux Btu/(hr.)(sq.ft.)
1-30-67	0	228.8	24	500	66,500
	4	228.85	22	500	66,500
	18	228.5	18	500	66,500
	29	228.4	19	500	66,500
	34	228.4	40	1000	66,500
	36	227.8	37	1000	66,500
	50	227.7	38	1000	66,500
1-31-67	0	231.7	22	500	122,000
	2	231.3	21	500	122,000
	5	231.1	19	500	122,000
	18	230.9	19	500	122,000
	26	230.9	36	1000	122,000
	27	230.7	35	1000	122,000
	44	230.85	36	1000	122,000
	51	230.85	36	1000	122,000
	56	230.85	73	1500	122,000
	58	230.0	68	1500	122,000
	68	231.0	69	1500	122,000

TABLE 7-B--Continued

B. Test Run to Establish Nature of DC-HTS(-) Voltage Effect on Heat Transfer to Nucleate Boiling Water (Coarse Grid Electrode at 1-inch Spacing)

Date of Run	Time, Minutes	Surface Temp., °F	Field Current Milliamp.	Applied Voltage	Heat Trans. Surface Polarity	Heat Flux Btu/(hr.) (sq.ft.)
6-13-67	0	226.8	15	500 DC	Negative	172,600
	0.5	227.2	15	500 DC	Negative	172,600
	1.5	---	18	500 DC	Negative	172,600
	2	226.8	21	500 DC	Negative	172,600
	3	226.8	25	500 DC	Negative	172,600
	4	226.1	34	500 DC	Negative	172,600
	5.5	226.2	45	500 DC	Negative	172,600
	6.5	--	52	500 DC	Negative	172,600
	7.5	226.5	60	500 DC	Negative	172,600
	8.5	226.9	65	500 DC	Negative	172,600
	10	226.8	72	500 DC	Negative	172,600
	11	226.8	77	500 DC	Negative	172,600
	12	--	82	500 DC	Negative	172,600
	13	227.5	86	500 DC	Negative	172,600
	14	227.9	91	500 DC	Negative	172,600
	16	228.3	93	500 DC	Negative	172,600
	18	228.6	92	500 DC	Negative	172,600
	20	228.9	94	500 DC	Negative	172,600
	23	229.6	94	500 DC	Negative	172,600
	25	230.2	94	500 DC	Negative	172,600

TABLE 7-B--Continued

Date of Run	Time, Minutes	Surface Temp., °F	Field Current Milliamp.	Applied Voltage	Heat Trans. Surface Polarity	Heat Flux Btu/(hr.) (sq.ft.)
6-13-67	28	230.8	94	500 DC	Negative	172,600
	30	231.2	93	500 DC	Negative	172,600
	34	232.0	92	500 DC	Negative	172,600
	39	233.1	91	500 DC	Negative	172,600
	43	234.0	91	500 DC	Negative	172,600
	48	235.1	90	500 DC	Negative	172,600
	51	235.6	88	500 DC	Negative	172,600
	55	236.4	87	500 DC	Negative	172,600
	60	237.6	86	500 DC	Negative	172,600
	60.5		VOLTAGE OFF			
		Water dumped and tank recharged				
6-14-67	0	238.51	20	500 DC	Positive	154,900
	1	238.3	22	500 DC	Positive	154,900
	2	238.2	24	500 DC	Positive	154,900
	4	237.8	27	500 DC	Positive	154,900
	7	237.4	32	500 DC	Positive	154,900
	13	237.0	36	500 DC	Positive	154,900
	18	236.4	39	500 DC	Positive	154,900
	24	236.3	40	500 DC	Positive	154,900
	31	236.1	39	500 DC	Positive	154,900
	36	235.7	37	500 DC	Positive	154,900
	41	235.9	36	500 DC	Positive	154,900
	49	235.6	36	500 DC	Positive	154,900

TABLE 7-B--Continued

Date of Run	Time, Minutes	Surface Temp., °F	Field Current Milliamp.	Applied Voltage	Heat Trans. Surface Polarity	Heat Flux Btu/(hr.) (sq.ft.)
6-14-67	50	235.6	70	1000 DC	Positive	154,900
	51	235.1	68	1000 DC	Positive	154,900
	54	235.2	61	1000 DC	Positive	154,900
	58	235.0	58	1000 DC	Positive	154,900
	63	235.0	56	1000 DC	Positive	154,900
	68	234.9	55	1000 DC	Positive	154,900
	71		VOLTAGE OFF			
C. Test Run Which Gave Indication of Effect of Current Level on Heat Transfer to Nucleate Boiling Water (Fine Grid Electrode at 1-inch Spacing)						
3-16-67	0	230.35	23	500 DC	Negative	150,000
	2	225.05	30	500 DC	Negative	150,000
	4	225.45	42	500 DC	Negative	150,000
	8	226.65	72	500 DC	Negative	150,000
	9	--	80	500 DC	Negative	150,000
	12	230.35	80	500 DC	Positive	150,000
	13	228.0	76	500 DC	Positive	150,000
	15	227.85	64	500 DC	Positive	150,000
	17		FILM BOILING			

TABLE 8-B

NUCLEATE BOILING HEAT TRANSFER DATA WITH AN AC APPLIED VOLTAGE

A. 0 - 500 Volts AC Data

Date of Run	Applied Voltage	Heat Flux Btu/(hr.)(sq.ft.)	Non-Field ΔT, °F	Heat Trans. Surface Polarity	Electrode Used	Elec. Spacing, Inches	% Surface Temp. Lowered	Field Current Milliamperes
12-10-66	273	58,000	21.2	+G*	FG	1	0.56	5
12-10-66	420	58,000	21.2	+G*	FG	1	2.4	12
1-5-67	210	59,000	20.4	+G*	FG	1	0.5	24.5
1-5-67	400	59,000	20.4	+G*	FG	1	1.0	61
5-17-67	500	61,500	16.4	+	FG	1	0.0	5
1-30-67	500	67,000	18.9	-	FG	¼	2.1	15
2-13-67	500	67,500	15.4	+	CG	¼	2.0	47
1-23-67	500	73,500	19.4	+	FG	1	0	10
1-17-67	500	80,000	22.3	+G*	FG	1	4.5	14
3-14-67	500	85,300	17.7	-	FG	1	4.0	15
11-22-66	345	87,000	22.7	+G*	FG	1	5.7	80
6-20-67	500	109,300	16.2	+	CG	¼	0.43	32.5
6-15-67	500	116,100	17.3	+	CG	¼	2.66	38
6-9-67	500	118,100	14.8	+	FG	1	0.75	2.5
6-1-67	500	120,700	14.8	+	CG	1	7.5	2.5
1-31-67	500	121,000	21.0	-	FG	¼	0.5	25

TABLE 8-B--Continued

Date of Run	Applied Voltage	Heat Flux Btu/(hr.) (sq.ft.)	Non-Field ΔT, °F	Heat Trans. Surface Polarity	Electrode Used	Elec. Spacing, Inches	% Surface Temp. Lowered	Field Current Milliamperes
2-13-67	500	123,000	21.6	+	CG	¼	3.7	54.5
1-25-67	500	123,000	20.4	+	FG	1	2.0	15
3-7-67	500	127,000	20.8	+	CG	1	-1.4**	10
6-19-67	500	142,700	18.9	+	CG	¼	7.21	7.5
5-29-67	500	145,000	14.9	+	CG	1	0	41
5-19-67	500	145,400	18.1	+	FG	1	1.9	5
5-21-67	500	146,500	14.3	+	CG	1	6	49.5
6-15-67	500	148,600	17.1	+	CG	¼	0.47	26.5
4-26-67	500	158,000	16.6	+	FG	1	-1.2**	1.0
5-17-67	500	164,000	19.6	+	FG	1	2.0	2.5
6-1-67	500	165,200	15.9	+	CG	1	6.3	2.5
6-19-67	500	167,800	19.4	+	CG	¼	-2.06**	21.5
6-10-67	500	188,000	17.8	+	CG	1	11.8	2.5
6-20-67	500	191,100	18.3	+	CG	¼	6.3	5.0
6-13-67	500	235,500	14.8	+	CG	1	7.96	2.5
B. 500 - 1000 Volts AC Data								
5-17-67	1000	61,500	16.4	+	FG	1	2.44	28
1-25-67	1000	67,000	18.9	-	FG	¼	4.8	42
2-13-67	1000	67,500	15.4	+	CG	¼	10.4	99

TABLE 8-B--Continued

Date of Run	Applied Voltage	Heat Flux Btu/(hr.) (sq.ft.)	Non-Field ΔT, °F	Heat Trans. Surface Polarity	Electrode Used	Elec. Spacing, Inches	% Surface Temp. Lowered	Field Current Milliamperes
1-23-67	1000	73,500	19.4	+	FG	1	0.5	36.5
1-17-67	1000	80,000	22.3	+G*	FG	1	8.5	75
3-14-67	1000	84,200	17.7	-	FG	1	7.4	39
6-15-67	1000	116,100	17.3	+	CG	¼	8.46	70
6-9-67	1000	118,100	14.3	+	CG	1	3.1	25.5
6-1-67	1000	120,700	14.8	+	CG	1	7.5	20
1-31-67	1000	121,000	21.0	-	FG	¼	0.5	53
1-25-67	1000	123,000	20.4	+	FG	1	7.4	44
2-13-67	930	123,500	21.6	+	CG	¼	5.8	112
3-7-67	1000	127,000	20.8	+	CG	1	1.0	28
6-19-67	1000	142,700	18.9	+	CG	¼	13.0	40.5
5-29-67	1000	145,000	14.9	+	CG	1	0	102
6-15-67	1000	148,600	17.1	+	CG	¼	5.74	55.5
6-9-67	1000	149,100	15.0	+	CG	1	2	22.5
4-26-67	1000	158,000	16.6	+	FG	1	-1.2**	25
5-17-67	1000	164,000	19.6	+	FG	1	3.3	20
6-1-67	1000	165,200	15.9	+	CG	1	8.2	10
6-19-67	1000	167,800	19.4	+	CG	¼	5.15	42.5
5-19-67	1000	186,800	20.6	+	FG	1	9.8	24
6-20-67	1000	191,100	18.3	+	FG	¼	7.7	32

TABLE 8-B--Continued

Date of Run	Applied Voltage	Heat Flux Btu/(hr.) (sq.ft.)	Non-Field ΔT, °F	Heat Trans. Surface Polarity	Electrode Used	Elec. Spacing, Inches	% Surface Temp. Lowered	Field Current Milliamperes
C. 1500 Volts and Above AC Data								
5-17-67	1500	61,500	16.4	+	FG	1	4.9	45
1-25-67	1500	67,000	18.9	-	FG	¼	6.9	65
1-23-67	1500	73,500	19.4	+	FG	1	0.5	76
1-17-67	1500	80,000	22.3	+G*	FG	1	9.0	134
3-14-67	1500	84,200	17.7	-	FG	1	9.9	62
6-20-67	1500	109,400	16.2	+	CG	¼	6.3	70.5
6-15-67	1500	116,100	17.3	+	CG	¼	15.4	104
6-9-67	1500	118,100	14.3	+	CG	1	3.8	45
6-1-67	1500	120,700	14.8	+	CG	1	7.5	29
1-31-67	1500	121,000	21.0	-	FG	¼	0.5	72
1-25-67	1500	123,000	20.5	+	FG	1	10.7	70
3-7-67	1500	127,000	20.8	+	CG	1	3.4	40
6-19-67	1500	142,700	18.9	+	CG	¼	17.6	63.5
5-19-67	1500	145,400	18.1	+	FG	1	9.1	38.5
5-31-67	1500	146,500	14.3	+	CG	1	19.1	44
6-15-67	1500	148,600	17.1	+	CG	¼	11.0	87
4-26-67	1500	158,000	16.8	+	FG	1	6.0	45
5-17-67	1500	164,000	19.6	+	FG	1	4.6	33
6-1-67	1500	165,200	15.9	+	CG	1	8.8	23.5
6-19-67	1500	167,800	19.4	+	CG	¼	13.9	63.5

TABLE 8-B--Continued

Date of Run	Applied Voltage	Heat Flux Btu/(hr.) (sq.ft.)	Non-Field ΔT, °F	Heat Trans. Surface Polarity	Electrode Used	Elec. Spacing, Inches	% Surface Temp. Lowered	Field Current Milliamperes
5-19-67	1500	186,800	20.6	+	FG	1	13.0	38
5-10-67	1500	188,000	17.8	+	CG	1	15.2	33
6-20-67	1500	191,100	18.3	+	CG	¼	9.86	53
5-20-67	1500	229,300	21.4	+	FG	1	14.0	32.5
6-13-67	1500	235,500	14.8	+	CG	1	11.3	48
1-25-67	2000	123,500	20.5	+	FG	1	11.2	100

*+G = Heat transfer surface grounded and of positive polarity

**Negative sign indicates an increase in surface temperature

TABLE 9-B

AVERAGED AC NUCLEATE BOILING DATA FROM RUNS IN TABLE 8-B

A. 500 Volt AC Data

Runs Averaged	Average Heat Flux Btu/(hr.)(sq.ft.)	Average % ΔT Lowered	Average Current, Milliamperes
5-17-67	67,400	1.25	19.2
1-30-67			
2-13-67			
1-23-67			
1-17-67	84,100	4.73	36.3
3-14-67			
11-22-66			
6-20-67	114,500	1.28	24.3
6-15-67			
6-9-67			
6-1-67	122,900	2.46	21.4
1-31-67			
1-25-67			
3-7-67			
6-19-67	145,600	3.12	25.8
5-29-67			
5-19-67			
5-31-67			
6-15-67			

TABLE 9-B--Continued

Runs Averaged	Average Heat Flux Btu/(hr.) (sq.ft.)	Average % ΔT Lowered	Average Current, Milliamperes
4-26-67	163,700	1.26	6.9
5-17-67			
6-1-67			
6-19-67			
6-10-67	189,600	9.05	3.75
6-20-67			
6-13-67	235,500	7.96	2.5
B. 1000 Volt AC Data			
5-17-67	67,400	4.54	56.31
1-25-67			
2-13-67			
1-23-67			
1-23-67	79,200	5.47	50.2
1-17-67			
3-14-67			
6-15-67	121,300	4.82	50.4
6-9-67			
6-1-67			
1-31-67			
1-25-67			
2-13-67			
3-7-67			

TABLE 9-B--Continued

Runs Averaged	Average Heat Flux Btu/(hr.) (sq.ft.)	Average % ΔT Lowered	Average Current, Milliamperes
6-19-67	146,400	5.19	55.1
5-29-67			
6-15-67			
6-9-67			
4-26-67	164,000	3.86	24.4
5-17-67			
6-1-67			
6-19-67			
5-19-67	189,000	8.75	28
6-20-67			
C. 1500 Volts AC Data			
5-17-67	67,300	4.1	62.0
1-25-67			
1-23-67			
1-23-67	79,200	6.45	91.0
1-17-67			
3-14-67			
6-20-67	114,500	8.50	72.3
6-15-67			
6-9-67			
6-15-67	121,000	6.88	60.0
6-9-67			
6-1-67			
1-31-67			

TABLE 9-B--Continued

Runs Averaged	Average Heat Flux Btu/(hr.) (sq.ft.)	Average % ΔT Lowered	Average Current, Milliamperes
1-25-67			
3-7-67			
6-19-67	145,800	14.2	55.8
5-19-67			
5-31-67			
6-15-67			
4-26-67	163,800	8.32	41.3
5-17-67			
6-1-67			
6-19-67			
5-19-67	188,600	13.01	41.3
6-10-67			
6-20-67			
5-20-67	232,400	12.65	40.3
6-13-67			
D. 2000 Volts AC Data			
1-25-67	123,500	11.2	100

TABLE 10-B

SUMMARY OF AC- AND DC-VOLTAGE FILM BOILING DATA

Date of Run	Applied Voltage	Heat Flux Btu/(hr.)(sq.ft.)	Surface Temp., °F	ΔT, °F	Elec. Grid Used	Heat Trans. Surface Polarity	Field Current Milliamp.	Time Applied, Minutes	Final Temp. w/ Volt.	Elec. Spacing, Inches
5-22-67	500 DC	15,200	458.5	248.1	FG	+	14-25	72	219.0	1
5-22-67	1000 DC	15,800	450.6	240.1	FG	+	17-44	22.5	219.0	1
5-23-67	1500 DC	16,100	467.9	251.8	FG	+	29.62	12.75	219.7	1
5-26-67	2000 DC	15,400	466.3	255.9	FG	+	58-115	8.5	219.1	1
5-31-67	500 DC	16,200	512.0	301.7	CG	+	9.24	94	219.1	1
6-1-67	1000 DC	16,400	531.7	320.8	CG	+	20-39	30.5	221.5	1
6-10-67	1500 DC	16,500	485.3	275.3	CG	+	56-72	43.5	222.2	1
6-13-67	1500 DC	17,000	448.5	238.1	CG	+	64-59	46	217.1	1
6-15-67	500 DC	24,900	416.8	206.6	CG	+	35-21.5	62	375.5	¼
6-20-67	500 DC	23,800	437.0	226.8	CG	+	26-19	45	376.6	¼
6-15-67	1000 DC	29,900	436.7	226.5	CG	+	69-56	32.5	218.9	¼
6-19-67	1500 DC	28,000	439.4	228.9	CG	+	70-105	15.5	223.2	¼
6-20-67	500 DC	23,800	427.6	217.4	CG	-	14-24	1.1	219.6	¼
5-17-67	500 AC	13,800	498.6	287.7	FG	+	0-5	3.83	220.2	1
5-26-67	500 AC	16,230	543.1	333.0	FG	+	0-5	3.25	219.0	1
6-14-67	500 AC	24,300	419.7	209.3	CG	+	0-5	1.5	219.4	1
6-10-67	500 AC	18,900	481.6	271.6	CG	+	0-5	21.0	299.3	1
6-10-67	1000 AC	18,900	299.3	89.3	CG	+	28-32	3.0	222.0	1

TABLE 10-B--Continued

Date of Run	Applied Voltage	Heat Flux Btu/(hr.) (sq.ft.)	Surface Temp., °F	ΔT, °F	Elec. Grid Used	Heat Trans. Surface Polarity	Field Current Milliamp.	Time Applied, Minutes	Final Temp. w/ Volt.	Elec. Spacing, Inches
5-29-67	1000 AC	16,740	522.5	312.5	FG	+	5	0.83	220.5	1
6-20-67	500 AC	26,900	432.9	222.5	CG	+	-	1.08	222.4	¼
6-19-67	500 AC	26,500	455.8	244.6	CG	+	24-18	40	416.9	¼
6-19-67	1000 AC	26,500	416.9	205.7	CG	+	55-46	16	357.2	¼
6-19-67	1500 AC	26,500	357.2	146.0	CG	+	84-76	15	225.3	¼

TABLE 11-B

DC-HTS (+) FILM DESTABILIZATION DATA FOR FINE GRID WITH 1-INCH ELECTRODE SPACING

Date of Run: 5-22-67; ΔT=248.1°F; 500V DC; Flux=15,200 Btu/(hr.)(sq.ft.)			Date of Run: 5-22-67; ΔT=240.1°F; 1000V DC; Flux=15,800 Btu/(hr.)(sq. ft.)		
Time, Minutes	Surface Temp., °F	Current, Milliamp.	Time, Minutes	Surface Temp., °F	Current, Milliamp.
0	458.6	9	0	451.4	17
0.5	444.4	9	1	426.1	17
1	437.7	9	1.5	417,2	17
1.5	432.3	9	2	411.2	19
2	427.8	9	2.5	405.2	19
2.5	423.6	9	3	401.0	19
3	420.7	9	3.5	396.8	19
3.5	417.6	9	4	393.4	19
4.5	413.0	9	5	386.5	20
5	411.0	9	6	380.7	21
5.5	409.5	9	7	375.2	22
6	408.0	10	8	369.7	24
7	405.5	10	9	365.0	24
8	403.4	10	10	360.4	25
10	399.7	10	11	355.0	26
12	396.6	11	12	350.5	27
18	388.5	11	13	344.5	29
21	384.9	11	14	337.1	29
25	380.8	12	15	329.1	30
27	378.0	12	16	319.9	30
30	374.5	14	17	307.3	31
36	365.2	14	17.5	300.2	31

TABLE 11-B--Continued

Time, Minutes	Surface Temp., °F	Current, Milliamp.	Time, Minutes	Surface Temp., °F	Current, Milliamp.
37	362.3	14	18	292.4	31
43	355.8	14	18.5	285.7	32
50	343.9	15	19	274.6	34
53	337.0	15	19.5	266.5	34
59	306.5	16	20	257.2	35
60	300.1	16	20.5	248.2	35
60.5	296.4	16	21	235.9	36
61	292.5	16	21.5	223.6	38
61.5	289.2	16	22	220.0	41
62	285.7	16	22.5	219.0	44
62.5	281.9	17			
63	278.3	17			
63.5	274.0	17			
64	270.4	17			
64.5	265.7	18			
65	262.1	18			
65.5	257.2	20			
66	252.8	20			
66.5	248.3	21			
67	243.8	22			
67.5	236.8	22			
68	227.9	22			
68.5	220.7	24			
69	219.0	25			

TABLE 11-B--Continued

Date of Run: 5-23-67; T=251.8°F; 1500V DC; Flux-16,100 Btu/(hr.)(sq.ft.)			Date of Run: 5-26-67; T=255.9°F; 2000V DC; Flux=15,415 Btu/(hr.)(sq.ft.)		
Time, Minutes	Surface Temp., °F	Current, Milliamp.	Time, Minutes	Surface Temp., °F	Current, Milliamp.
0	462.9	29	0	466.1	58
1	424.4	31	0.5	430.5	58
1.5	413.9	31	1	419.2	59
2	406.5	32	1.5	408.2	61
2.5	399.3	32	2	399.2	63
3	393.1	34	2.5	390.0	66
3.5	387.0	34	3	381.2	67
4	382.2	35	3.5	371.6	70
4.5	376.1	36	1	361.7	70
5	371.1	37	4.5	352.0	75
5.5	366.5	39	5	339.4	75
6	361.3	39	5.5	324.3	80
6.5	357.2	41	6	304.1	82
7	352.0	42	6.5	278.4	84
7.5	345.0	43	7	246.2	95
8	339.4	45	7.5	228.8	98
8.5	333.1	46	8	220.7	107
9	326.1	46	8.5	219.1	115
9.5	316.2	47			
10	303.3	49			
10.5	287.5	52			
11	269.3	54			
11.5	249.6	55			
12	227.8	57			
12.5	223.6	60			
13	219.7	62			

TABLE 12-B

AC WATER FILM DESTABILIZATION DATA AT 1-INCH ELECTRODE SPACING

Date of Run: 5-17-67; ΔT=287.7°F
500 Volts; Heat Flux=13,800 Btu/(hr.)(sq.ft.) Fine Grid Electrode

Time, Minutes	Surface Temp., °F	Field Current, Milliamp.
0	498.6	~3
1	363.5	~3
2	292.9	~3
2.5	256.3	~3
2.83	220.2	~3

Date of Run: 5-26-67; ΔT=333.0°F
500 Volts; Heat Flux=16,230 Btu/(hr.)(sq.ft.) Fine Grid Electrode

Time, Minutes	Surface Temp., °F	Field Current, Milliamp.
0	541.8	~3
0.5	478.3	~3
1	441.4	~3
1.5	410.6	~3
2	376.4	~3
2.5	328.2	~3
3	260.0	~3
3.25	223.6	~3

Date of Run: 5-29-67; ΔT=312.5°F
1000 Volts; Heat Flux=16,740 Btu/(hr.)(sq.ft.) Fine Grid Electrode

0	522.1	5
0.5	390.7	5
0.75	294.7	5
0.83	220.5	5

Date of Run: 6-14-67; ΔT=209.3°F
500 Volts; Heat Flux=24,300 Btu/(hr.)(sq.ft.) Coarse Grid Electrode

0	419.9	~3
.5	364.1	~3
1	300.1	~3
1.5	219.6	~3

TABLE 13-B

DC-HTS(+) FILM DESTABILIZATION DATA FOR COARSE GRID WITH 1-INCH ELECTRODE SPACING

Date of Run: 5-31-67; ΔT = 301.7°F
Flux = 16,160 Btu/(hr.)(sq.ft.); 500 Volts

Time, Minutes	Temp., °F	Current, Milliamperes
0	511.5	9
0.5	490.7	9
1	479.8	9
1.5	469.3	9
2	461.5	9
2.5	452.9	10
3	450.2	10
3.5	446.1	10
4	442.3	10
4.5	439.5	10
5	436.6	10
6	431.5	10.5
7	427.4	10.5
8	423.8	10.5
9	420.7	10.5
10	418.3	10.5
11	416.4	10.5
12	414.4	10.5
13	412.6	10.5
14	410.7	11
15	409	11
16	408	11

TABLE 13-B--Continued

Time, Minutes	Temp., °F	Current, Milliamperes
17	406.9	11
18	405.7	11
19	404.3	11
20	403.2	11
21	402.1	11
22	401.4	11
23	400.4	11
25	398.7	12
27	397.0	12
30.5	394.9	12
32.5	393.2	13
35	391.3	13.5
37.5	389.3	14
40	387.5	14
42.5	386.3	14
45	385.1	14
47.5	383.9	14
50	382.2	14.5
52.5	380.4	14.5
55	378.9	14.5
57.5	376.4	14.5
59	375.2	14.8
62.5	372.6	14.8
65	369.1	15.1
67.5	364.9	15.3
70	361.5	15.3
71.5	356.7	15.3
72.5	354.1	16

TABLE 13-B--Continued

Time, Minutes	Temp., °F	Current, Milliamperes
74	349.3	16
75	347.3	16
76	341.8	16
77	337.1	16
78	331.8	16
79	326.2	16
80	320.1	16
81	313.3	16
82	306.0	16
83	297.8	16.5
84	289.7	16.5
85	281.3	17
86	273.7	17
86.5	269.4	17
87	265.4	17.5
88	257.2	18
88.5	253.7	18
89	249.6	18.5
89.5	246.2	19
90	242.8	19
91	234.0	19.5
91.5	226.2	19.5
92	222.0	21
92.5	221.2	21
93	220.4	21
94	219.1	24

TABLE 13-B--Continued

DC-HTS(+) FILM DESTABILIZATION DATA FOR COARSE GRID WITH 1-INCH ELECTRODE SPACING

Date of Run: 6-1-67; ΔT=320.8°F
Flux=16,400 Btu/(hr.)(sq.ft.); 1000 Volts

Time, Minutes	Temp., °F	Current, Milliamperes
0	530.6	20
0.75	497.0	20
1	488.8	20
1.5	476.7	21
2	465.3	21
2.5	456.5	21
3	448.7	21
3.5	442.1	21
4	436.7	22
4.5	432.1	22
5	427.2	22.5
5.5	422.6	22.5
6	419.1	23
7	412.6	23.5
8	407.2	23.5
9	401.7	24
10	397.1	24
11	393.0	24
12	389.5	24.5
13	386.1	24.5
14	382.6	25
15	379.5	25
16	376.1	25

TABLE 13-B--Continued

Time, Minutes	Temp., °F	Current Milliamperes
17	372.4	25
18	368.0	25.5
19	364.1	25.5
20	359.7	26
21	354.6	26
22	349.2	26
23	342.2	26.5
24	334.2	27
25	322.5	28
25.5	315.1	28
26	306.9	28.5
26.5	297.4	29
27	287.9	29
27.5	277.3	30
28	267.0	30
28.5	256.9	31
29	246.2	31
29.5	231.2	35
30	223.2	35
30.5	222.4	37
31	221.7	39
32	221.5	32

TABLE 14-B

WATER FILM DESTABILIZATION DATA WITH ¼-INCH ELECTRODE SPACING

A. DC-HTS(+) Film Destabilization Data with the Coarse Grid

Date of Run: 6-15-67; ΔT=206.6°F *
500 Volts; Heat Flux=29,900 Btu/(hr)(sq.ft.)

Time, Minutes	Surface Temp. °F	Field Current Milliamperes
0	416.6	35
0.5	395.6	35
1	386.0	35
1.5	379.8	35
2	376.6	34
3	373.8	34
4	373.0	34
5	371.8	34
6	371.1	33
8	370.4	33
10	371.5	31
13	371.3	29
17	372.1	28
21	372.2	26
29	374.4	25
35	374.6	23
43	376.4	23.5
51	375.7	22
61	375.5	21.5

*The run of 6-15-67 at 500 volts DC was affected by surface condition and is not felt to be representative of the system.

TABLE 14-B--Continued

Date of Run; 6-15-67; ΔT=226.5 of
1000 Volts; Heat Flux=29,900 Btu/(hr)(sq.ft.)

Time, Minutes	Surface Temp., °F	Field Current Milliamperes
0	437.2	69
0.5	394.4	69
1	378.8	69
1.5	367.5	69
2	359.4	66
2.5	353.7	66
3	348.8	66
4	341.7	61
5	337.9	59
6	335.2	59
7	332.6	58
8	329.9	56
9	327.5	55
10	325.5	55
11	323.1	55
12	321.2	55
13	318.5	55
14	315.5	55
15	312.5	55
16	309.0	55
17	305.5	55
18	301.3	55
19	296.8	55
20	291.1	55
21	285.1	55.5

TABLE 14-B--Continued

Time, Minutes	Surface Temp., °F	Field Current Milliamperes
22	277.0	56
23	267.4	56
23.5	261.3	57
24	254.3	57
24.5	246.7	58
25	238.3	60
25.5	228.5	64
26	224.5	65
26.5	223.0	65
27	222.4	65
28	221.4	66
29	220.4	67
30	219.7	67
31	218.9	67

Date of Run: 6-19-67; ΔT=228.9°F
1500 Volts; Heat Flux=28,000 Btu/(hr.)(sq.ft.)

0	439.2	105
0.5	411.4	104
1	394.2	100
1.5	383.6	--
2	374.2	91
3	360.4	85
3.5	354.7	81
4	348.6	81
4.5	343.8	--

TABLE 14-B--Continued

Time, Minutes	Surface Temp., °F	Field Current Milliamperes
5	339.2	77
5.5	334.1	76
6	331.9	75
7	322.9	74
8	315.4	72
9	308.8	71
9.5	305.2	71
10	302.2	71
10.5	298.9	70
11	297.6	70
11.5	292.3	70
12	288.8	70
13	281.5	70
13.5	276.6	70
14	271.7	70
14.5	264.2	70
15	247.8	71
15.5	226.2	79
16	223.6	80
16.5	223.5	80
17	223.2	80

B. Other ¼-Inch Electrode Spacing Coarse Grid Runs

Date of Run: 6-20-67; ΔT=222.5°F
500 Volts AC; Heat Flux=26,900 Btu/(hr)(sq.ft.)

Time, Minutes	Surface Temp., °F	Field Current Milliamperes
0	432.4	--
0.5	334.7	--
1.5	222.4	--

Date of Run: 6-20-67; ΔT=217.4°F
500 Volts DC HTS(-); Heat Flux=23,800 Btu/(hr)(sq.ft.)

0	427.6	14
0.5	339.1	14
1	276.6	--
1.5	219.6	24

TABLE 15-B

SURFACE CONDITION AFFECTED APPLIED VOLTAGE FILM BOILING WATER DATA

Date of Run: 6-10-67 Heat Flux = 18,902 Btu/(hr)(sq.ft.)
ΔT = 271.6°F; Course Grid Electrode at 1-Inch Spacing

Time, Minutes	Surface Temp., °F	Field Current Milliamperes	Applied Voltage
0	481.6	~3	500 AC
.5	429.2	~3	500 AC
1	397.8	~3	500 AC
1.25	383.2	~3	500 AC
1.5	369.9	~3	500 AC
1.75	357.9	~3	500 AC
2	348.5	~3	500 AC
2.25	341.2	~3	500 AC
2.5	333.8	~3	500 AC
2.75	327.1	~3	500 AC
3	321.8	~3	500 AC
3.5	314.5	~3	500 AC
3.75	311.7	~3	500 AC
4	308.8	~3	500 AC
4.25	307.3	~3	500 AC
4.75	305.3	~3	500 AC
5.5	304.1	~3	500 AC
6	303.9	~3	500 AC
7	303.5	~3	500 AC
9.5	303.3	~3	500 AC
11	302.7	~3	500 AC
13	301.9	~3	500 AC

TABLE 15-B--Continued

Time, Minutes	Surface Temp., °F	Field Current Milliamperes	Applied Voltage
14	301.8	~3	500 AC
15	300.4	~3	500 AC
17	300.1	~3	500 AC
18	299.9	~3	500 AC
19	299.3	~3	500 AC
21	299.3	28	1000 AC
21.25	276.6	28	1000 AC
21.5	265.9	28	1000 AC
21.75	254.5	28	1000 AC
22	243.2	28	1000 AC
22.25	232.3	28	1000 AC
22.5	225.1	30	1000 AC
22.75	223.2	30	1000 AC
23	222.4	30	1000 AC
23.5	222.0	30	1000 AC
24	222.0	32	1000 AC

Film reformed when voltage removed

Date of Run: 6-19-67; Heat Flux = 26,500 Btu/(hr)(sq.ft.)
ΔT = 244.6°F; Course Grid Electrode at ¼-Inch Spacing

0	455.8	20	500 AC
1	434.0	24	500 AC
2	426.0	24	500 AC
3	422.0	21	500 AC
4	419.7	20	500 AC
5	418.4	20	500 AC

TABLE 15-B--Continued

Time, Minutes	Surface Temp., °F	Field Current Milliamperes	Applied Voltage
6	417.6	18	500 AC
7	417.0	18	500 AC
8	416.9	18	500 AC
9	416.9	55	1000 AC
9.5	406.0	55	1000 AC
10	401.0	55	1000 AC
11	343.1	54	1000 AC
12	388.5	53	1000 AC
13	384.7	53	1000 AC
14	382.2	51	1000 AC
15	380.2	50	1000 AC
16	378.6	50	1000 AC
17	377.0	44	1000 AC
18	375.9	49	1000 AC
19	374.5	49	1000 AC
20	373.3	49	1000 AC
24	368.9	46	1000 AC
27	367.1	46	1000 AC
30	365.9	46	1000 AC
33	364.3	46	1000 AC
36	362.3	46	1000 AC
42	359.4	46	1000 AC
48	357.2	46	1000 AC
49	357.2	80	1500 AC
49.5	344.5	80	1500 AC
50	338.4	78	1500 AC
51	328.5	78	1500 AC

TABLE 15-B--Continued

Time, Minutes	Surface Temp., °F	Field Current Milliamperes	Applied Voltage
52	320.8	78	1500 AC
53	314.7	77	1500 AC
54	308.7	77	1500 AC
55	303.3	77	1500 AC
56	298.1	77	1500 AC
58	292.9	77	1500 AC
59	287.9	77	1500 AC
60	283.0	76	1500 AC
61	277.3	76	1500 AC
62	269.6	76	1500 AC
63	245.9	79	1500 AC
63.5	226.6	84	1500 AC
64	225.4	84	1500 AC
65	225.3	84	1500 AC
66	Voltage off		

Film reformed when voltage removed

TABLE 16-B

FREON-112 BOILING HEAT TRANSFER DATA

Date of Run	Heat Flux Btu/(hr) (sq.ft.)	ΔT °F	Voltage Applied	Heat Transfer Surface Polarity	Electrode Spacing, Inches
8-4-67	1,100	11.4	None	--	--
8-4-67	5,300	21.4	None	--	--
8-4-67	13,200	26.8	None	--	--
8-9-67	15,800	42.2	2000 AC	Positive	¼
8-9-67	16,300	41.5	None	--	--
8-6-67	20,100	30.7	None	--	--
8-6-67	21,800	28.2	1000 DC	Positive	¼
8-4-67	23,200	34.6	None	--	--
8-9-67	30,600	49.7	2000 AC	Positive	¼
8-6-67	34,540	36.3	2800 DC	Negative	¼
8-6-67	35,200	36.7	None	--	--
8-6-67	36,900	36.8	1000 DC	Positive	¼
8-4-67	37,300	41.5	None	--	--
8-9-67	46,600	51.6	2000 AC	Positive	¼
8-6-67	47,500	41.0	None	--	--
8-6-67	47,840	41.4	2800 DC	Negative	¼
8-6-67	51,700	38.2	1000 DC	Positive	¼
8-4-67	53,600	46.7	None	--	--
8-6-67	63,700	49.1	None	--	--
8-6-67	63,960	48.8	2800 DC	Negative	¼
8-6-67	66,900	42.9	1000 DC	Positive	¼
8-9-67	67,700	57.5	2000 AC	Positive	¼
8-4-67	67,800	51.7	None	--	--
7-13-67	82,440	Burnout	None	--	--
8-6-67	85,890	Burnout	1000 DC	Positive	¼
8-7-67	87,770	Burnout	2800 DC	Negative	¼

TABLE 16-B--Continued

Date of Run	Heat Flux Btu/(hr) (sq.ft.)	ΔT, °F	Voltage Applied	Heat Transfer Surface Polarity	Electrode Spacing, Inches
8-9-67	11,160	203.7	None	--	--
12-18-67	13,390	370.5	None	--	--
12-18-67	13,390	356.4	None	--	--
9-10-67	13,570	354.8	None	--	--
9-10-67	15,050	371.1	None	--	--
11-11-67	17,010	370.8	None	--	--
11-11-67	17,830	345.5	None	--	--
9-10-67	17,980	341.5	None	--	--
9-10-67	20,180	362.1	None	--	--

TABLE 17-B

FREON FILM DESTABILIZATION DATA

Date of Run: 9-10-67; ΔT = 371.1°F
2000 Volts DC HTS(-); Heat Flux = 15,050 Btu/(hr)(sq.ft.)
Course Grid at ¼-Inch Spacing

Time, Minutes	Surface Temp., °F	Field Current Milliamperes
0	569.1	~2
1	562.6	~2
2	557.9	~2
3.5	551.3	~2
5	544.8	~2
7	537.4	~2
9	530.6	~2
11	524.6	~2
14	516.5	~2
16	511.9	~2
18	507.3	~2
20	503.4	~2
22	499.5	~2
24	496.5	~2
26	492.8	~2
28	489.9	~2
30	487.6	~2
32	486.2	~2
34	484.8	~2
36	482.7	~2
38	480.7	~2
40	478.7	~2
42	476.5	~2
44	475.3	~2
46	474.7	~2

TABLE 17-B--Continued

Time, Minutes	Surface Temp., °F	Field Current, Milliamperes
48	473.8	~2
50	472.3	~2
52	471.5	~2
52.5	Voltage off	
53	472.8	
55	476.2	

Date of Run: 11-11-67; ΔT = 345.5°F
2800 Volts DC HTS(+); Heat Flux = 17,830 Btu/(hr)(sq.ft.)
Course Grid at ¼-Inch Spacing

0	543.6	~4
1	527.7	~4
2	516.7	~4
3	508.1	~4
5	495.2	~4
6	490.1	~4
7	485.7	~4
9	478.3	~4
10	475.1	~4
11	472.3	~4
12	469.2	~4
13	466.3	~4
14	463.5	~4
15	460.6	~4
16	457.7	~4
17	455.2	~4
18	452.8	~4
19	450.5	~4

TABLE 17-B--Continued

Time, Minutes	Surface Temp., °F	Field Current Milliamperes
20	448.2	~4
21	446.1	~4
22	443.8	~4
24	439.6	~4
26	434.4	~4
28	430.3	~4
30	426.0	~4
32	422.1	~4
35	416.1	~4
38	409.9	~4
41	406.4	~4
45	405.9	~4
--	Heater Current Increased	
49	413.4	~4
53	418.8	~4
57	421.8	~4
60	426.2	~4
65	430.9	~4
70	434.2	~4

Date of Run: 11-11-67; ΔT = 370.8°F
2800 Volts, DC HTS(-); Heat Flux = 17,010 Btu/(hr)(sq.ft.)
Course Grid at ¼-Inch Spacing

0	568.6	~4
1	557.6	~4
2	550.1	~4
3.5	541.3	~4

TABLE 17-B--Continued

Time, Minutes	Surface Temp., °F	Field Current Milliamperes
4	538.8	~4
5	534.6	~4
7	526.0	~4
8	521.0	~4
9.5	516.3	~4
10.5	512.9	~4
11.5	509.9	~4
12.5	507.3	~4
14	503.5	~4
15	501.3	~4
16	499.1	~4
18	494.6	~4
20	490.6	~4
23	487.3	~4
26	483.8	~4
29	480.2	~4
34	473.1	~4
39	466.6	~4
44	467.9	~4
49	469.9	~4
54	468.5	~4
59	466.0	~4
60	Voltage off	

Date of Run: 12-18-67; ΔT = 356.4°F
2800 Volts DC HTS(+); Heat Flux = 13,390 Btu/(hr)(sq.ft.)
Course Grid at 1-Inch Spacing

0	553.1	~4

TABLE 17-B--Continued

Time, Minutes	Surface Temp., °F	Field Current Milliamperes
.5	547.4	~4
1	544.0	~4
2	538.9	~4
3	535.6	~4
4	532.0	~4
5	529.0	~4
6	526.4	~4
7	524.5	~4
8	522.9	~4
10	519.1	~4
13	514.2	~4
18	510.0	~4
24	508.4	~4
29	505.3	~4
32	503.0	~4
36	501.2	~4
42	500.2	~4
47	499.2	~4
53	497.2	~4
62	491.2	~4
71	489.7	~4
78	490.4	~4
80	489.8	~4

TABLE 17-B--Continued

Date of Run: 9-10-67; ΔT = 362.1°F
2000 Volts DC HTS(+); Heat Flux = 20,200 Btu/(hr)(sq.ft.)
Course Grid at ¼-Inch Spacing

Time, Minutes	Surface Temp., °F	Field Current Milliamperes
0	560.3	~2
1	553.8	~2
3	546.3	~2
5	537.1	~2
7	528.9	~2
10	518.8	~2
15	503.2	~2
18	491.0	~2
21	481.7	~2
26	470.5	~2
31	465.2	~2
Shut down as heater current dropping		

Date of Run: 9-10-67; ΔT = 341.5
2000 Volts AC; Heat Flux = 18,000 Btu/(hr)(sq.ft.)
Course Grid at ¼-Inch Spacing

0	539.5	30
1	538.0	30
3	536.1	30
6	535.2	30
9	534.6	30
12	527.8	30
Shut down as heater current dropping		

TABLE 17-B--Continued

Date of Run: 12-18-67; ΔT = 370.5°F
2800 Volts AC; Heat Flux = 13,390 Btu/(hr)(sq.ft.)
Course Grid at ¼-Inch Spacing

Time, Minutes	Surface Temp., °F	Field Current Milliamperes
0	567.2	36
1	565.9	36
2	564.9	36
3	564.3	36
4	563.6	36
5	562.9	36
9	561.2	36
12	560.2	36
17	558.8	36
23	558.5	36
35	560.0	37

APPENDIX C

BASIC ELECTRIC FIELD THEORY

BASIC ELECTRIC FIELD THEORY

Since the forces arising from the application of a voltage to a boiling medium are directly related to the electric field intensity, $\vec{E}$, the answer to the question of what occurs electrically in a two-phase medium should be apparent from an investigation of the electric field in a two-dielectric medium. Our interest is, thus, in what electric field theory predicts for the field intensity in dielectric mediums and what boundary conditions, or criteria, apply at a dielectric interface. In seeking answers to these questions, we shall first briefly consider dielectrics in general and then develop some boundary conditions for dielectric interfaces.*

The characteristic which all dielectrics have in common, whether solid, liquid, or gas, is their ability to store energy. This storage takes place by a shift in the relative positions of the internal positive and negative charges against normal atomic

*A development of these concepts can be found in most any book on electromagnetic theory. In this particular development the texts of Hayt [10] and Whitmer [31] were heavily relied on.

and molecular forces. This displacement against a restraining force is analogous to lifting a weight or stretching a spring and represents potential energy with, in this case, the source of the energy being the external field. Quantitatively, this additional stored energy shows up as an increase in permittivity. For example, the stored energy in any capacitor with a vacuum between the plates is as shown below:

$$\text{P.E.} = \frac{1}{2} \int_{\text{vol}} \epsilon_o E^2 dv \qquad \text{(C-1)}$$

It is numerically equal to the work required to charge the condenser plates to a certain voltage. In the case of a dielectric material between the condenser plates, the electric field is still considered the same, but the additional stored energy is accounted for by replacing ϵ_o, the permittivity of a vacuum, by ϵ, the permittivity of the dielectric. Thus, for a fixed electrode arrangement with a non-conducting medium between the plates, the electric field intensity is considered to be the same as that for a vacuum, and the difference in the energy storage capacity, which is a function of the medium between the plates, is accounted for by the permittivity of the medium.

Another way of looking at the method of accounting for the increased energy storage capacity of dielectrics is from the aspect of free and bound charge. Since the electric field causes an orientation of dipoles, the positive conducting con-

denser plate attracts negative dipole ends and vice versa. At the conductor-dielectric interface, these oppositely-charged dipole ends tie up some of the free charge on the conductor surface. The effect of this bound charge couplet on the electrical parameters can best been seen from an example.* Consider a flat plate capacitor of constant potential difference, V_o, with each plate of infinite area. The electric field intensity for this capacitor, with plate spacing d, is $E = V_o/d$. For a constant applied voltage and plate spacing, the value of the field intensity remains constant and is not affected by the addition of a dielectric. This type of argument, however, cannot be used for the electric flux density, $\overline{D}$, which is defined as the number of charge lines passing through a unit area of surface with one flux line representing each unit of charge. It is related to the field intensity through the permittivity and for a free space capacitor is defined as $\vec{D} = \epsilon_o \vec{E}$. While the dielectric surface charge (bound charge) is not the same as that of the free surface charge on the capacitor plates, its effect, as far as flux density is concerned, is the same as that of the free surface charge. In the case of the flat

---

*Bound charge refers to both the charge tied up on the conductor and the charge tied up in the dielectric at the conductor-dielectric interface. Bound charge, as such, can mean either of these.

plate condenser the flux density is $\epsilon_o V_o/d$. This value is not changed by the addition of the dielectric, for the effect of the positive and negative charge in the region between the plates is one of cancellation. Flux, however, must terminate at the bound or free charge on each plate and, as such, we find that there must be a greater surface charge on the capacitor plates than existed without the dielectric because some electric flux arriving at a plate must have originated from the dielectric bound surface charge. This increase in surface charge on the conductor plate had to flow through the external source and represents an increase in stored energy. To simplify the physical conditions it is customary to ignore the dielectric bound surface charge (but not the surface charge on the conductor) and ascribe a permittivity to the dipole assemblage which is greater than that of free space. As such, the effect of a dielectric material between the plates of a capacitor as compared to free space is to:

(a) Change the permittivity from ϵ_o to $K\epsilon_o = \epsilon$, where ϵ is the permittivity of the dielectric medium and K the dielectric constant.

(b) Increase the electric flux density by a factor K, $(\overline{D} = \epsilon_o K\overline{E})$.

(c) Increase the surface charge on the capacitor plates and the stored energy by a factor K.

In terms of flux density, account of the dielectric medium is normally taken by definition of the polarization as shown in Equation (C-2) where $\vec{P}$ is in coulombs per square meter.

$$\vec{P} = \vec{D} - \epsilon_o \vec{E} \qquad \text{(C-2)}$$

For an ideal dielectric, that is, a substance which is homogenous (same throughout), isotropic (behaves the same in every direction which rules out crystalline materials but not liquids), and linear (field directly proportional to strength of source), one can represent $\vec{D}$ by the expression $\vec{D} = \epsilon\vec{E}$. Thus, Equation (C-2) can be rephrased as shown below:

$$\vec{P} = (\epsilon - \epsilon_o)\ \vec{E} = (K-1)\ \epsilon_o \vec{E} \qquad \text{(C-3)}$$

Previously we found that insertion of the dielectric between the capacitor plates at constant potential led to an increase in the surface charge on the conductor plates, the new charge being greater than the old by the magnitude of the bound charge at the conductor-dielectric interface. The ratio of the surface charge with and without the dielectric between the plates is related to the dielectric constant by the following:

$$K = \frac{\epsilon}{\epsilon_o} = \frac{|\rho_{s_o}| + |\rho_{sb}|}{|\rho_{s_o}|} = 1 + \frac{|\rho_{sb}|}{|\rho_{s_o}|} \qquad \text{(C-4)}$$

The quantity ρ_{s_o} is the surface charge density without the dielectric and ρ_{sb} is the bound surface charge density on the

dielectric. The polarization may then be written as in Equation (C-5) since $|\rho_{s_o}| = \epsilon_o|\vec{E}|$.

$$|\vec{P}| = (K-1)\epsilon_o|\vec{E}| = (1 + \frac{|\rho_{sb}|}{|\rho_{s_o}|} - 1)\rho_{s_o} = |\rho_{sb}| \qquad \text{(C-5)}$$

Equation (C-5) shows that the polarization, $\vec{P}$, in the dielectric medium at the conductor-dielectric interface is equal to the absolute value of the bound surface charge density. For the case of the infinite parallel flat plate capacitor with an ideal dielectric between the plates, Equation (C-5) also describes the polarization throughout the dielectric medium between the conductor plates. For other electrode arrangements, particularly those resulting in non-uniform electric fields, the polarization will change in magnitude and direction from point to point within the dielectric, equaling the bound surface charge density only at the dielectric-conductor interface. A general expression for polarization which applies to all electrode arrangements is given by

$$\rho_{sb} = \frac{Nqd_qS}{S} = Nqd_q = P = \frac{\text{Total number of dipoles in layer of thickness } d_q \text{ and area A}}{\text{Surface Area}} \qquad \text{(C-6)}$$

d_q = Charge displacement distance in a dipole

N = Number of dipoles per unit volume

S = Area of width d_q

q = Charge on each end of a dipole

The above expression defines the polarization as a dipole movement per unit volume, and applies throughout the dielectric medium when the field is non-uniform.

The question of what occurs at a dielectric-conductor interface and a dielectric-dielectric interface between conducting plates can now be considered. In considering the dielectric-conductor interface problem, we consider a statically-charged conductor next to which is an insulating dielectric material as shown in Figure C-1(a). To keep all other considerations as general as possible it is assumed that the $\vec{E}$ and $\vec{D}$ extending from the conductor surface into the fluid are not normal to the surface and, as such, have both tangential and normal components to the surface as shown in Figure C-1(a). On consideration of the tangential component, it can be intuitively seen that it must be zero. If it were not zero, a tangential force would be applied to elements of the surface charge, resulting in its motion and non-static conditions. Such a condition would defy the possibility of a static charged condition, which is in contrast to experimental observation. Gauss's law provides the answer to the question concerning the normal component. It states that the electric flux crossing the boundaries of an enclosed volume must be

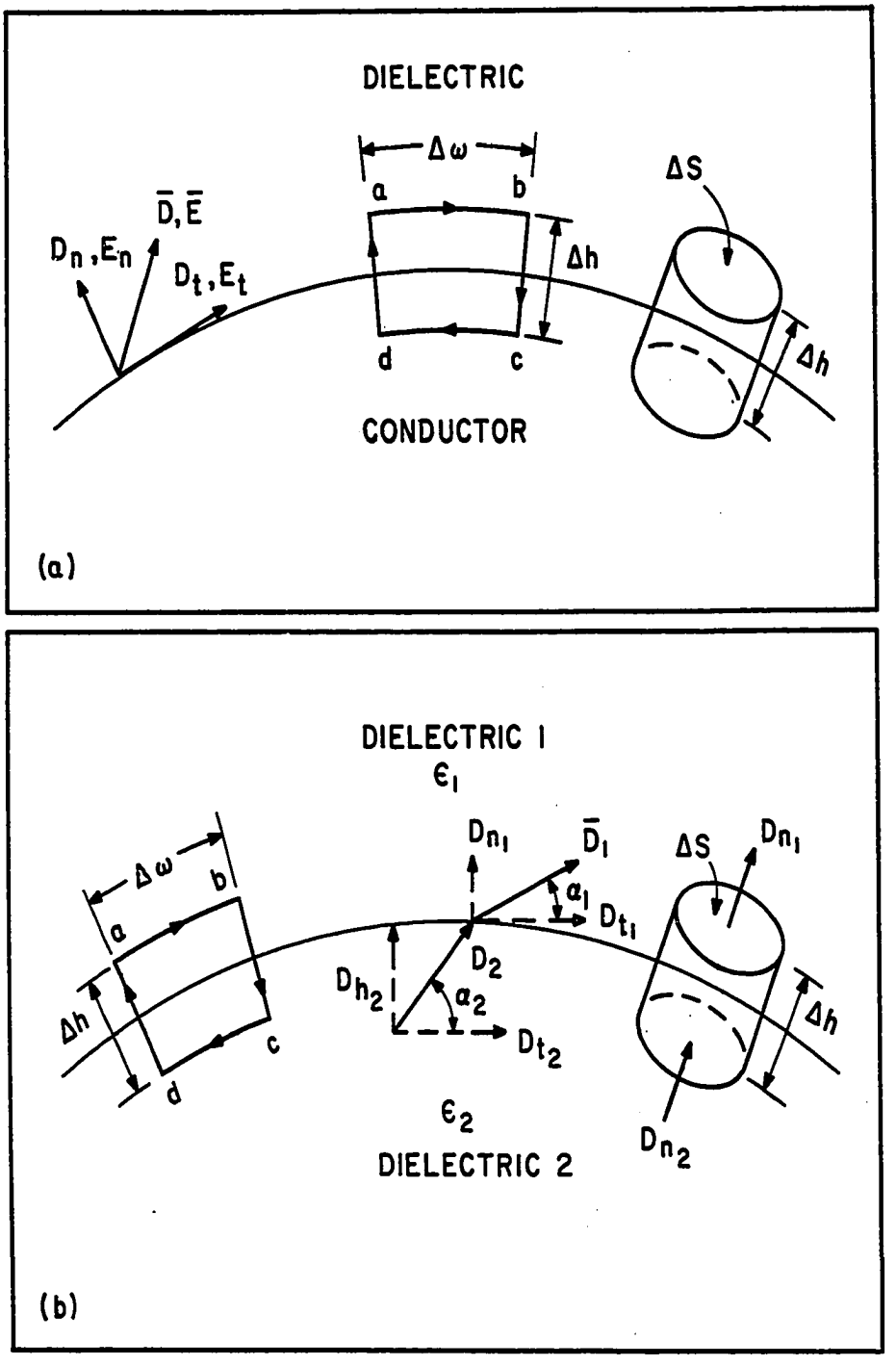

Figure C-1. Electric Field Intensity Vectors Across a Dielectric-Conductor and Dielectric-Dielectric Interface [10]

equal to the charge contained within the volume. In this case the flux cannot leave the surface tangentially for this component is zero, and it cannot penetrate into the conductor for the total field there is zero. It must, thus, leave normally from the surface. Quantitatively, we say the electric flux density in coulombs per meter squared, leaving the surface in a normal direction, is equal to the surface charge density, or $D_n = \rho_s$.

Approaching this problem mathematically we know both the field and the flux ($\vec{E}$ and $\vec{D}$) are zero in the conductor since no field can exist inside a conductor with static charge or the surface charge would move. The tangential field may be determined by applying Equation (C-7) around abcd, as shown in Figure C-1(a).

$$\Delta\text{Potential} = \int \vec{E} \cdot d\vec{L} = 0 = \int \vec{F} \cdot d\vec{L} = \text{Work} \qquad \text{(C-7)}$$

This expression merely states that in going around a closed loop the change in potential or work is zero. To carry out the integration, the line integral is broken into four parts.

$$\int_a^b \vec{E} \cdot d\vec{L} + \int_b^c \vec{E} \cdot d\vec{L} + \int_c^d \vec{E} \cdot d\vec{L} + \int_d^a \vec{E} \cdot d\vec{L} = 0 \qquad \text{(C-8)}$$

The lengths a to b, and c to d, being Δw, and b to c, and d to a, being Δh, the following result is obtained:

$$E_{tan}\Delta w - \frac{1}{2} E_n \Delta h + 0 + \frac{1}{2} E_n \Delta h = 0 \qquad \text{(C-9)}$$

The reason for the 1/2 with the normal components and no contribution of the integral from c to d is that the field in the conductor is zero. Since we are only interested in E_{tan} we can let Δh approach zero, keeping Δw small but finite. Hence, it makes no difference whether or not the normal fields are equal at a and b for Δh causes these terms to become negligibly small. Hence, $E_{tan}\Delta w = 0$ and $E_{tan} = 0$.

The condition on the normal field intensity is found by considering a small cylindrical Gaussian surface of height Δh and circular top and bottom areas of ΔS, as shown in Figure C-1(a). Again letting Δh approach zero and integrating Gauss's law (Equation (C-10) given below) over the three individual areas, the expression for the normal flux intensity is obtained in Equation (C-11).

$$\oint_S \vec{D}\cdot d\vec{S} = Q$$

$$\int_{top} \vec{D}\cdot d\vec{S} + \int_{bottom} \vec{D}\cdot d\vec{S} + \int_{sides} \vec{D}\cdot d\vec{S} = Q \qquad \text{(C-10)}$$

$$D_{top}\Delta S = D_n \Delta S = Q = \rho_s \Delta S$$

Therefore,

$$D_n = \rho_s \qquad \text{(C-11)}$$

The last two terms in the integration are zero as $\vec{D}$ is zero in the conductor and the sides are perpendicular to the normally-directed D_n, and thus $\vec{D}\cdot d\vec{S}$ is zero.

The desired boundary conditions at a conductor-dielectric interface in electrostatics are, thus, as shown in Equations (C-12) and (C-13).

$$D_{tan} = E_{tan} = 0 \tag{C-12}$$

$$D_n = \epsilon E_n = \rho_S \tag{C-13}$$

In summary, these boundary conditions say that the electric flux density leaves the conductor in a direction normal to the surface (no tangential component), and its magnitude is numerically equal to the surface charge density. The electric field intensity may then be found when the permittivity of the insulating material is specified.

The boundary conditions at an interface between two different dielectrics are generated in the same manner as those for a conductor-dielectric interface. Again, we start with an interface as shown in Figure C-1(b). Integrating the field around the closed path indicated, the tangential component boundary condition is obtained (Equation (C-14)).

$$\oint \vec{E}\cdot d\vec{L} = 0$$

$$E_{tan_1} \Delta w - E_{tan_2} \Delta w = 0 \qquad \text{(C-14)}$$

$$E_{tan_1} = E_{tan_2}$$

The only difference from the conductor-dielectric situation is that a field exists on both sides of the interface and, as such, we find that the tangent components of the field intensity must be equal. The normal component boundary condition (See Equation (C-15)below) is again found through use of Gauss's law on the small pillbox shown in Figure C-1(b). Again, the side contribution to this integral is zero as $\vec{D} \cdot \Delta\vec{S} = D\Delta S \cos 90° = 0$.

$$\oint_S \vec{D} \cdot d\vec{S} = Q$$

$$\int_{top} \vec{D} \cdot d\vec{S} + \int_{bottom} \vec{D} \cdot d\vec{S} + \int_{sides} \vec{D} \cdot d\vec{S} = Q$$

$$D_{n_1} \Delta S - D_{n_2} \Delta S = \rho_s \Delta S$$

$$D_{n_1} - D_{n_2} = \rho_s \qquad \text{(C-15)}$$

The question now is as to what ρ_s represents. It cannot be bound surface charge density as we agreed to treat its effect as an increase in permittivity. It is extremely unlikely that any free charge is on the interface for no free charge is available in this perfect dielectric. Thus, except for the special case that charge be placed in the dielectrics deliberately, we

may assume that ρ_s is zero on the interface and the normal components of the flux density are equal across the dielectric interface, as given in Equation (C-16).

$$D_{n_1} = D_{n_2} \tag{C-16}$$

Since the electric field intensity is related to the flux density through $\vec{D} = \epsilon\vec{E}$ it is evident that, while the tangential component of the field intensity is continuous across the interface, the normal component is discontinuous. Likewise, while the normal component of the flux density is continuous, the tangential component is discontinuous. In summary, the boundary conditions which hold across a dielectric-dielectric interface in electrostatics are:

$$\begin{aligned}
&\text{(a)} \quad E_{tan_1} = E_{tan_2} \\
&(a_1) \quad \frac{D_{tan_1}}{D_{tan_2}} = \frac{\epsilon_1}{\epsilon_2} \\
&\text{(b)} \quad D_{n_1} = D_{n_2} \\
&(b_1) \quad \epsilon_1 E_{n_1} = \epsilon_2 E_{n_2}
\end{aligned} \tag{C-17}$$

These conditions may be combined to show the change in direction of the $\vec{D}$ and $\vec{E}$ vectors across the interface. Consider the following sketch:

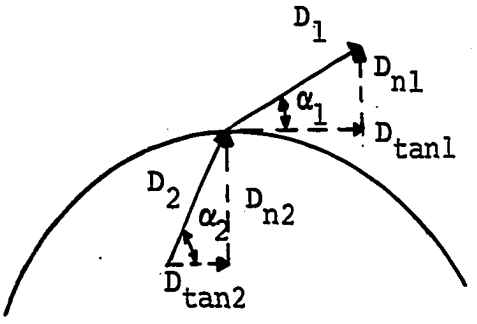

If $\vec{D}_1$ makes an angle α_1 with the interface, the normal and tangential components of the vectors can be expressed as follows:

$$D_1 \sin \alpha_1 = D_2 \sin \alpha_2$$

$$\frac{D_1 \cos \alpha_1}{\epsilon_1} \quad \frac{D_2 \cos \alpha_2}{\epsilon_2} \tag{C-18}$$

$$\epsilon_1 E_1 \sin \alpha_1 = \epsilon_2 E_2 \sin \alpha_2$$

$$E_1 \cos \alpha_1 = E_2 \cos \alpha_2 \tag{C-19}$$

Division of the normal components by the tangential components then gives the relationship between the angles α_1 and α_2 as given in Equation (C-20),

$$\tan \alpha_2 = \frac{\epsilon_1}{\epsilon_2} \tan \alpha_1 \tag{C-20}$$

The magnitudes of $\vec{D}$ and $\vec{E}$ in region 2 of the sketch above are obtained by the Pythagorean theorem and are in relation to the known fields of region 1, as shown by the following:

$$D_2 = D_1 \left[\sin^2 \alpha_1 + \left(\frac{\epsilon_2}{\epsilon_1}\right)^2 \cos^2 \alpha_1\right]^{\frac{1}{2}} \tag{C-21}$$

$$E_2 = E_1 \left[\cos^2 \alpha_1 + \left(\frac{\epsilon_1}{\epsilon_2}\right)^2 \sin^2 \alpha_1\right]^{\frac{1}{2}} \tag{C-22}$$

An inspection of these equations shows that D is larger in the region of smaller E, and vice versa. The direction of the vectors ($\vec{D}$ and $\vec{E}$) are the same in each region as these two vectors are directly proportional to each other.

These boundary conditions, and the magnitude and direction relations derived from them, allow one to find quickly the field and/or flux on one side of the boundary, if the field on the other side is known. A practical problem most often does not fit these conditions. Usually something is known about the fields on each side of the interface, and the boundary conditions must be used to determine both fields.

As a conclusion of this discussion, let us take a simple case, that of a parallel plate capacitor, and consider two cases of dielectric orientation. The two orientations are shown in Figures C-2(a) and C-2(b). In both cases the capacitor area is S and spacing d, with the usual assumption that d is small compared to the linear dimensions of the plates. Between these plates as shown we have two dielectrics of permittivities ϵ_1 and ϵ_2. For the situation in Figure C-2(a), when a voltage $V_o = E_1 d_1 + E_2 d_2$. At the dielectric interface $\vec{E}$ is normal to the interface and $\alpha_1 = \alpha_2 = 90$ degrees. As such, the relationships between E_1 and E_2, as well as D_1 and D_2, can easily be

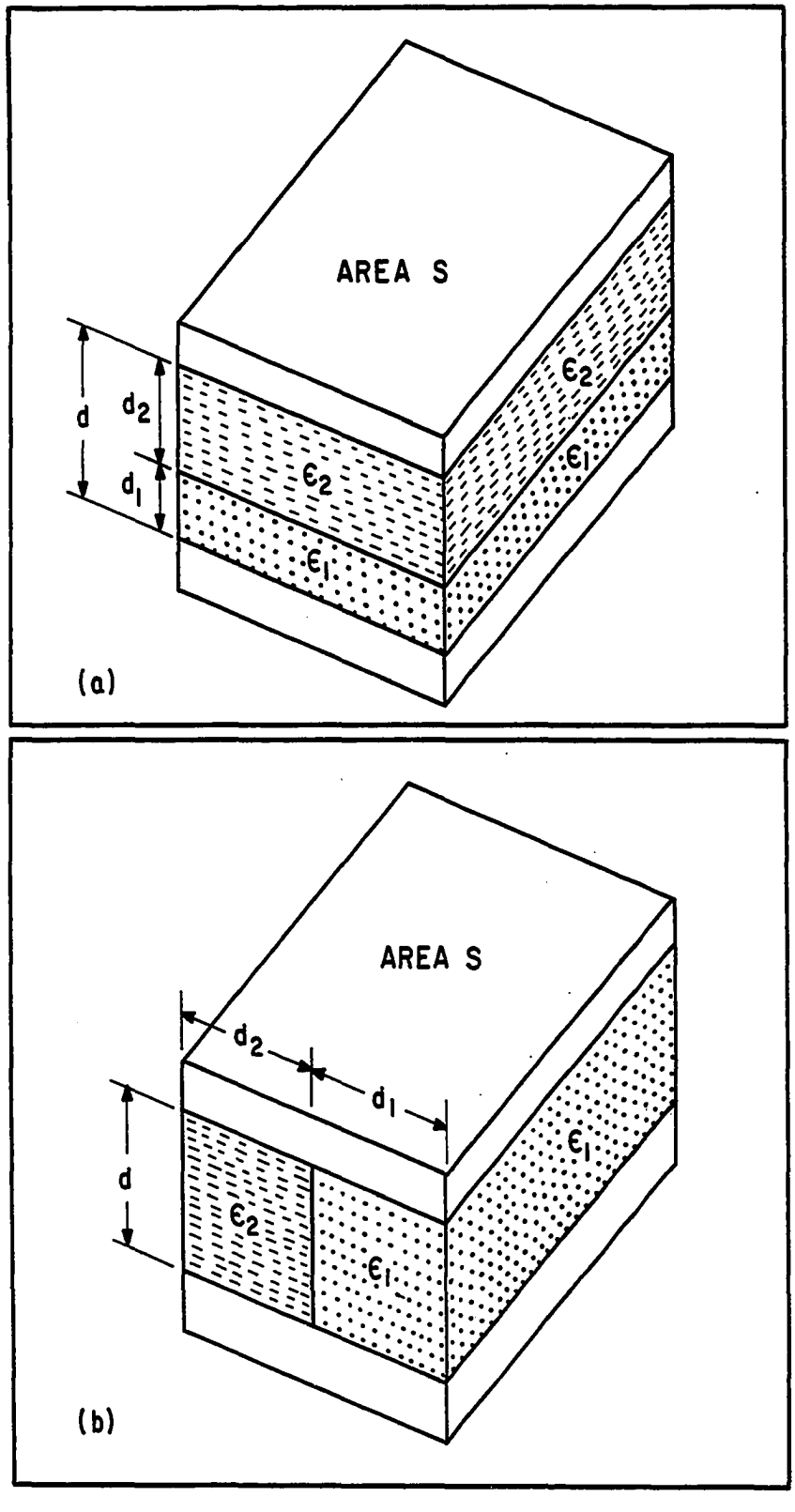

Figure C-2. Horizontal and Vertical Dielectric Configuration Between Flat Parallel Plate Electrodes

found from Equations (C-21) and (C-22), as shown by Equations (C-23) and (C-24).

$$E_2 = E_1[\cos^2(90°) + (\frac{\epsilon_1}{\epsilon_2})^2 \sin^2(90°)]^{\frac{1}{2}} = E_1 \frac{\epsilon_1}{\epsilon_2}$$

$$D_2 = D_1[\sin^2(90°) + (\frac{\epsilon_2}{\epsilon_1})^2 \cos^2(90°)]^{\frac{1}{2}} = D_1$$

$$V_0 = E_1 d_1 + E_1 d_2 \frac{\epsilon_1}{\epsilon_2}$$

$$\text{(a) } E_1 = \frac{V_0}{d_1 + d_2 \frac{\epsilon_1}{\epsilon_2}} \qquad \text{(C-23)}$$

$$\text{(b) } E_2 = \frac{\epsilon_1}{\epsilon_2}\left[\frac{V_0}{d_1 + d_2 \frac{\epsilon_1}{\epsilon_2}}\right]$$

$$D_1 = D_2 = \frac{E_1 V_0}{d_1 + d_2 \frac{\epsilon_1}{\epsilon_2}} \qquad \text{(C-24)}$$

A plot of the magnitudes of $\vec{E}$ and $\vec{D}$ as a function of d, for the assumptions $d_2 = 2d_1$ and $\epsilon_2 = 2\epsilon_1$ is shown in Figure C-3(a) for this dielectric configuration. As shown, the flux intensity is continuous while the field intensity is discontinuous.

For the case when the two dielectric layers are normal to the conducting plates, as shown in Figure C-2(b), with a potential difference V_0 between the plates, the electric field intensities in both regions are tangent to the dielectric interface. As such, the angles α_1 and α_2 are both zero degrees and the

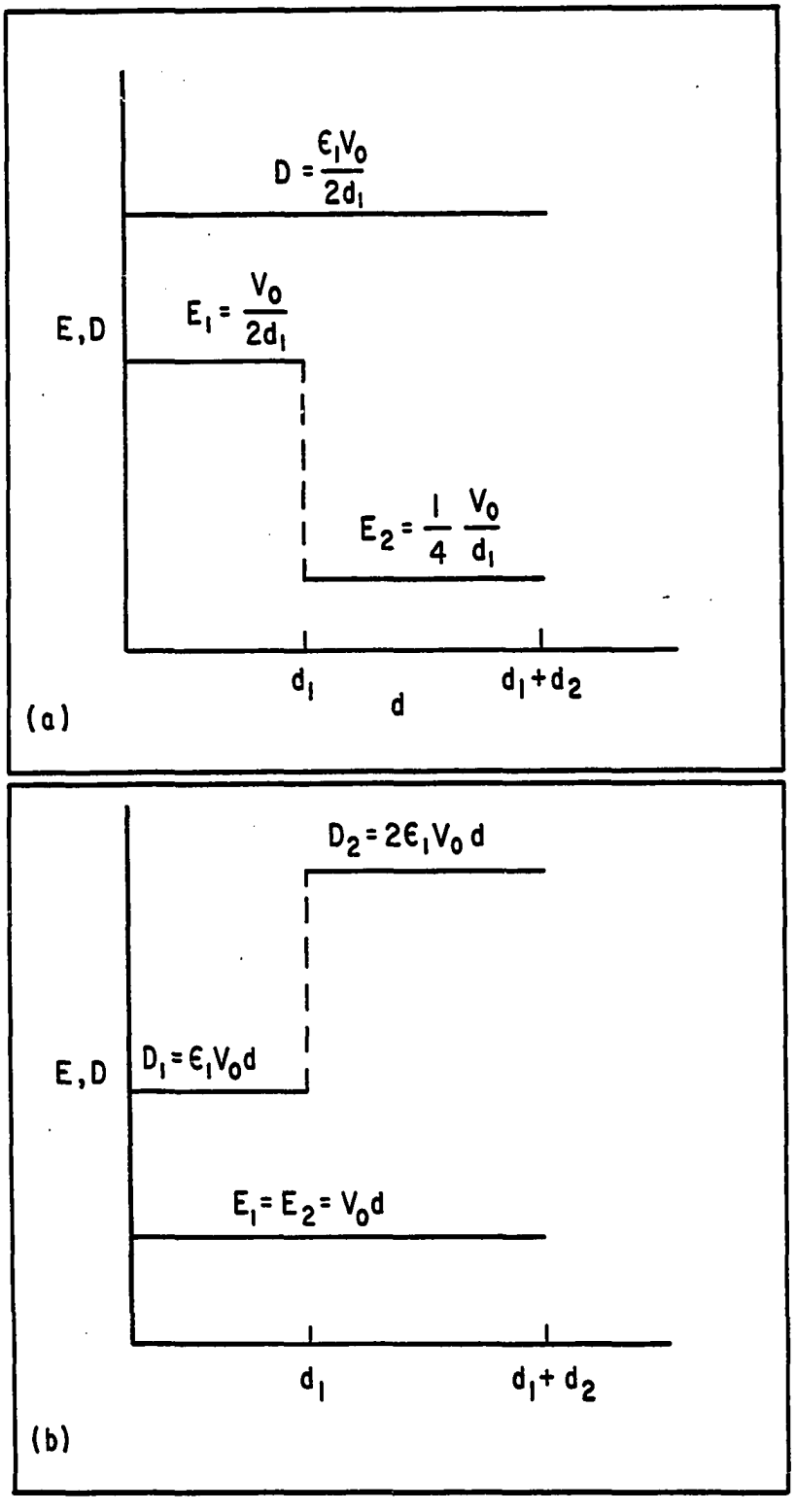

Figure C-3. Plots of E and D vs d for Vertical and Horizontal Dielectric Configurations in Figure C-2 [10]

field intensity and flux intensity in the two regions are as shown in Equations (C-25) and (C-26).

$$E_2 = E_1[\cos^2(0^0) + (\frac{\epsilon_1}{\epsilon_2})^2 \sin^2(0)]^{\frac{1}{2}} = E_1$$

$$D_2 = D_1[\sin^2(0^0) + (\frac{\epsilon_2}{\epsilon_1})^2 \cos^2(0^0)]^{\frac{1}{2}} = \frac{\epsilon_2}{\epsilon_1} D_1$$

$$V_0 = \frac{E_1}{d} = \frac{E_2}{d}$$

(a) $E_1 = V_0 d$ (C-25)

(b) $E_2 = V_0 d$

(a) $D_1 = \epsilon_1 E_1 = \epsilon_1 V_0 d$ (C-26)

(b) $D_2 = \epsilon_2 E_2 = \epsilon_2 V_0 d$

A plot of the magnitudes of $\vec{E}$ and $\vec{D}$ as a function of d for this dielectric configuration, for the same assumptions as in the previous case, is shown in Figure C-3(b). For this case the field intensity is continuous.

These two configurations represent the extremes in terms of dielectric-dielectric interfaces between a flat plate capacitor. In applying these results it must be remembered that these derivations were made for a statically charged system and do not hold for a conducting media, i.e., a media in which charges exist between the plates and a current flow is experienced.

APPENDIX D

DEVELOPMENT OF DIELECTROPHORETIC FORCE EQUATION

DEVELOPMENT OF DIELECTROPHORETIC FORCE EQUATION [6]

A derivation of the force from dielectrophoresis begins with Gauss's law as written in the form shown by

$$\rho_s dA = \vec{D}\cdot\vec{n}dA \qquad \text{(D-1)}$$

where dA is an element of area on the surface which contains the surface charge ρ_s, and $\vec{n}$ is the unit vector normal to the elemental surface area dA. To obtain the polarization form of Gauss's law the substitution $\vec{D} = K\epsilon_0\vec{E}$ is first made in Equation (D-1), yielding

$$\frac{\rho_s}{K} dA = \epsilon_0\vec{E}\cdot\vec{n}dA \qquad \text{(D-2)}$$

in which K is the dielectric constant of the medium between the conducting plates. If the polarization shown by

$$\vec{P} = \vec{D} - \epsilon_0\vec{E} \qquad \text{(D-3)}$$

is now dotted with the surface normal vector and multiplied by dA, the following is obtained:

$$\vec{P}\cdot\vec{n}dA = \vec{D}\cdot\vec{n}dA - \epsilon_0\vec{E}\cdot\vec{n}dA \qquad \text{(D-4)}$$

Substitution of Equation (D-1) and (D-2) into Equation (D-4) yields

$$\vec{P}\cdot\vec{n}dA = \rho_s\left(1 - \frac{1}{K}\right)\, dA \qquad \text{(D-5)}$$

which is Gauss's law for polarization.

If $\vec{D} = K\epsilon_0\vec{E}$ is substituted into Equation (D-3), one obtains:

$$\vec{P} = \epsilon_0\vec{E}\ (K\text{-}1) \qquad \text{(D-6)}$$

To proceed further with the analysis, the polarization is defined in terms of the dipole moment, $\vec{\mu}$, which is given by

$$\vec{\mu} = q\vec{d} \qquad \text{(D-7)}$$

where d is the distance of dipole charge separation and q is the dipole charge. The polarization, which is defined as the dipole moment per unit volume, is then

$$\vec{P} = N\vec{\mu} \qquad \text{(D-8)}$$

where N is the number of dipoles per unit volume of dielectric. If $\vec{E}'$ represents the local electric field strength, torque, $\vec{T}$, as given by the following expression is exerted on the dipole.

$$\vec{T} = \vec{\mu} \times \vec{E}' \qquad \text{(D-9)}$$

This torque tends to align the dipole in the field direction. If the field is non-uniform, one end of the dipole experiences a larger torque than the other and a net transitional motion is experienced. The force producing this motion can be obtained by simply adding the forces acting on the + and - ends of the dipole, as shown by

$$\vec{F} = \vec{F}- + \vec{F}+ = \vec{E}'(-q) + [\vec{E}' + (\vec{d}\cdot\nabla)\vec{E}'](+q)$$

$$\vec{F} = q\vec{d}\cdot\nabla\vec{E}' = \vec{\mu}\cdot\nabla\vec{E}' \qquad \text{(D-10)}$$

As might be expected the dipole moment, $\vec{\mu}$, is directly proportional to the field intensity, $\vec{E}'$, as shown by

$$\vec{\mu} = \lambda\vec{E}' \qquad \text{(D-11)}$$

where the proportionality constant λ is the polarizability. Substitution of Equation (D-11) into Equation (D-10) yields

$$\vec{F} = \lambda\vec{E}' \cdot \nabla\vec{E}' \qquad \text{(D-12)}$$

Intuitively, it might be expected that the locally acting field, $\vec{E}'$, will be identical with the externally applied field, $\vec{E}$, if the interaction between the molecules can be neglected (gases at low pressure). However, in liquid dielectrics the field acting on a particle might be expected to be modified by the polarization of the surrounding particles. The exact determination of $\vec{E}'$ is prohibitively difficult; however, a reasonable approximation for non-polar fluids is the Mosotti field, given by

$$\vec{E}' = \vec{E} + \frac{\vec{P}}{3\epsilon_0} \qquad \text{(D-13)}$$

Substitution of Equation (D-6) into Equation (D-13) yields

$$\vec{E}' = \frac{\vec{E}}{3}(K+2) \qquad \text{(D-14)}$$

Combining Equations (D-6), (D-8), and (D-11), the polarization is redefined as

$$\vec{P} = N\lambda\vec{E}' = (K-1)\epsilon_0\vec{E} \qquad \text{(D-15)}$$

Substituting the Mossotti equation, as given by Equation (D-14), into (D-15) yields (D-16):

$$\frac{(K-1)}{(K+2)} = \frac{N\lambda}{3\epsilon_0} \qquad \text{(D-16)}$$

On solving for λ, one obtains

$$\lambda = \frac{3\epsilon_0}{N}\frac{(K-1)}{(K+2)} \qquad \text{(D-17)}$$

Substituting Equation (D-17) for λ, and Equation (D-14) for $\vec{E}'$, into Equation (D-12) and multiplying through by N, the final result is obtained:

$$\vec{F}_V = \frac{\epsilon_0}{6}(K-1)(K+2)\ \vec{\nabla}E^2 \qquad \text{(D-18)}$$

Another approach to obtain this result is presented by Choi [6]. Using a force expression from electrodynamics of more general validity, he derived Equation (D-18), the volume force on a continuous homogeneous dielectric medium in a non-uniform field. The force equation with which he worked is shown by

$$\vec{F}_V = \frac{\epsilon_0}{2}\nabla E^2 \frac{\partial K}{\partial \rho}\rho \qquad \text{(D-19)}$$

where ρ is the dielectric density. Equation (D-18) is obtained by defining N as shown by

$$N = \frac{N_o\rho}{M} \qquad \text{(D-20)}$$

where N_o = Avagadros number

M = Dielectric molecular weight

ρ = Dielectric density

If the Mossotti relationship is assumed and Equation (D-20) is substituted in Equation (D-17), an expression for the density in terms of K is obtained as shown by

$$\rho = \frac{3\epsilon_o M}{N_o \lambda} \frac{(K-1)}{(K+2)} \qquad \text{(D-21)}$$

From this, the derivative is obtained.

$$\frac{\partial K}{\partial \rho} = \frac{No\lambda}{9\epsilon_o M} (K+2)^2 \qquad \text{(D-22)}$$

Substitution of Equations (D-21) and (D-22) into Equation (D-19) yields Equation (D-18).

APPENDIX E

DEVELOPMENT OF THE ELECTRIC FIELD INTENSITY INSIDE AND OUTSIDE OF A SPHERE OF DIELECTRIC CONSTANT K_1 IMBEDDED IN A BULK MEDIUM OF DIELECTRIC CONSTANT K_2 WHICH IS SUBJECTED TO A UNIFORM ELECTRIC FIELD

DEVELOPMENT OF THE ELECTRIC FIELD INTENSITY INSIDE AND OUTSIDE OF A SPHERE OF DIELECTRIC CONSTANT K_1 IMBEDDED IN A BULK MEDIUM OF DIELECTRIC CONSTANT K_2 WHICH IS SUBJECTED TO A UNIFORM ELECTRIC FIELD

In general, the electrical potential in a charge free medium surrounding a charged surface is given by Laplace's equation,

$$\nabla^2 V = 0 \qquad \text{(E-1)}$$

The electric field intensity, $\vec{E}$, in turn is related to the electric potential through the following expression.

$$\vec{E} = - \vec{\nabla} V \qquad \text{(E-2)}$$

The solution of these two equations for the case of a dielectric material of dielectric constant K_1 existing in spherical shape within a bulk dielectric medium of dielectric constant K_2, all of which is subjected to a uniform electric field, E_o, as produced by two flat plate charged electrodes, is what is desired. For the situation of a sphere of specified radius r_1, as depicted in Figure E-1, the potential on the inside of the spherical particle, V_1, is given by Laplace's equation in spherical coordinates as shown in Equation (E-3).

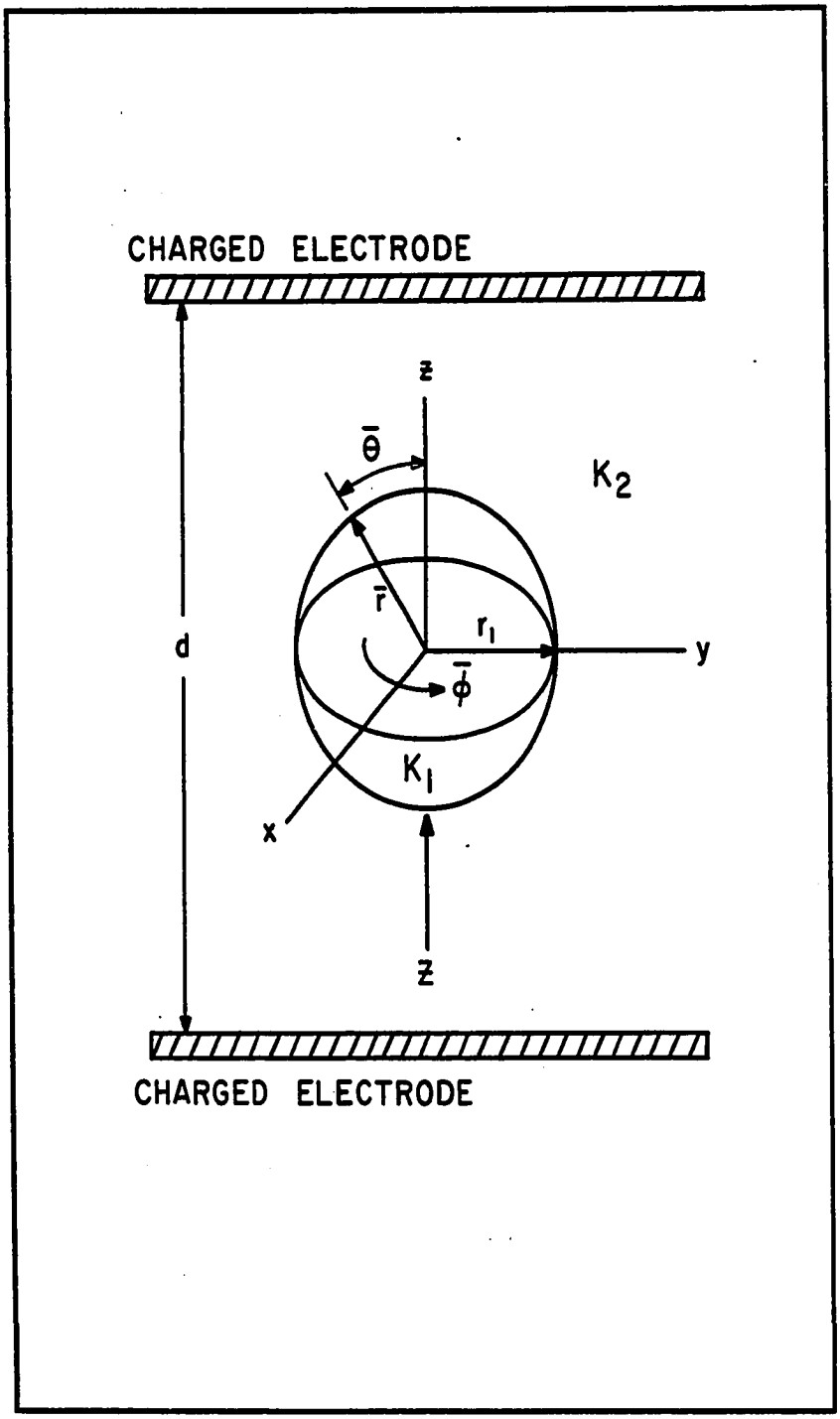

Figure E-1. Geometry of a Sphere of Dielectric Constant K_1 in a Bulk Medium of Dielectric Constant K_2 all Being Subjected to a Uniform Electric Field

$$\nabla^2 V_1 = \frac{1}{r^2}\frac{\partial}{\partial r}\left(r^2 \frac{\partial V_1}{\partial r}\right) + \frac{1}{r^2 \sin\theta}\frac{\partial}{\partial \theta}\left(\sin\theta \frac{\partial V_1}{\partial \theta}\right) + \frac{1}{r^2 \sin^2\theta}\frac{\partial^2 V_1}{\partial \Phi^2} = 0 \qquad \text{(E-3)}$$

The solution of this equation yields the potential inside the sphere, ($r<r_1$), which is due to the induced charge distribution on the sphere. The potential in the bulk medium surrounding the sphere ($r>r_1$) is given by the following expression.

$$V_2 = V_o + V_2' \qquad \text{(E-4)}$$

where

$$\nabla^2 V_2' = \frac{1}{r^2}\frac{\partial}{\partial r}\left(r^2 \frac{\partial V_2'}{\partial r}\right) + \frac{1}{r^2 \sin\theta}\frac{\partial}{\partial \theta}\left(\sin\theta \frac{\partial V_2'}{\partial \theta}\right) + \frac{1}{r^2 \sin^2\theta}\frac{\partial^2 V_2'}{\partial \Phi^2} = 0 \qquad \text{(E-5)}$$

and

$$V_o = E_o Z = - E_o r \cos\theta \qquad \text{(E-6)}$$

Equation (E-4) simply states that the potential in the bulk medium surrounding the spherical particle, V_2, is given by the combined potential of the induced charge on the sphere, V_2', and the potential of the charge distributed on the flat plate electrodes V_o. The potentials V_1 and V_2 are related through the following boundary conditions.

$$V_1 = V_2 \text{ at } r = r_1 \tag{E-7}$$

$$K_1 \frac{\partial V_2}{\partial r} = K_2 \frac{\partial V_2}{\partial r} \text{ at } r = r_1 \tag{E-8}$$

These boundary conditions, which state that the potential is continuous across the dielectric-dielectric interface, and that the normal component of the electric field intensity on each side of the interface are related through the respective dielectric constants, were discussed in Appendix C.

The general solution to Equations (E-3) and (E-5) is identical and is obtained by the separation of variables technique. Assuming a solution of the following form

$$V_2' = V = R(r) \cdot \Theta(\theta) \cdot \bar{\Phi}(\Phi) \tag{E-9}$$

Equations (E-3) and (E-5) can be resolved to

$$\frac{1}{r^2 R} \frac{d}{dr}\left(r^2 \frac{dr}{dr}\right) + \frac{1}{r^2(\sin\theta)\,\Theta} \frac{d}{d\theta}\left(\sin\theta \frac{d\Theta}{d\theta}\right) + \frac{1}{r^2(\sin^2\theta)\Phi} \frac{d^2\bar{\Phi}}{d\bar{\Phi}^2} = 0 \tag{E-10}$$

The above equation may be separated into the following three ordinary differential equations.

$$\frac{d^2\bar{\Phi}}{d\Phi^2} = -m^2\bar{\Phi} \tag{E-11}$$

$$\frac{d}{dr}\left(r^2 \frac{dr}{dr}\right) = n(n+1)R \tag{E-12}$$

$$\frac{1}{\Theta \sin\theta} \frac{d}{d\theta}\left(\sin\theta \frac{d\Theta}{d\theta}\right) = \frac{m^2}{\sin^2\theta} - n(n+1) \qquad \text{(E-13)}$$

Equation (E-13) is a form of the Legendere differential equation. Solution to the above three equations are respectively

$$\bar{\Phi} = C_1 \sin(m\,\Phi) + C_c \cos(m\,\Phi) \qquad \text{(E-14)}$$

$$R = C_3 r^n + \frac{C_4}{r^{n+1}} \qquad \text{(E-15)}$$

$$\Theta = C_5 P_n^m(\cos\theta) + C_6 P_n^m(\cos\theta) \qquad \text{(E-16)}$$

The complete general solution as given by (E-9) is thus

$$V_2' = V_1 = \sum_{n=0}^{\infty} \sum_{n=0}^{\infty} (C_1 \sin(m\Phi) + C_2 \cos(m\Phi))\left(C_3 r^n + \frac{C_4}{r^{n+1}}\right)\left(C_5 P_n^m(\cos\theta) + C_6 Q_n^m(\cos\theta)\right) \qquad \text{(E-17)}$$

For the problem under consideration there is no variation in the Φ direction. As such m is equal to zero. Further, for V_2' the influence of the induced charge on the sphere must become negligible as r increases. Therefore for the V_2' solution C_3 is chosen to be zero*. In an analogous fashion, since V_1 must hold at r equal to zero, C_4 is set equal to zero for the solution inside the sphere. Finally, since $Q_n(\cos\theta)$ becomes unbounded for $\theta = k\pi$ the constant C_6 is

*This condition involves the assumption that the sphere is relatively far removed from the conducting electrodes.

equated to zero. With these restrictions which apply to the problem under consideration the solution for the potential inside and outside the sphere due to the induced charge on the sphere become

$$V_1 = \sum_{n=0}^{\infty} a_n r^n P_n(\cos\theta) \tag{E-18}$$

$$V_2' = \sum_{n=0}^{\infty} \frac{b_n P_n(\cos\theta)}{r^{n+1}} \tag{E-19}$$

In the above equations the $P_n(\cos\theta)$ term refers to Legendere polynomials in $\cos\theta$, the first four of which are shown below.

$$P_o(\cos\theta) = 1 \tag{E-20}$$

$$P_1(\cos\theta) = \cos\theta \tag{E-21}$$

$$P_2(\cos\theta) = \tfrac{1}{2}(3\cos^2\theta - 1) \tag{E-22}$$

$$P_3(\cos\theta) = \tfrac{1}{2}(5\cos^3\theta - 3\cos\theta) \tag{E-23}$$

Substitution of Equation (E-21) and (E-19) into Equation (E-4) and (E-6) respectively, and then of (E-6) into (E-4), yields the total potential in the bulk medium around the sphere.

$$V_2 = -E_o r P_1(\cos\theta) + \sum_{n=0}^{\infty} b_n \frac{P_n(\cos\theta)}{r^{n+1}} \tag{E-24}$$

The constants a_n and b_n in Equations (E-18) and (E-24) are obtained by application of the boundary conditions given in

(E-7) and (E-8). By equating like coefficients of $P_n(\cos\theta)$ the following is obtained.

$$a_o = b_o = 0 \tag{E-25}$$

$$a_1 = - \frac{3K_2}{(K_1+2K_2)} E_o \tag{E-26}$$

$$b_1 = \frac{(K_1-K_2)}{(K_1+2K_2)} r_1^3 E_o \tag{E-27}$$

$$a_n = b_n = 0 \quad \text{for } n > 2 \tag{E-28}$$

The resultant potential inside and outside the sphere is then

$$V_2 = - E_o r\cos\theta + \frac{(K_1-K_2)}{(2K_2+K_1)} r_1^3 \frac{E_o \cos\theta}{r^2} \tag{E-29}$$

$$V_1 = - \frac{3K_2}{(K_1+2K_2)} E_o r\cos\theta = - \frac{3K_2}{(K_1+2K_2)} E_o Z \tag{E-30}$$

Application of Equation (E-2) to Equations (E-29) and (E-30) yields the desired electric field intensity inside and outside the spherical particle.

$$\vec{E}_1 = - \vec{\nabla} V_1 = \frac{3K_2 E_o}{(2K_2+K_1)} \vec{k} \tag{E-31}$$

$$\vec{E}_2 = - \vec{\nabla} V_2 = E_o\cos\theta\left[1+ \frac{2r_1^3(K_1-K_2)}{r^3(2K_2+K_1)}\right]\vec{r} + E_o\sin\theta\left[\frac{r_1^3(K_1-K_2)}{r^3(K_1+2K_2)} -1\right]\vec{\theta} \tag{E-32}$$

As is apparent from Equation (E-31) the electric field intensity inside the sphere is invariant. This is not true, however, on the outside of the sphere. In the case of nucleate boiling the inside of a spherical bubble consists of vapor and the outside of liquid. As such the electric field intensity in the liquid region in the vicinity of the vapor liquid interface is non-uniform.

Before use of Equations (E-31) and (E-32) are made for the boiling situation it is well to recall the assumption made in their development. Of particular interest along these lines is a basic assumption made in resolving Equation (E-17) to (E-19) for V_2'. In this step it was assumed that a_n had to be zero so that V_2 (E-24) resolved to the applied potential from the charged electrodes as r becomes large. In essence equating a_n to zero assumes that the sphere is distant from the charged electrodes. In the boiling situation the vapor bubbles are generated at one of these electrodes and this basic assumption is not valid. Including the a_n term in Equation (E-19) would require an additional boundary condition for solution. This boundary condition would specify the location of the bubble with respect to the electrode heat transfer surface. How inclusion of this term would affect the final result for $\vec{E}_2$ is not known. As such, Equation

(E-32) involves the assumption that the field intensity $\vec{E}_2$ is not affected by bubble location with respect to the heat transfer surface.

APPENDIX F

DEVELOPMENT OF ELECTRICAL FORCE EXPRESSION WHICH APPLY TO THE BOILING SITUATION

DEVELOPMENT OF ELECTRICAL FORCE EXPRESSION WHICH APPLY TO THE BOILING SITUATION

Stratton [26] presents the development for the stress which exists across a dielectric-dielectric interface.

$$\vec{S} = \frac{\epsilon_o}{6}\{\frac{1}{K_1}(K_2^2K_1^2+4K_2^2K_1 - 6K_2K_1^2 - 3K_2^2 + 2K_2 + 2)E_{n_2}^2 + [K_1(K_1-2) - K_2(K_2-2)]E_{tan_2}^2\}\vec{n}_1 \qquad (F\text{-}1)$$

The stress is normal to the interface and directed toward medium 1. If medium 1 is gaseous, whose dielectric constants are very slightly greater than unity, Equation (F-1) can be reduced to the following form.

$$\vec{S} = \frac{\epsilon_o(K_2-1)}{6}(2E_{n_2}^2 - E_{tan_2}^2)\vec{n}_1 \qquad (F\text{-}2)$$

Since in the boiling situation the gaseous region is the vapor region Equation (F-2) can be rewritten

$$\vec{S} = \frac{\epsilon_o(K_\ell-1)}{6}[2E_{n_\ell}^2 - E_{tan_\ell}^2]\vec{n}_v \qquad (F\text{-}3)$$

where subscripts ℓ and v refer to the liquid and the vapor.

The development of the general expression for the

electrical body force on a continuous dielectric medium is also given in Stratton [26].

$$\vec{F}_v = - \tfrac{1}{2} E^2 \epsilon_o \vec{\nabla} K + \tfrac{1}{2} \epsilon_o \vec{\nabla} \left(E^2 \rho \frac{\partial K}{\partial \rho} \right) \qquad \text{(F-4)}$$

Through use of the Mosotti relationship, as shown in Appendix D, Equation (F-4) can be resolved to the following form.

$$\vec{F}_v = -\tfrac{1}{2} E^2 \epsilon_o \vec{\nabla} K + 1/6 \, \epsilon_o \vec{\nabla} \left[E^2 (K-1)(K+2) \right] \qquad \text{(F-5)}$$

If the medium dielectric constant is uniform the above expression resolves to

$$\vec{F}_v = 1/6 \, \epsilon_o (K-1)(K+2) \vec{\nabla} E^2 \qquad \text{(F-6)}$$

Of interest now are the expression for the interfacial stress, as given by Equation (F-2), and the body force in the bulk medium, as given by Equation (F-6), for the configurations shown in Figures C-2 and E-1 respectively. In these figures regions 1 and 2 represent the vapor and the liquid respectively. For the laminated configuration shown in Figure C-2 the body force, F_v, is zero since the electric field is uniform in each of bulk mediums. Since the uniform electric field intensity vectors are all normal to the interface the stress at the interface is as follows, where $(E_o)_\ell$ is the electric field intensity in the liquid as produced by the conducting

electrodes.

$$\vec{S} = \frac{\epsilon_o}{3}(K_\ell - 1)^2 (E_o)_\ell^2 \vec{n}_v \qquad \text{(F-7)}$$

For the spherical configuration shown in Figure E-1 the interfacial stress is tabulated from the liquid side electric field intensity given by Equation (E-32). The normal and tangent components of the electric field intensity from this equation are respectively

$$E_{n_\ell} = E_o \cos\theta \left[1 + \frac{2r_1^3 (K_1 - K_2)}{r^3 (2K_2 + K_1)}\right] \qquad \text{(F-8)}$$

$$E_{\tan_\ell} = E_o \sin\theta \left[\frac{r_1^3 (K_1 - K_2)}{r^3 (K_1 - 2K_2)} - 1\right] \qquad \text{(F-9)}$$

Substitution of Equations (F-8) and (F-9) at $r = r_1$ into Equation (F-3) yields the expression for the electrical stress around a spherical bubble, which when simplified is

$$\vec{S} = \frac{3\epsilon_o (K_\ell - 1)^2 E_o^2}{2(K_v + 2K_\ell)^2} \left[\cos^2\theta (K_\ell^2 + 2K_v^2) - K_\ell^2\right] \vec{n}_v \qquad \text{(F-10)}$$

Substitutions of Equations (E-31) and (E-32) into Equation (F-6) yields the body force, F_v, in the vapor and liquid regions of the spherical configuration which are Inside the bubble (liquid region)

$$\vec{F}_v = 0 \qquad \text{(F-11)}$$

Outside the bubble (liquid region)

$$F_v)_r = \frac{6E_o^2(K_\ell - K_v)r_1^3}{(K_v+2K_\ell)r^4}\left\{2\cos^2\theta\left[1 - \frac{2r_1^3(K_\ell-K_v)}{r^3(K_v+2K_\ell)}\right] - \sin^2\theta\left[1+\frac{r_1^3(K_\ell-K_v)}{r^3(K_v+2K_\ell)}\right]\right\}$$

(F-12)

$$F_v)_\theta = \frac{2E_o^2\sin\theta\cos\theta}{r}\left\{\left[\frac{r_1^3(K_\ell-K_v)}{r^3(K_v+2K_\ell)} + 1\right]^2 - \left[1 - \frac{2r_1^3(K_\ell-K_v)}{r^3(K_v+2K_\ell)}\right]^2\right\}$$

(F-13)

Equations (F-12) and (F-13) are the r and θ components of the body force in the liquid region outside the vapor bubble. At the interface, $r = r_1$, the body force in the liquid becomes

$$\vec{F}_v = \frac{3E_o^2(K_\ell-1)(K_\ell+2)\epsilon_o}{r_1(K_v+2K_\ell)^2}\left[(K_\ell-K_v)(2K_v\cos^2\theta - K_\ell\sin^2\theta)\vec{r} + \cos\theta\sin\theta \times (K_\ell^2 - K_v^2)\vec{\theta}\right]$$

(F-14)

Another case of interest is the value of the electrical body force for a fluid of variable dielectric constant in a uniform electric field. For this situation Equation (F-5) becomes

$$\vec{F}_v = -\tfrac{1}{2}E^2\vec{\nabla}K + \frac{1}{6}\epsilon_o E^2\vec{\nabla}\left[(K-1)(K+2)\right] \qquad \text{(F-11)}$$

On manipulation the above expression can be resolved to the following result.

$$\vec{F}_v = \frac{\epsilon_o E^2}{3} (K-1) \vec{\nabla} K \qquad (F-12)$$

APPENDIX G

EXAMPLE CALCULATIONS OF ELECTRICAL FORCE QUANTITIES

EXAMPLE CALCULATIONS OF ELECTRICAL FORCE QUANTITIES

A. Stress Across the Vapor-Liquid Interface of a Flat Vapor Film (Film Boiling Analogy).

$$\vec{S} = \frac{\epsilon_o (K_\ell - 1)^2}{3} E_o^2 \, \vec{n}_v$$

Sample Point: water at E_o = 1000 volts/inch and

$$K_\ell = 56.1$$

$$\epsilon_o = 8.85 \times 10^{-12} \ (\text{coul})^2/(\text{n})(\text{m})^2$$

$$\vec{S} = \frac{8.85\text{x}10^{-12} \frac{(\text{coul})^2}{(\text{n})(\text{m})^2} \text{x} (56.1-1)^2 \left[1000 \frac{\text{volts}}{\text{inch}} \text{x} 100 \frac{\text{cm}}{\text{m}} \frac{\text{inch}}{2.54 \text{ cm}}\right]^2 \text{x} 1.45\text{x}10^{-4} \frac{\text{psi}}{\text{n}/(\text{m})^2}}{3} \vec{n}_v$$

$$\vec{S} = 2.0 \times 10^{-3} \, \vec{n}_v$$

B. Stress Across the Vapor-Liquid Interface of a Spherical Vapor Bubble.

$$\vec{S} = \frac{3\epsilon_o (K_\ell - 1)^2 E_o^2}{2(K_v + 2K_\ell)^2} [2K_v^2 \cos^2 \theta - K_\ell^2 \sin^2 \theta] \vec{n}_v$$

Sample Point: water at E_o = 1000 volts/inch = 39,370 $\frac{\text{volts}}{\text{meter}}$ and

$$\theta = 30°$$

$$K_v = 1.0$$

$$K_\ell = 56.1$$

$$\cos^2 \theta = 0.750$$

$$\sin^2 \theta = 0.250$$

$$\epsilon_o = 8.85 \times 10^{-12} \cdot (\text{coul})^2 (\text{n}) (\text{m})^2$$

$$\vec{S} = \frac{3(8.85\times10^{-12}) \frac{(\text{coul})^2}{(\text{n})(\text{m})^2} (56.1-1)^2 (39{,}370 \frac{\text{volts}}{\text{meter}})^2}{2(1.0+2(56.1))^2 / 1.45\times10^{-4} \text{psi/n/(m)}^2} [2(1.0)^2(0.75) - (56.1)^2 (0.25)] \vec{n}_v$$

$$S = -5.563 \times 10^{-4} \vec{n}_v$$

C. Body Force and Electrical Acceleration in the Liquid at the Vapor-Liquid Interface of a Vapor Bubble.

$$\vec{F}_V = \frac{+3E_o^2 (K_\ell - 1)(K_\ell + 2)\epsilon_o}{r_1 (K_v + 2K_\ell)^2} [(K_\ell - K_v)(2K_v \cos^2\theta - K_\ell \sin^2\theta)\vec{r} + (\cos\theta \sin\theta)(K_\ell^2 - K_v^2)\vec{\theta}]$$

$$|F_V| = \sqrt{\vec{r} \cdot \vec{r} + \vec{\theta} \cdot \vec{\theta}}$$

$$|g_e| = \frac{|F_V|}{\rho_\ell} g_c$$

Angle of intersection of body force with surface normal at bubble vapor-liquid interface

$$\tan \Psi = \frac{r}{\theta}$$

Bubble departure diameter as given by Fritz correlation given in Rohsenow [24]

$$r_1 = \frac{A}{2} \left[\frac{2\sigma g_c}{g(\rho_\ell - \rho_v)}\right]^{1/2} \left(\frac{6}{\pi}\right)^{1/3}$$

Sample Point: water at $E_o = 1000 \frac{\text{volts}}{\text{inch}} = 39{,}700 \frac{\text{volts}}{\text{inch}}$ and

$$\theta = 30°$$

$$K_\ell = 56.1$$

$$K_v = 1.0$$

$$\cos^2 \theta = 0.750$$

$$\sin^2 \theta = 0.250$$

$$\sin \theta \cos \theta = 0.433$$

$$\rho_\ell = 59.88 \text{ lbm/(ft)}^3$$

$$\rho_v = 0.03595 \text{ lbm/(ft)}^3$$

$$\sigma = 4.03 \times 10^{-3} \text{ lb}_f/\text{ft}$$

$$g_c = 32.2 \text{ (ft)(lbm)/(lb}_f\text{)(sec)}^2$$

$$g = 32.2 \text{ ft/(sec)}^2$$

$A = 0.20$ for contact angle, β_o, of 20°

$$r_1 = \frac{0.20}{2}\left(\frac{6}{\pi}\right)^{1/3}\left[\frac{(2)(4.03\times10^{-3})\frac{\text{lb}_f}{\text{ft}}\ 32.2\ \frac{\text{ft lbm}}{\text{lb}_f(\text{sec})^2}}{32.2\ \frac{\text{ft}}{(\text{sec})^2}(59.88-.03595)\ \frac{\text{lbm}}{(\text{ft})^3}}\right]^{1/2} \times (12)\ \frac{\text{inches}}{\text{ft}}$$

$$r_1 = 0.01728 \text{ inches}$$

$$\vec{F}_V = \frac{+3(39{,}700)^2(56.1-1)(56.1+2)\ 8.85\times10^{-12}}{(.01728)(1.0+2(56.1))^2/1.45\times10^{-4}}[(56.1-1.0)[(2)(1.0)(0.75)$$

$$-(56.1)(0.25)]\vec{r} + 0.433\ [(56.1)^2-(1.0)^2]\vec{\theta}]\ 1728\ \frac{\text{in}^3}{\text{ft}^3}$$

$$\vec{F}_V = [-101.3\ \vec{r} + 200.0\ \vec{\theta}]$$

$$F_V = 224.9\ lb_f/ft^3$$

$$|g_e| = \frac{224.9}{59.88}\ (32.2) = 120.5\ \frac{ft}{(sec)^2}$$

$$\tan\ \Psi = \frac{-101.3}{200} = -.507$$

D. Condenser Effect Stress

$$\frac{F}{A} = \frac{\epsilon_o}{2}\ \vec{E} \cdot \vec{E}$$

$\vec{E}$ calculated assuming that the full voltage is across the vapor film δ.

$$\delta = \frac{k\Delta T}{q/A}$$

$$\vec{E} = \frac{V_o}{\delta} = \frac{V_o q}{k\Delta T A}\ \vec{r}$$

Sample Point: water at V_o = 1000 volts and

$$\Delta T = 285°F$$

$$q/A = 13{,}000\ BTU/(hr)\,(ft)^2$$

$$k = 0.016 \text{ BTU/(hr)(ft)(°F)}$$

$$\epsilon_o = 8.85 \times 10^{-12} (\text{coul})^2/\text{n}(\text{m})^2$$

$$E = \frac{(1000)(13{,}000)(100)}{(.016)(285)(12)(2.54)} = 9.35 \times 10^6 \frac{\text{volts}}{\text{inch}}$$

$$\frac{F}{A} = \frac{(8.85 \times 10^{-12})}{2} (1.45 \times 10^{-4}) (9.35 \times 10^6)^2 = 561 \times 10^{-4} \text{psi}$$

E. Volume Force and Electrical Acceleration Evaluated at the Wire Heated Surface for Choi's Freon-113 Apparatus

$$(F_V)_{wire} = \frac{\epsilon_o}{6}(K_\ell - 1)(K_\ell + 2)\nabla E^2 = \frac{-\epsilon_o}{3}(K-1)(K+2)\left[\frac{V_o}{\ln \frac{r_w}{r_o}}\right]^2 \frac{1}{r_w^3}$$

Sample Point: Freon-113 at $V_o = 5{,}250$ volts and

$$r_o = 0.75 \text{ inches}$$

$$r_w = 0.01005 \text{ inch} = 2.553 \times 10^{-4} \text{ meters}$$

$$K_\ell = 2.392$$

$$\epsilon_o = 8.85 \times 10^{-12} (\text{coul})^2/(\text{n})(\text{m})^2$$

$$1 \text{ n/m}^3 = 3.683 \times 10^{-6} \text{lb}_f/\text{in}^3$$

$$(F_V)_{wire} = \frac{(8.85\times10^{-12})(2.392-1)(2.392+2)(3.683\times10^{-6})}{3(2.553\times10^{-4})^3} \times$$

$$\left[\frac{5,250}{\ln(\frac{.01005}{.75})}\right]^2 (1728) = 10,357 \frac{lb_f}{ft^3}$$

$$|g_e| = \frac{|F_V|}{\rho_\ell} g_c = \frac{10,357}{95.33} 32.2 = 3,498 \frac{ft}{(sec)^2}$$

F. Volume Force and Electrical Acceleration Within the Superheated Boundary Layer Adjacent to a Heated Surface.

$$F_V = + \frac{1}{3} \epsilon_o E^2 (\frac{\partial K_\ell}{\partial T})(\frac{\partial T}{\partial X})[K_\ell - 1]$$

$$|g_e| = \frac{|F_V|}{\rho_\ell} g_e$$

From Lange [13]

$$K = 78.54[1-4.579\times10^{-3}(T-25)+1.19\times10^{-5}(T-25)^2-2.8\times10^{-8}(T-25)^3]$$

and therefore

$$(\frac{\partial K}{\partial T}) = 78.54[-4.579\times10^{-3}+2.38\times10^{-5}(T-25)-8.4\times10^{-8}(T-25)^2]$$

Sample Point: water at E = 1000 volts/inch = 39,370 v/m and

$$\epsilon_o = 8.85\times10^{-12}(coul)^2/n(m)^2$$

$$q/A = 100{,}000 \text{ BTU/(hr)(ft)}^2$$

$$K_\ell = 56.1$$

From Bobst [4]

$$T_{surface} = 237°F$$

$$\left(\frac{\partial T}{\partial X}\right)_{x=0} = -9{,}406°F/\text{inch}$$

Therefore

$$\left(\frac{\partial K}{\partial T}\right) = -0.349°F^{-1}$$

$$F_V = +\frac{1}{3}(8.85\text{x}10^{-12})(39{,}370)^2(1728)(1.45\text{x}10^{-4})(-9{,}406)(-0.349)(56.1-1)r$$

$$F_V = 205.1 \text{ lb/ft}^3$$

$$|g_e| = \frac{205}{59.88} \text{ x } 32.2 = 110.3 \text{ ft/(sec)}^2$$

APPENDIX H

NOMENCLATURE

NOMENCLATURE

AC	alternating current
AF	amplification factor as defined by Equation (4)
BP	boiling point
C	unspecified constant
C_p	specific heat
d	diameter or length
DC	direct current
$\vec{E}$	electric field intensity vector
El	electrical dimensionless group as defined by Equations (6) and (7)
$\vec{F}$	force vector
$\vec{F}_v$	electrical body force vector
F/A	force per unit area or stress
g	acceleration of gravity
g_e	electrical acceleration as defined by Equation (16)
g_o	term representing all types of induced acceleration
g_c	Newton's law constant for British engineering units
g_t	total acceleration
Gr	Grashof number

HTS (+)	refers to DC voltage operation with the heat transfer surface of positive polarity
HTS (-)	refers to DC voltage operation with the heat transfer surface of negative polarity
H_{fg}	heat of vaporization
$\vec{i}_r$	unit vector in radial direction
K	dielectric constant
k	thermal conductivity
$\vec{n}$	unit vector
Nu	Nusselt number
Pr	Prandtl number
p_w	pressure of saturated fluid at T_w
p	pressure of saturated fluid at normal boiling point
Δp	$p_w - p$
q/A	heat flux
q^+	electrical charge
r	radial coordinate in cylindrical or spherical coordinates
r_1	radius of a vapor bubble
$\vec{r}$	unit vector directed in a radial direction
s	variation of dielectric constant with temperature
$\vec{S}$	electrical stress vector at a dielectric interface
t	variation of electrical conductivity with temperature
T	temperature
ΔT	heated surface minus saturated fluid temperature difference

V	voltage or electrical potential
V_o	voltage difference between conducting electrodes
α, β	parameters which characterize isotropic dielectric media
β_o	contact angle
ϵ_o	electrical permittivity of free space
ϵ	electrical permittivity of a fluid
θ	angular coordinate
μ	fluid viscosity
ρ	fluid density
σ	surface tension
τ	dynamic viscosity of a fluid
χ	dielectric susceptibility
Ψ	angle subtended by the interface normal and the respective F_v vector

Subscripts

i	refers to inner cylinder of concentric cylinder electrode configuration
l	liquid value
n	normal or perpendicular component of a vector
o	refers to outer cylinder of concentric cylinder electrode configuration except where specifically defined otherwise
p	particle value
tan	refers to tangent component of a vector
w	evaluated at heated surface wall

1,2	region designation

Appendix A

ΔT	heated surface minus saturated fluid temperature difference
ΔT_{CB}	conduction block temperature differences
$(\Delta T_{CB})_{avg.}$	average value of the six conduction block temperature differences

Appendix B

CG	coarse grid
FG	fine grid
F	film boiling
+G	heat transfer surface grounded and of positive polarity
HTS(+)	heat transfer surface of positive polarity
HTS(-)	heat transfer surface of negative polarity
ΔT	heated surface minus saturated fluid temperature difference

Appendix C

$\vec{D}$	electric flux density vector
d	characteristic distance
d_q	charge displacement distance in a dipole
$\vec{E}$	electric field intensity vector
Δh	length increment normal to a dielectric interface

K	dielectric constant
L	linear distance or length
N	number of dipoles per unit volume
$\vec{P}$	electric polarization vector
PE	potential energy
Q	total charge contained within a Gaussian surface
q	charge
S	area
V_o	voltage difference between conducting electrodes
v	volume
α	angle between $\vec{D}$ and D_{tan}
ϵ_o	electrical permittivity of free space
ϵ	electrical permittivity of a fluid
ρ_s	surface charge density
ρ_{sb}	bound surface charge density
Δw	length increment tangent to a side of a dielectric interface

Subscripts

$\vec{n}$	normal or perpendicular component of a vector
tan	tangent component of a vector
1,2,3	region designation

Appendix D

A	area
$\vec{D}$	electric flux density vector
$\vec{E}$	electric field intensity vector
E'	local electric field intensity vector
N	number of dipoles per unit volume
N_o	Avagadros number
$\vec{n}$	unit vector in the normal direction
M	molecular weight
$\vec{P}$	electric polarization vector
$\vec{T}$	torque
ϵ_o	electrical permittivity of free space
λ	polariability
$\vec{\mu}$	dipole moment vector
ρ	fluid density
ρ_s	surface charge density

Appendix E

C	integration constant
$\vec{E}$	electric field intensity vector
E_o	electric field intensity magnitude from an applied potential of V_o
K	dielectric constant
m,n	constants arising from separation of variables

P, Q	refer to Legendere polynomials
r	radial direction designation in spherical coordinates
r_1	sphere radius
V_1	potential inside sphere due to induced charge
V_2	total potential outside the sphere
V_2'	potential outside the sphere due to induced charge
V_o	potential outside the sphere due to the charged flat plate electrodes
Z	vertical direction in orthogonal cartesian coordinates
θ, Φ	the two angular directions in spherical coordinates

Subscripts

ℓ	liquid
v	vapor
1	designation for region inside the sphere
2	designation for region outside the sphere

Appendix F

$\vec{E}$	electric field intensity vector
E_o	electric field intensity magnitude as produced by the charge on the flat plate electrodes
$\vec{F}_v$	electrical body force vector
K	dielectric constant
$\vec{n}$	unit vector normal to a surface or interface
$\vec{S}$	electrical stress vector at a dielectric interface

r,θ,Φ spherical coordinate directions

r_1 radius of sphere

ϵ_o electrical permittivity of free space

ρ fluid density

Subscripts

n refers to the normal component of a vector

ℓ liquid

tan refers to the tangent component of a vector

v vapor

1,2 region designation

Appendix G

A Fritz bubble departure diameter correlation constant

$\vec{E}$ electric field intensity vector

F/A condenser effect stress

$\vec{F}_V$ electrical body force vector

g_e electrical acceleration as defined by Equation (16)

g_c Newton's law constant for British engineering units

K dielectrical constant

k thermal conductivity

$\vec{n}$ surface unit normal vector

q/A heat flux

r	radial coordinate in cylindrical or spherical coordinates
r_1	radius of a vapor bubble
$\vec{S}$	electrical stress or traction vector
T	temperature
ΔT	heated surface minus saturated fluid temperature difference
V_o	voltage difference between conducting electrodes
β_o	contact angle
δ	film boiling vapor film thickness
ϵ_o	electrical permittivity of free space
$\vec{\theta}$	angular coordinate unit vector
θ	angle as defined in Figure E-1
ρ	fluid density
σ	surface tension
Ψ	angle subtended by the interface normal and the respective F_V vector

Subscripts

ℓ	liquid value
o	refers to outer cylinder of concentric cylinder electrode configuration except where specifically defined otherwise
v	vapor value
w	heated wall surface